CERENKOV LIGHT PRODUCTION IN A WATER MODERATED NUCLEAR REACTOR

by

Robert William Madey

Thesis submitted to the Faculty of the Graduate School
of the University of Maryland in partial fulfillment
of the requirements for the degree of
Doctor of Philosophy
1963

APPROVAL SHEET

Title of Thesis: Cerenkov Light Production in a Water Moderated Nuclear Reactor

Name of Candidate: Robert William Madey
Doctor of Philosophy, 1963

Thesis and Abstract Approved:

Dick Duffey

Dick Duffey - Professor
Nuclear Reactor Director
Chemical Engineering
Department

Date Approved:
22 April 1963

ABSTRACT

Title of Thesis: Cerenkov Light Production in a Water Moderated Nuclear Reactor

Robert William Madey, Doctor of Philosophy, 1963

Thesis directed by Dr. Dick Duffey, Professor

An experimental investigation of the production of Cerenkov radiation in a water moderated nuclear reactor is conducted using a photomultiplier as a light sensor. The variations in light intensity are studied during various phases of reactor operation, namely: startup, steady state and shutdown. The relevant theory is presented as an aid in interpreting and extrapolating the experimental results.

It is found that for transients such as startup, the light signal is directly related to reactor power for periods (e - folding time) faster than about 20 seconds. Additional transient data acquired from measurements performed on a TRIGA pulsed-type reactor illustrate the excellent agreement between the Cerenkov detector and a conventional ionization chamber for measuring pulse characteristics such as peak power, pulse half-width, and prompt period. The proportionality between reactor power and Cerenkov signal is no longer valid for whole core measurements made at steady state power level because of the gradual increase of the Cerenkov signal as a result mainly of fission product

contributions. Selective scanning of the Cerenkov spectrum through the use of interference filters over the wavelength range 3500 Å to 5530 Å results in a lower buildup fraction. Indications are that measurements further into the short wavelength region may yield a light sensor, and hence a good power detector, independent of any fission product buildup. The decrease in the Cerenkov light intensity after shutdown is measured for reactor operating times from 20 minutes to 4 hours. Comparison of the empirical data with theoretical considerations results in good agreement for shutdown times ranging from 500 seconds to 10,000 seconds.

Spectral measurements made through 17 feet of water with a Hilger quartz spectrograph show a spectral distribution ranging from 2500 Å to 6000 Å. A calculated spectral distribution is compared with the measured spectrum after correcting for water attenuation.

ACKNOWLEDGEMENT

The author wishes to express his appreciation to Dr. Dick Duffey for the opportunity to undertake this work and for his interest and encouragement throughout the course of the investigation. He is especially grateful to Dr. C. O. Muehlhause for suggesting the problem and to Dr. Joseph Silverman for many stimulating discussions regarding the problems encountered in this work.

Grateful recognition is also extended to the many friends who assisted in the experiments and preparation of the thesis material. Particular notice is taken of the invaluable help given by Mr. Chieh Ho in maintaining the operational status of the University of Maryland Reactor.

To all these individuals, and to my wife Gloria for her constant encouragement, assistance and patient understanding, I extend my thanks.

TABLE OF CONTENTS

TABLE OF CONTENTS (CONT'D)

LIST OF TABLES

LIST OF FIGURES

LIST OF FIGURES (CONT'D)

LIST OF FIGURES (CONT'D)

LIST OF FIGURES (CONT'D)

CHAPTER I

INTRODUCTION

A. The Cerenkov Effect

1. History[1]

The discovery of the blue light emitted from transparent substances when irradiated by radioactive sources dates back to Mallet (1926, 1928-1929). He noted that the spectrum of the light was continuous and did not possess the line or band structure characteristic of fluorescence. Mallet, however, did not attempt to offer any explanation of the phenomenon and it was not until 1934 that the Russian physicist, Cerenkov, studied the phenomenon more systematically. He showed, in particular, the fundamental difference between this light and that produced by fluorescence, namely the addition of known fluorescent inhibitors had no effect upon the light. Furthermore, his experiments showed the light to be partially polarized. The correct theoretical explanation of the phenomenon was not established until 1937 by Frank and Tamm.

2. Descriptive Account[1,2,3,4]

Whenever a fast charged particle traverses a dielectric medium it produces a local polarization along its path. The polarized atoms return to their normal states with the emission of light immediately after the particle has passed. When the velocity of the particle is less than the phase

velocity of light in the same medium, the light pulses from the individual atoms are damped out due to destructive interference. However, if the velocity of the particle is greater than the phase velocity of light in the medium, the wavelets from all portions of the trace are in phase with one another and a resulting radiation known as Cerenkov radiation is observed. Referring now to Figure 1, the wavelets which are sent out while the particle traverses the distance AB are propagated along a wavefront BC, the velocity of propagation being $\frac{c}{n}$ where n is the refractive index of the medium and c is the velocity of light in vacuo. Coherence exists whenever the time taken by the particle to traverse the distance AB is the same as the time taken by the wavefront to traverse the distance AC, e.g., the spherical waves arrive in phase along BC. The direction of emission of the radiation is along the line AC, at right angles to BC. The distance the particle travels in a time Δt is $AB = v\Delta t$, where v is the velocity of the particle in the medium. In the same time, the light travels a distance $AC = \frac{c}{n}\Delta t$. The resulting expression, known as the Cerenkov relation, obtained from these two expressions is:

$$\cos\theta = \frac{1}{\beta n} \tag{1}$$

where $\beta = \frac{v}{c}$ and is related to the kinetic energy E of the particle and to its rest mass m_o by the equation:

$$E = m_o c^2 \cdot \left[\frac{1}{\sqrt{1 - \beta^2}} - 1 \right] \tag{2}$$

Fig. 1 Huyghens Construction to Illustrate Coherence

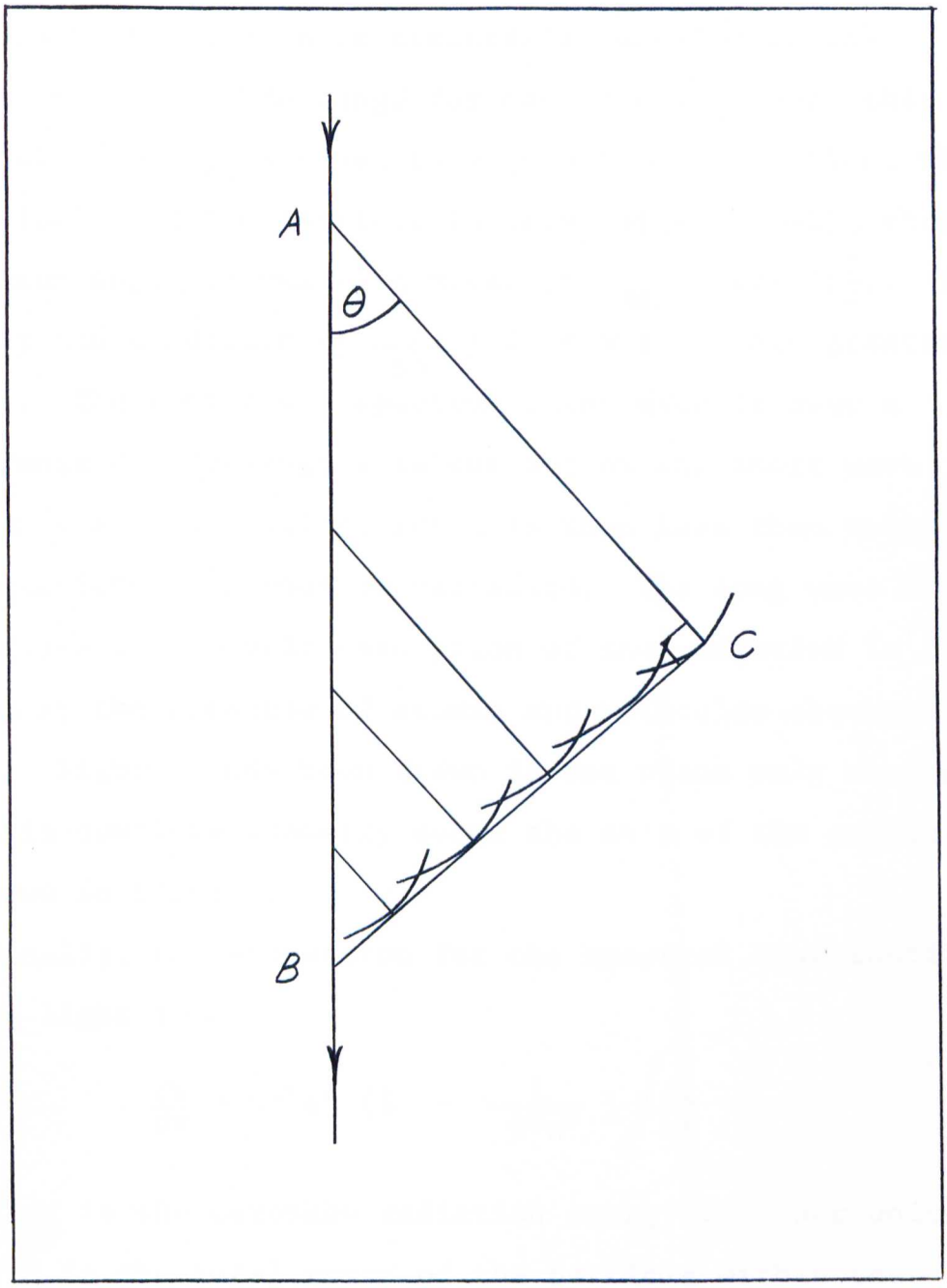

Therefore, Cerenkov radiation is not possible unless $0 \leq \frac{1}{\beta n} \leq 1$ which says, in effect, that there is a critical velocity below which a particle is not able to produce the Cerenkov effect. In general, the index of refraction is a function of wavelength. However, to a first approximation, n is essentially wavelength independent over a wide range for many media. Hence this critical velocity is equal to $v_{min} = \frac{c}{n}$. In addition, when the velocity of the particle is very large ($\beta \rightarrow 1$), there is a maximum angle of emission given by $\theta_{max} = \cos^{-1}(\frac{1}{n})$. To satisfy the condition $0 \leq \frac{1}{\beta n} \leq 1$, n must remain greater than 1. The continuous spectrum which extends over a wide range of wavelengths is cut off on the short wave side in the x-ray region, for n is then less than unity and equation (1) cannot be satisfied. The long wave cut-off arises due to self absorption of the radiation in the medium by the presence of atomic and molecular absorption bands. Figure 1 has been drawn in one plane only whereas there is complete symmetry about the axis of the particle as shown in Figure 2.

Finally, the expression for the spectral distribution of the light is[1]

$$\frac{dW}{dx} = 4\pi^2 e^2 \left(1 - \frac{1}{\beta^2 n^2}\right) \int \frac{d\lambda}{\lambda^3} \qquad (3)$$

where $\frac{dW}{dx}$ is the Cerenkov radiation energy loss per unit path, x is the total range of the particle within the medium, e is the charge of the particle and λ is the wave-

Fig. 2 Formation of the Cerenkov Cone

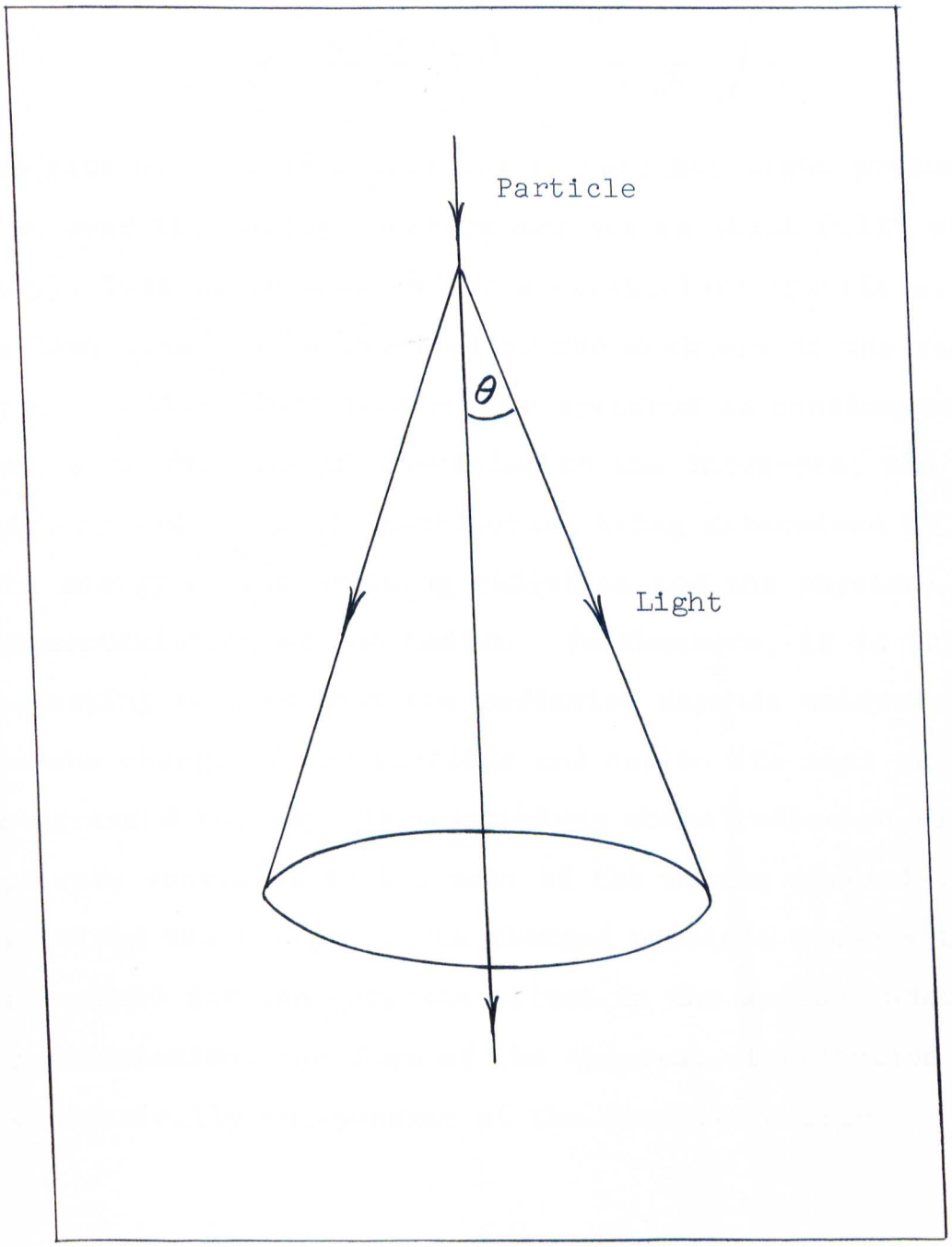

length of the light. Since the intensity of light of wavelength λ may be written as $W = N_p \cdot \frac{hc}{\lambda}$ where N_p is the number of Cerenkov light photons and h is Planck's constant, the expression for the production of light in units of photons per unit path as derived by Frank and Tamm is given by:

$$\frac{dN_p}{dx} = \frac{4\pi^2 e^2}{hc} \left(1 - \frac{1}{\beta^2 n^2}\right) \int \frac{d\lambda}{\lambda^2} \qquad (4)$$

The rate of loss of energy due to Cerenkov light production over the entire spectrum amounts to about 0.1%[3] of the energy loss by ionization for a relativistic particle, so some idea may be obtained of the weakness of the radiation. Unlike fluorescence, the spectrum is continuous extending from the ultra-violet to the infra-red; the intensity and spectral distribution being determined by the energy of the exciting radiation and the physical characteristics of the medium. Furthermore, it is interesting to note that the radiation depends uniquely on the charge of the particle and not on its mass as contrasted to, say, bremsstrahlung whose radiation yield is very sensitive to the mass of the moving particle. Provided the energy of the charged particle exceeds the threshold for the Cerenkov effect in the medium under consideration, the form of the spectral distribution is theoretically independent of the particle energy.

CHAPTER II

CERENKOV RADIATION IN WATER MODERATED REACTORS

A. Source of Cerenkov Radiation

1. General

The Cerenkov light intensity produced in a transparent dielectric medium is dependent upon the nature of the particles appearing in the medium and upon its physical properties. In the experimental investigation described herein, the Cerenkov light intensity from the core of a light-water moderated reactor has been investigated under varying conditions of reactor operation. The index of refraction of light-water is approximately $\frac{4}{3}$ as indicated by Table I. Hence, only particles having a velocity greater than $\frac{3}{4}$ c, (where c is the velocity of light, 3×10^{10} cm per sec), are able to produce light by the Cerenkov effect.

The kinetic energy of particles having such a velocity as calculated from equation (2) is seen to be:

260 kev for electrons
475 Mev for protons
960 Mev for deuterons
2 Bev for alpha particles

The three latter particles have energies much too high to be of importance in reactors. On the contrary, there exists

Table I - Refractive Index of Water at 20°C For Various Wavelengths[5]

Wavelength (Å)	Refractive Index
12560	1.3210
6708	1.3308
6563	1.3311
6438	1.3314
5893	1.3330
5461	1.3345
5086	1.3360
4861	1.3371
4800	1.3374
4047	1.3428
3034	1.3581

Temperature Coefficient of Index of Refraction:

-1.0×10^{-4} per °C

in the reactor a large number of electrons having energies greater than or equal to 260 kev. These fast electrons can be produced either directly as beta particles from radioactive nuclei or indirectly by gamma rays.

2. Beta Radiation

The constituent materials of the University of Maryland reactor are essentially the water moderator, the uranium elements clad in aluminum, and the aluminum fuel element containers, experimental ports and tank. The aluminum cladding of the elements stop, to a great extent, the beta particles emitted by the fission products. Based on beta ray spectra of the fission products of U-235,[13,23] it is conservatively estimated that less than five percent of the total number of beta particles produced per fission penetrate the aluminum cladding. On the other hand, beta particles emitted by the aluminum slow down in the water and are capable of producing the Cerenkov effect. Al-27, under bombardment by neutrons gives rise to Al-28 which is radioactive and emits beta particles having a maximum energy of 2.86 Mev and gamma rays of approximately 1.8 Mev.[6] The half-life of Al-28 is 2.3 minutes and the beta particles are of sufficient energy for producing light by the Cerenkov effect.

3. Gamma Radiation

The main sources of the gamma radiation[7,8,9] throughout the reactor include the following:

(a) prompt fission gamma rays

(b) gamma rays from neutron capture in the uranium, construction materials and the moderator

(c) fission product gamma rays

(d) gamma rays from the disintegration of capture products

The first two sources are proportional to the number of neutrons present in the reactor; hence a function of power level, whereas the latter two depend upon the power and history of the reactor in a more complex way. Gamma rays from inelastic scattering in aluminum and uranium as well as neutron capture in U-238 and the graphite reflector are not considered due to their relatively low intensities.

The importance of gamma radiation, with respect to production of light by the Cerenkov effect, depends essentially on the probability of a gamma ray producing fast electrons. Gamma rays produce electrons by the photoelectric effect, Compton effect, and pair production[10,11] but only those electrons having an energy greater than 260 kev are considered. Table II illustrates the relative importance of these processes in water. In the photoelectric effect, the energy of the incident gamma ray photon is transferred completely to an orbital electron in an atom which is then ejected with a kinetic energy

TABLE II

Relative Importance of Photoelectric, Compton, and Pair Absorption Coefficients in Water[12]

Photon energy, Mev	Total mass absorption coefficient, cm^2/gm	Compton (σ_c/ρ) % of total	Photoelectric and Pair (σ_{pe}/ρ) % of total
0.10	0.171	98.8	1.2
0.20	0.137	99.7	0.3
0.30	0.119	100	0
0.40	0.106	100	0
0.50	0.0966	100	0
0.60	0.0896	100	0
0.80	0.0786	100	0
1.0	0.0706	100	Pair
1.5	0.0575	99.8	0.2
2.0	0.0493	98.6	1.4
3.0	0.0396	97.2	2.8
4.0	0.0339	94.7	5.3
5.0	0.0301	92.0	8.0
6.0	0.0275	89.1	10.9
8.0	0.0240	83.3	16.7
10.0	0.0219	78.1	22.9

$E_k = h\nu - I$, I being the ionization potential of the level at which the electron is found, and ν the frequency of the incident gamma ray photon. For the K electron level, the ionization potential is approximately equal to $R_y Z^2$ (Z being the atomic number and R_y the Rydberg constant which is equal to 13.5 ev), e.g. the ionization potential for aluminum and uranium is 2 kev and 108 kev respectively. For the subsequent levels further out, the ionization potential becomes smaller. A photoelectron, therefore, is able to produce light by the Cerenkov effect if the energy of the incident photon is greater than $h\nu = E_k + I$, ($h\nu$ = 262 kev for aluminum). Examination of the cross-section curve in Figure 3 and Table II shows that gamma rays with energies greater than or equal to 262 kev have a very small probability of producing electrons. As a rough approximation,[8]

$$\text{Probability of photoelectric interaction} \approx \text{const.} \times \frac{Z^n}{E_k^3}$$

where n varies from 3, for gamma rays of low energy, to 5, for high energy rays. The photoelectric effect is important mostly at the lower energies for which the electrons are unable to produce light in the water by the Cerenkov effect.

In the pair production process, a gamma ray photon with energy in excess of 1.02 Mev may be annihilated

Fig. 3 Mass Absorption Coefficients for Water as a Function of Photon Energy

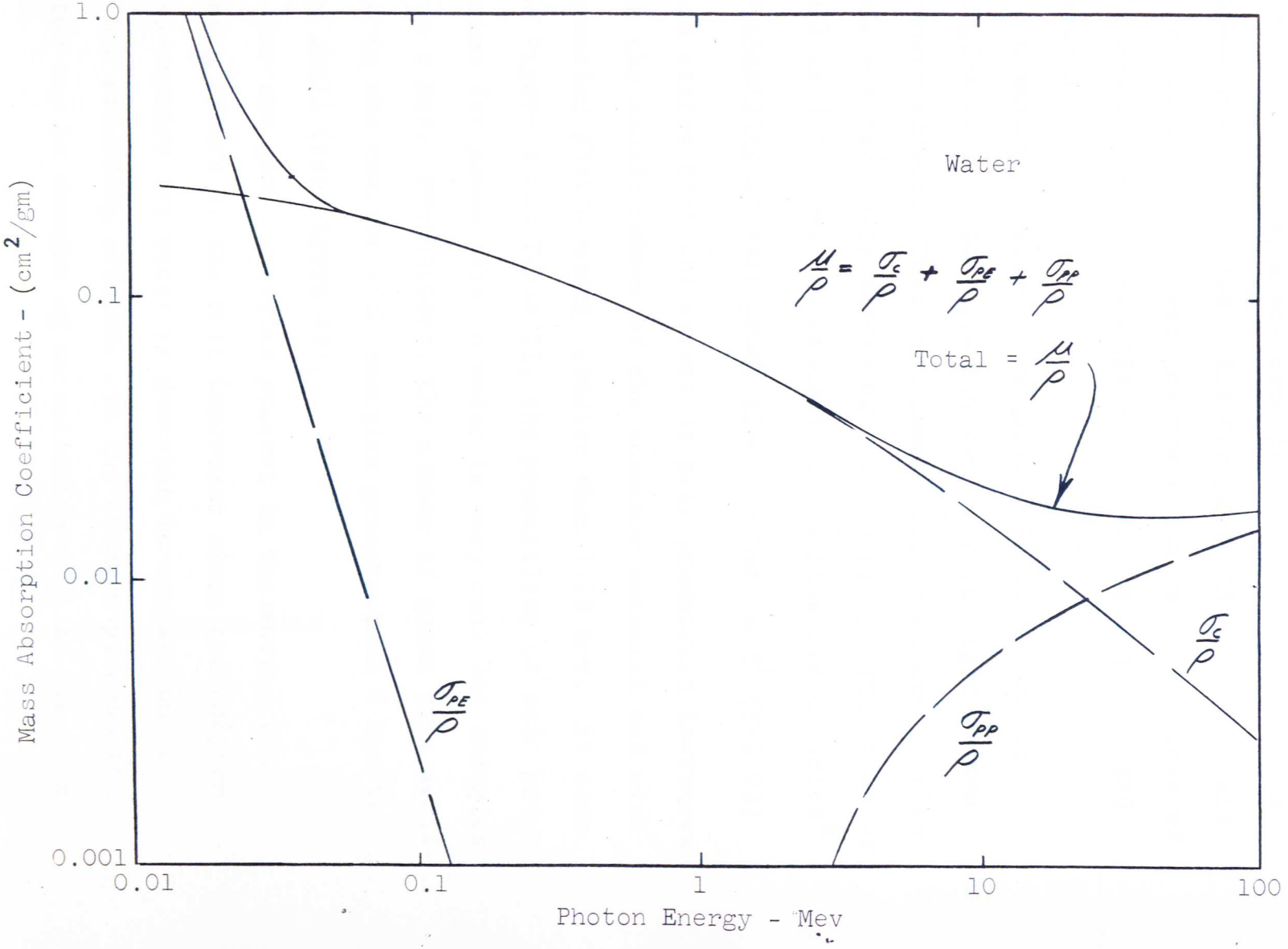

with the subsequent formation of a positron - electron pair. Since the energy equivalent of the total mass of an electron and a positron is 1.02 Mev, this is the minimum energy necessary for the production of the pair of particles. Any energy of the gamma rays in excess of 1.02 Mev appears as kinetic energy of the electron and positron.

In water, positive or negative electrons having energies greater than 260 kev can produce light by the Cerenkov effect. Thus, the gamma rays which are able to produce these pairs should have an energy greater than or equal to 1.54 Mev. In general, it is possible to write[8]

$$\text{Probability of pair production} \approx \text{const.} \times Z^2 \, (E-1.02)$$

which states that the extent of pair production increases with the atomic number of the absorber material and with increasing photon energy greater than 1.02 Mev. As seen from Figure 3 and Table II, the probability of pair production for gamma rays in water is very weak for energies up to 6 Mev. Furthermore, the number of gamma rays available in the reactor with energies greater than 6 Mev is very small (see Figure 43).

For the gamma energies present in the reactor the Compton effect is the most important since the Compton cross-section for water is dominant in comparison to the two preceding effects. In the Compton process the photon may be thought of as colliding with an electron

which is usually considered free (e.g. the binding energy is neglected). In the collision, part of the energy of the incident photon is transferred to the electron and at the same time the photon is scattered from its initial direction. Since in Compton scattering each electron may be considered to be free, its magnitude depends on the atomic number of the absorber. As a rough approximation,[8]

$$\text{Probability of Compton interaction} \approx \text{const.} \times \frac{Z}{E}$$

The probability of a gamma ray photon producing an electron capable of emitting light by the Cerenkov effect depends on the energy of the incident gamma ray and at the same time on the energy of the scattered electron; the minimum photon energy which can produce an electron capable of emitting Cerenkov light being 0.407 Mev.[35]

The beta rays from the radioactive decay of the Al-28 and the fission products are accompanied by a source of gamma radiation called bremsstrahlung, which is secondary radiation resulting from the deceleration of the beta particles in the atomic electric field of the material adjacent to the point of beta emission. The amount of energy radiated as bremsstrahlung increases with the atomic number of the material in which the electrons are brought to rest so that an upper limit for bremsstrahlung production in a reactor is obtained by assuming that the beta particles are completely stopped by the uranium. Based on this assumption, one finds that the upper limit

of the contribution of bremsstrahlung energy is less than 15% of the total gamma energy released from fission products per fission.[13] The percentage falls rapidly to about 1% if the beta stopping material has an effective Z of 13, e.g. aluminum.[13] Therefore, the effect is clearly negligible if the effective Z of the beta stopping material is small. The total energy radiated by the bremsstrahlung process is in general considerably higher than that by the Cerenkov process but in the visible region the contribution from the bremsstrahlung is significantly small.[3] Moreover, any Cerenkov radiation produced by bremsstrahlung is clearly negligible, being only a second order effect of an already minor contribution.

CHAPTER III

EXPERIMENTAL DESIGN

A. Brief Description of the Reactor[14]

The University of Maryland Reactor, hereafter referred to as the UMR, is a 10 kilowatt swimming pool reactor moderated by ordinary water and reflected by graphite. The fuel is an alloy of fully-enriched uranium (93.5 percent U-235, the remainder being U-238) and aluminum in the form of flat, aluminum clad plates. Each plate is essentially a sandwich; the center 0.026 inches is the uranium-aluminum alloy, the outer side is a layer of aluminum cladding 0.027 inches thick bonded to each side of the center. The cladding serves two purposes; it prevents contamination of the pool and air by sealing in the radioactive fission products and it prevents corrosion of the uranium by the water. All the experiments except the final series dealing with spectrographic and filter measurements are conducted on the original core as shown in Figure 4. The original reactor core consists of 16 fuel assemblies in a 4 x 4 array; three 6 plate assemblies, twelve 10 plate assemblies and one 9 plate assembly. The six plate assemblies accommodate the three control rods of which two are boron carbide shim-safety rods and one is a stainless steel regulating rod. Each fuel element assembly is open at the top and bottom and is surrounded

Fig. 4 Initial Reactor Core Geometry, #1

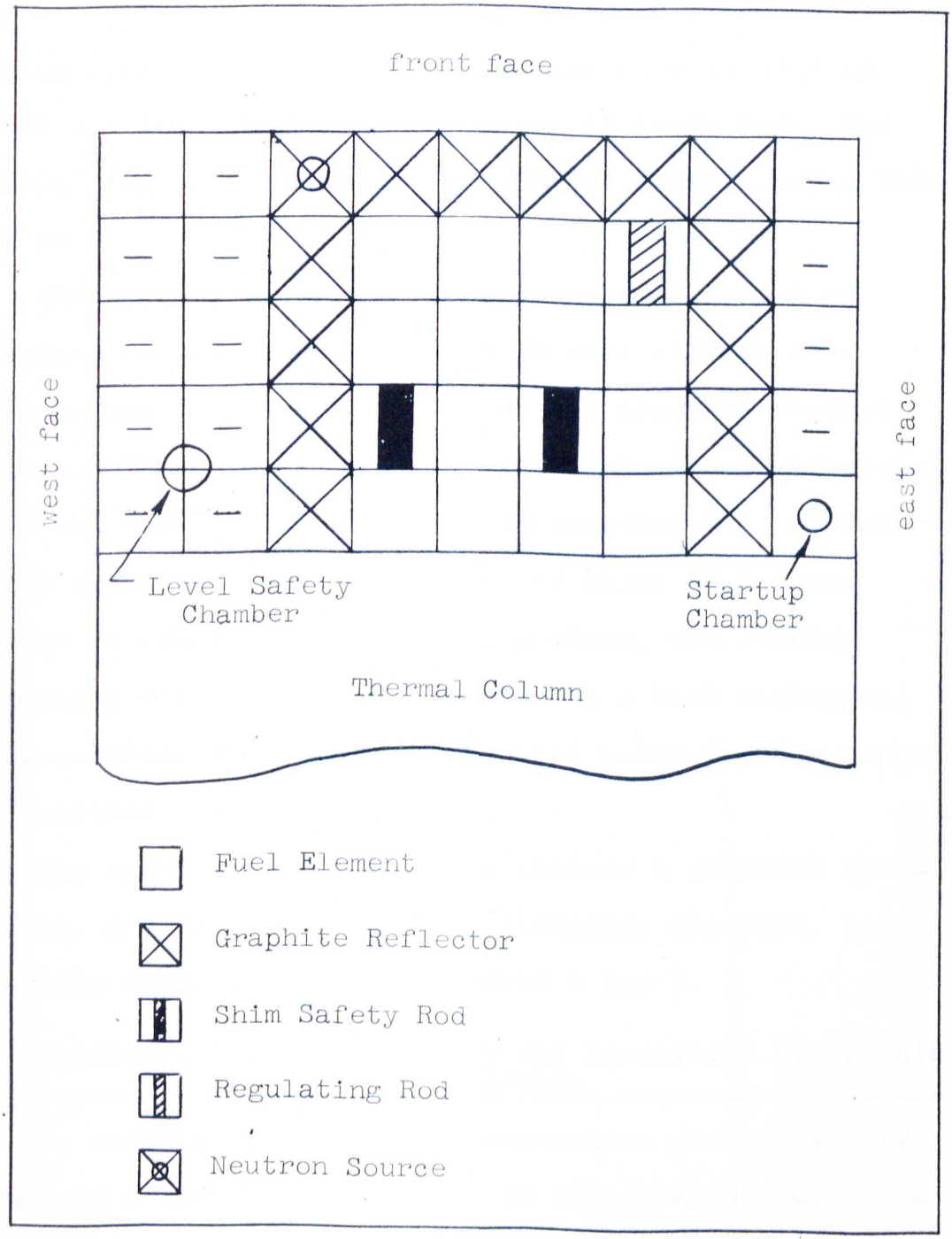

by a fuel element container of aluminum which is 0.064 inches thick. Water flowing up through the core by natural convection passes between the fuel plates which are 0.182 inches apart, removing the heat produced during operation. Figure 5 shows the core loading on which the final experimental series is conducted. Two special fuel elements containing experimental sample holes are provided as shown.

The core is reflected on three vertical sides by aluminum canned graphite blocks in fuel element containers and on the fourth side by the graphite thermal column. The core is supported in an aluminum grid plate near the tank wall. The water surrounding the reactor which covers the core to a depth of about 17.0 feet, serves as moderator, reflector, coolant, and shield. The water circulation system includes a heat exchanger, demineralizer and filter. A typical value for the water conductivity is 1.60 micormhos.

The experimental facilities include a graphite thermal column, a through tube passing alongside the core, and two beam tubes as shown in Figures 6 and 7.

B. Detector, Detector Assembly and Associated Electronic Equipment

In order to simplify the measurement problem and to maintain a certain versatility in the intended study, it seems preferable to study the light emitted from the whole

Fig. 5 Final Reactor Core Geometry, #2

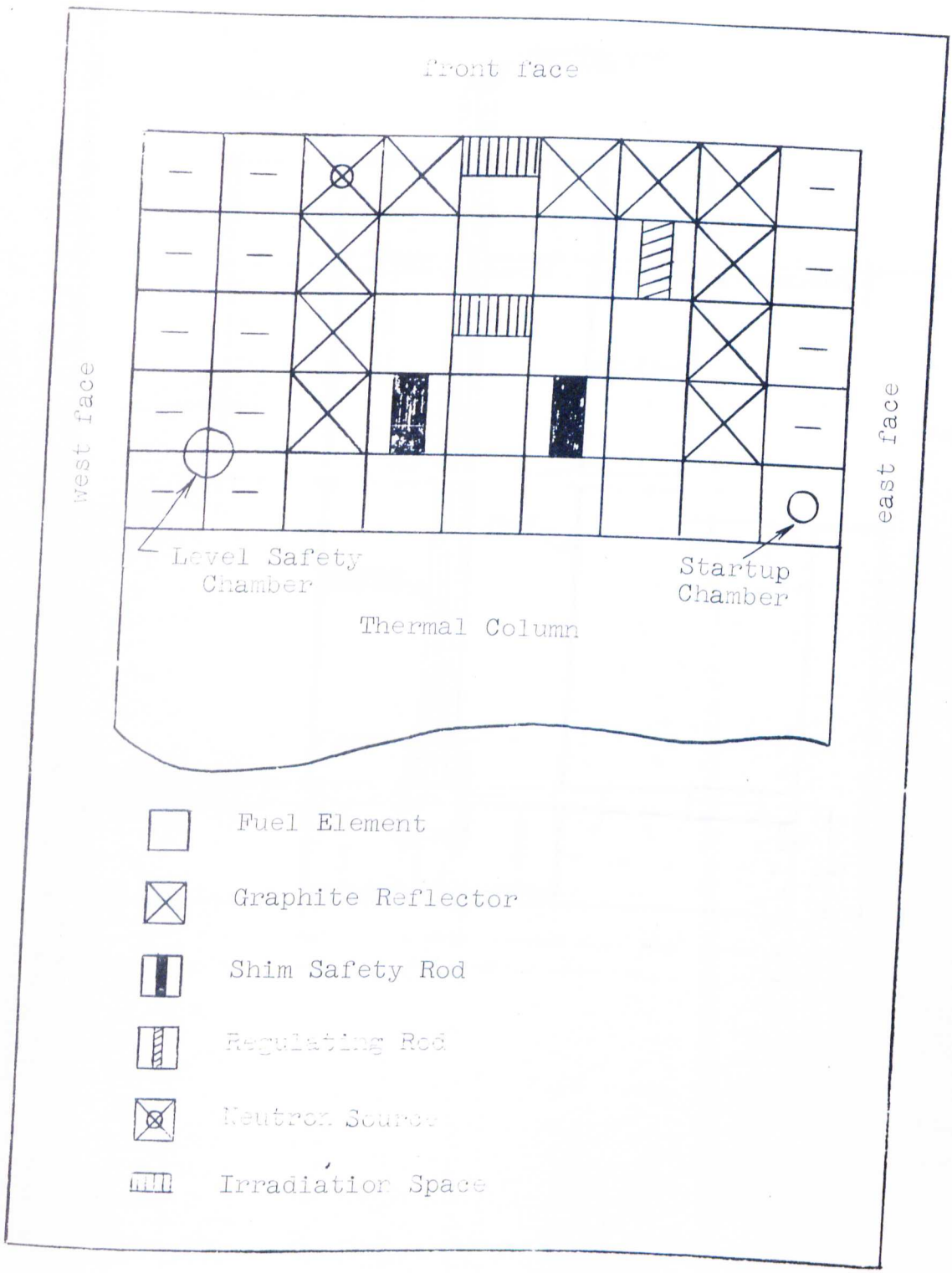

FIGURE 6
VERTICAL CROSS-SECTION OF THE UNIVERSITY OF MARYLAND REACTOR

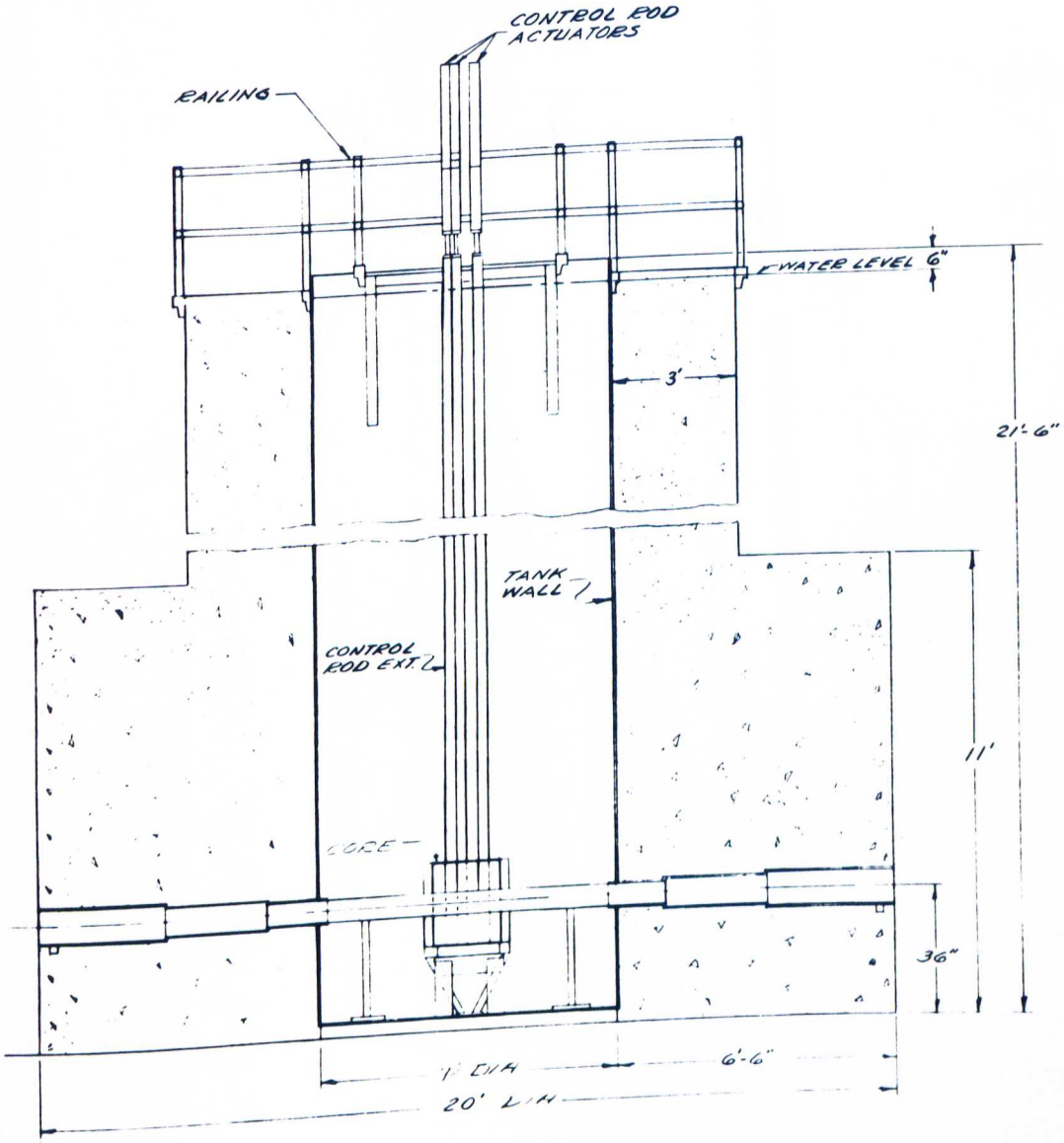

FIG. 7 TOP VIEW OF THE UNIVERSITY OF MARYLAND REACTOR CORE

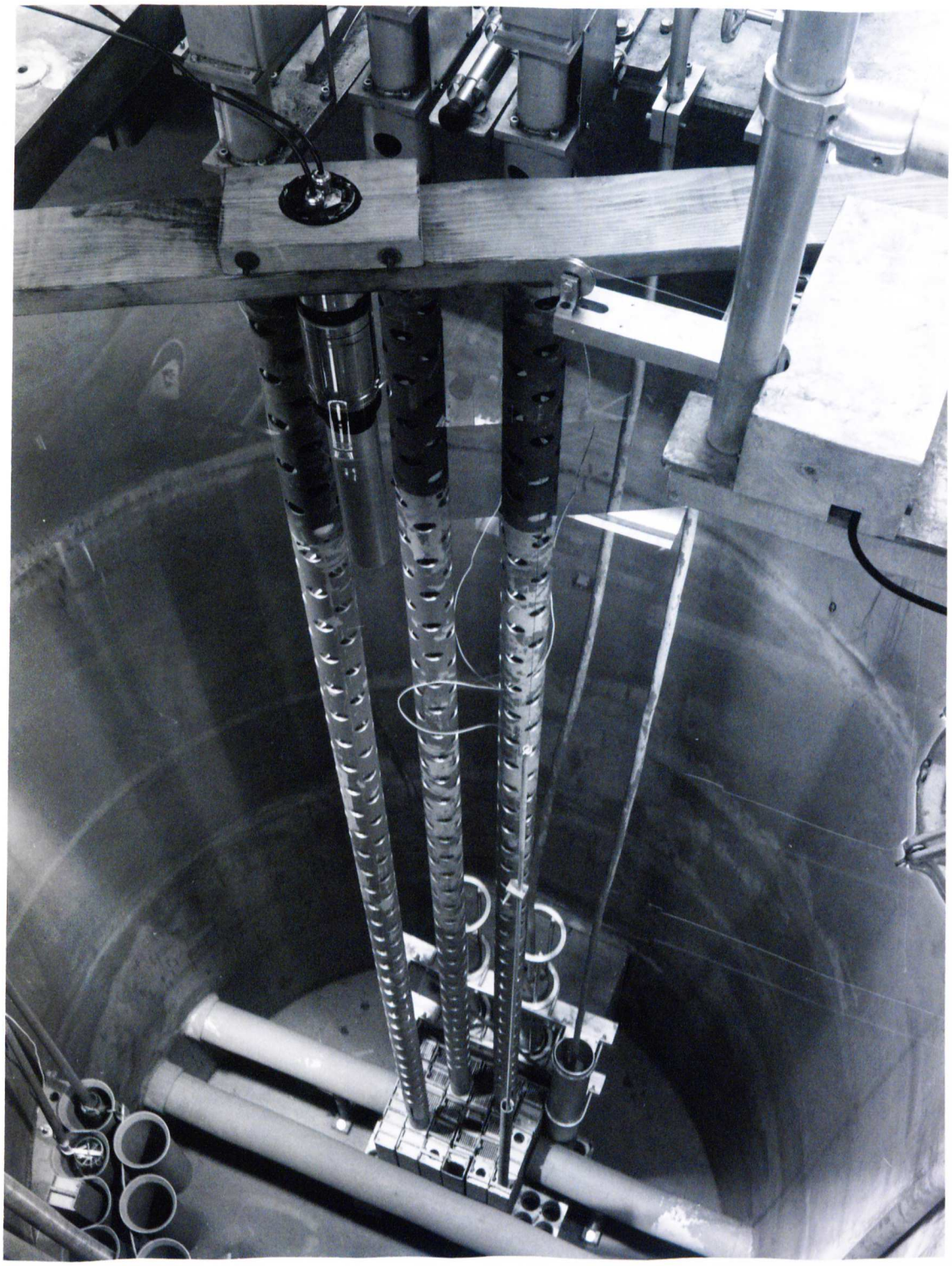

core. The interpretation of the measurements carried out on the light produced in the core indeed seems complex because of the absorption and attenuation of the light through the large depth of water and the numerous reflections on the aluminum which composes the structural components inside the tank and the fuel elements. Moreover, this method does not allow a simple analysis of the contribution of the different radiations on the emission of the light. However, it does not require ultrasensitive apparatus since the light intensity is quite strong for most measurements. In addition, protection of personnel from either gamma rays or neutrons is not required. The apparatus is easily mounted and disassembled and no problem arises as to activation of materials. Finally, measurements made on the whole core are relatively independent of geometry and control rod configuration.

Shown in Figure 8 is the photomultiplier tube which is mounted inside a cylindrical housing containing the voltage divider network. A 20 inch cylindrical aluminum tube, which fits over the photomultiplier and is attached to the main housing serves as a light collimator. The entire assembly consisting of photomultiplier tube, housing and collimator is suspended at the top of the pool directly over the core by means of a guide bar which is clamped to the edge of the tank as illustrated

FIG. 8 PHOTOMULTIPLIER DETECTOR ASSEMBLY

in Figure 7. When properly adjusted, the photomultiplier is in optical contact with the water in order to minimize reflection losses. The location of the detector assembly throughout the experiment series is insured by marking the tank for exact placement of the guide bar. During the final series of experiments the Cerenkov spectrum is observed through interference type filters which provide a convenient means of isolating specific spectral bands. Transmission type interference filters possess narrow pass bands and consequently transmit light of high spectral purity. Each filter consists of two highly reflecting but partially transmitting films with an interposing film of non-absorbing material. The separation of the two cover films determines the wavelength position of the pass band and hence the color of the light which the filter will transmit. The filters in each case are mounted atop of a metal shield which fits snugly over the photomultiplier and the entire assembly is mounted over the core as in earlier measurements.

Figure 9 illustrates the parameters which optically characterize interference filters, namely, the wavelength position, λ, of the peak of the pass band, the transmittance, T, at the peak of the pass band and the half-width HW. The half-width is convenient for expressing filter selectivity. It is defined as the spectral width of the pass band at the level where the transmittance is

Fig. 9 Pass Band Characteristics of Interference Filters

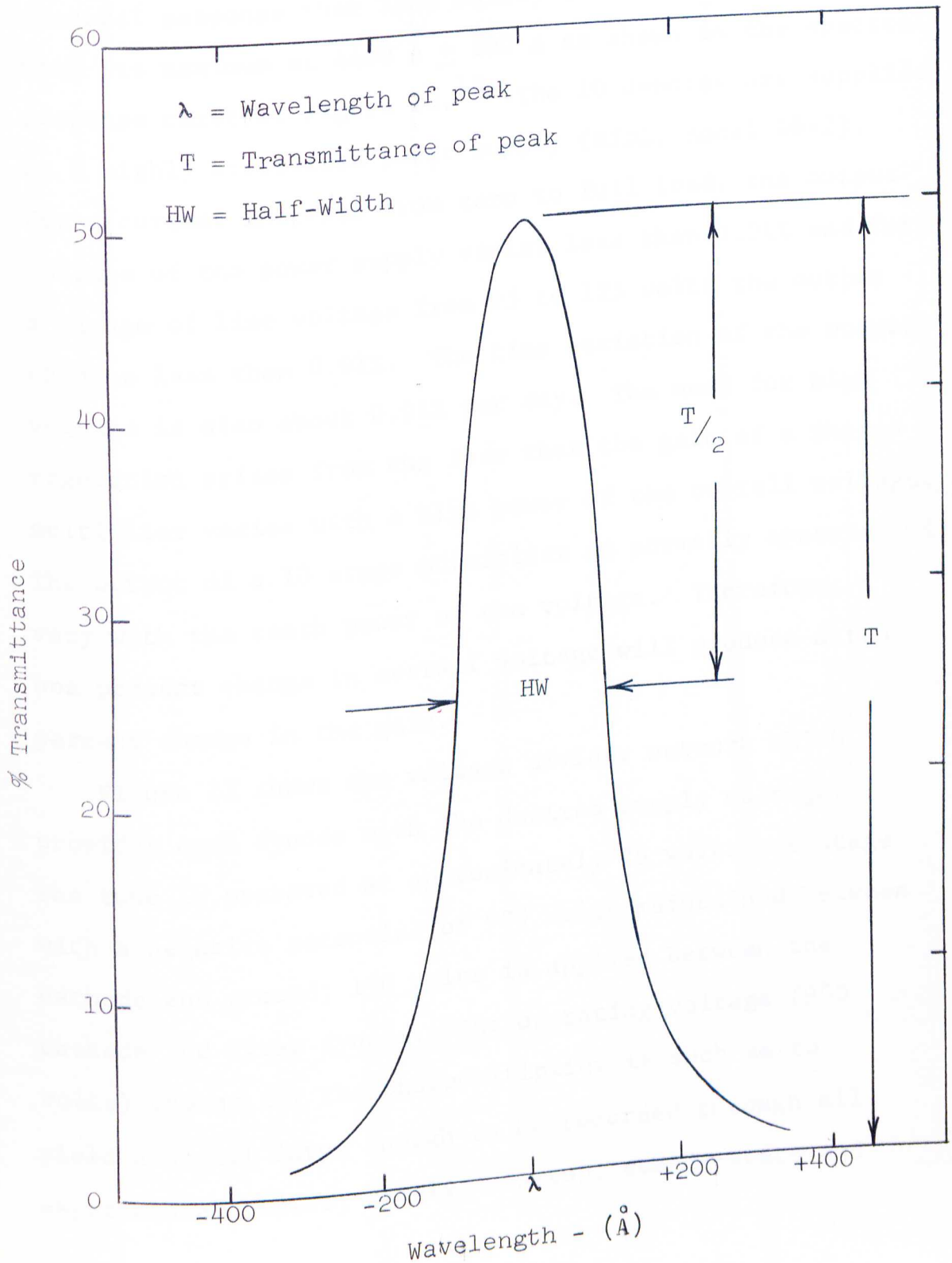

one half the peak transmittance.

The photomultiplier is a DuMont 6292, 10 stage device with a circular end-on photocathode having a spectral response that lies mainly in the visible region with its maximum at 4400 Å ± 500 Å as shown in the spectral response curve of Figure 10.[15] The 10 dynodes are supplied by a highly stabilized power supply (RIDL, Model 40-2). For a current increase from zero to full load, the output voltage of the power supply varies less than 0.01% and for a change of line voltage from 95 to 125 volts the output changes less than 0.01%. The time variation of the output voltage is also about 0.01% per day. The need for high regulation arises from the fact that the gain of a photo-multiplier varies with a high power of the overall voltage. The output of a 10 stage multiplier as normally operated will vary with the tenth power of the voltage. Therefore, a one percent change in overall voltage will produce a ten percent change in the gain.

Figure 11 shows the voltage divider network which provides each dynode with the desired supply voltage. The tube is operated at approximately 75 volts per stage with a negative potential of 900 volts maintained between cathode and ground; 150 volts is applied between the cathode and first dynode. The operating voltage (900 volts) chosen for the photomultiplier is such as to yield a signal large enough to be recorded through all experimental phases, namely, startup, steady-state and

Fig. 10 Photomultiplier Spectral Sensitivity

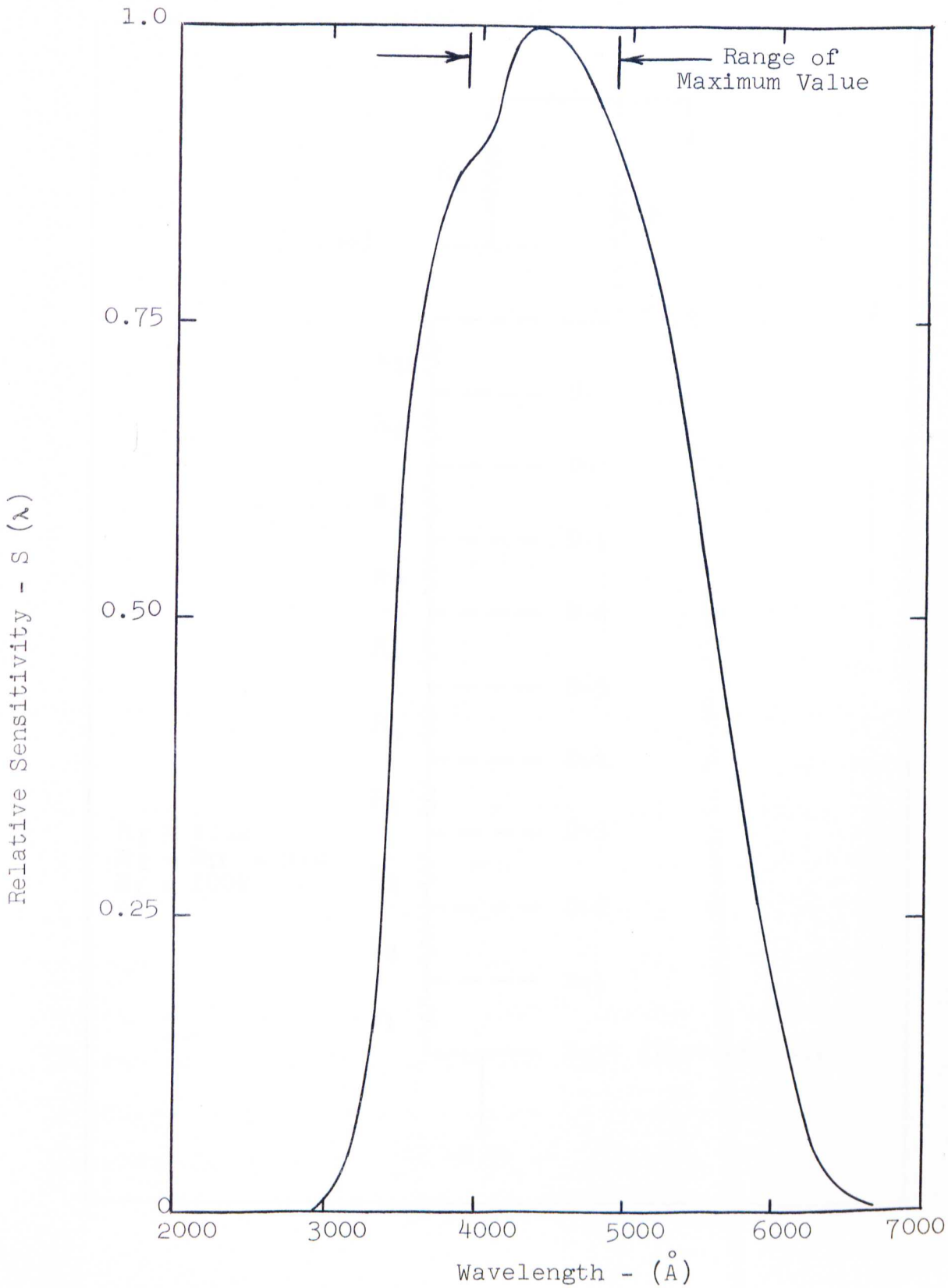

Fig. 11 Photomultiplier Bleeder Network

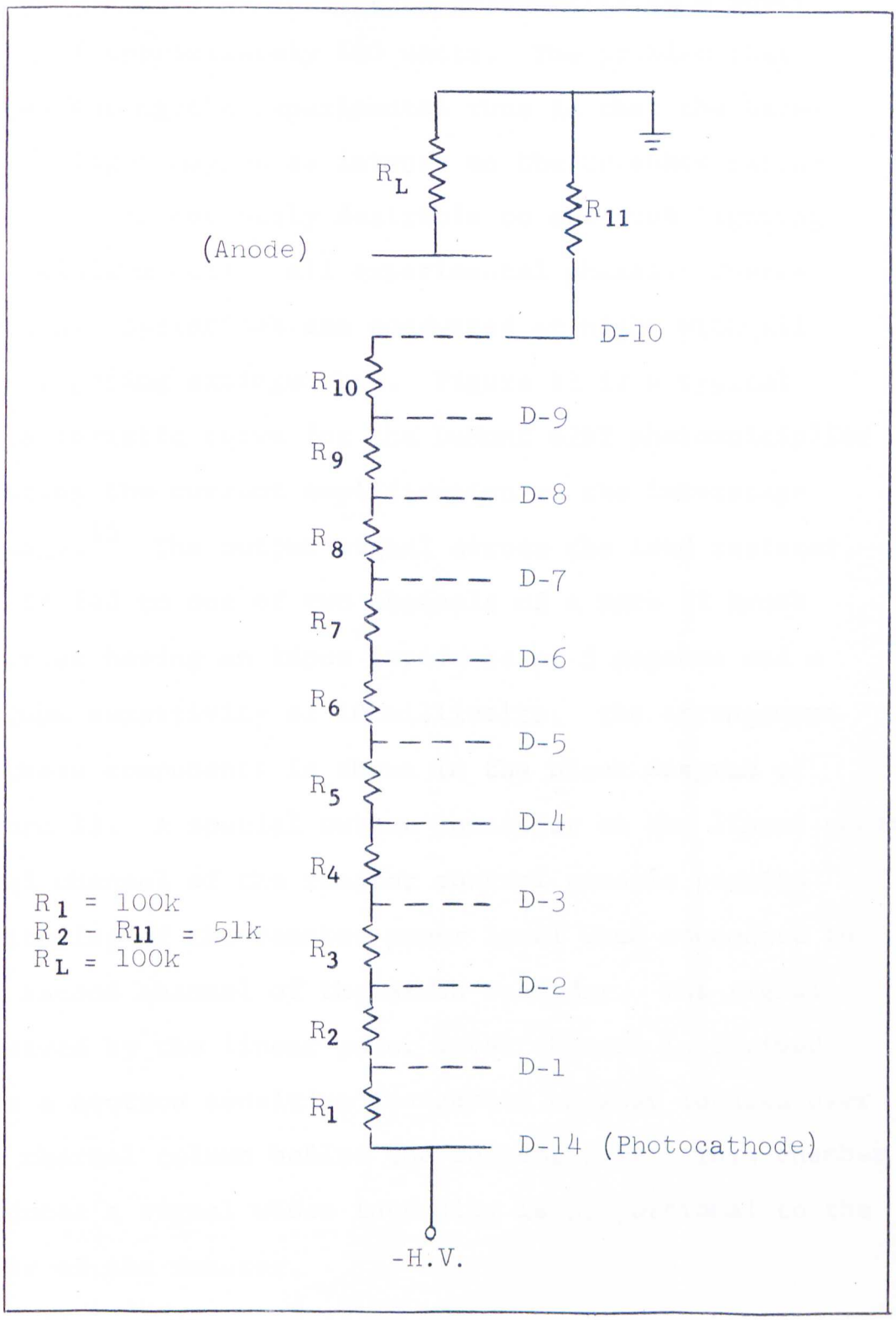

shutdown while still maintaining linearity between the incident radiation and the photoelectric current. The detector begins to respond satisfactorily at a power level of approximately 100 watts. The problem that arises during the experimental runs is that the background light may be as intense as the Cerenkov radiation. It is obviously desirable to cut room lighting to a minimum during all experimental phases. Therefore, all operations are conducted at night with all room lighting extinguished. Figure 12 is a typical characteristic curve for the DuMont 6292 photomultiplier relating the current amplification to the interstage voltage.[15] The output signal across the load resistor, R_L, is fed to one of two channels of a Mark II Brush recorder having an input impedance of 5 megohms and a maximum sensitivity of 10 millivolts. The arrangement of these components is shown in the block diagram of Figure 13. A special output connector on the linear power level channel of the reactor control console permits monitoring of the reactor power level when connected to the second channel of the Brush recorder. The signal received by the linear power level channel is derived from a neutron sensitive ionization chamber located over the thermal column behind the reactor core. This chamber produces a signal whose intensity is proportional to the power of the reactor.

Fig. 12 Average Photomultiplier Characteristic

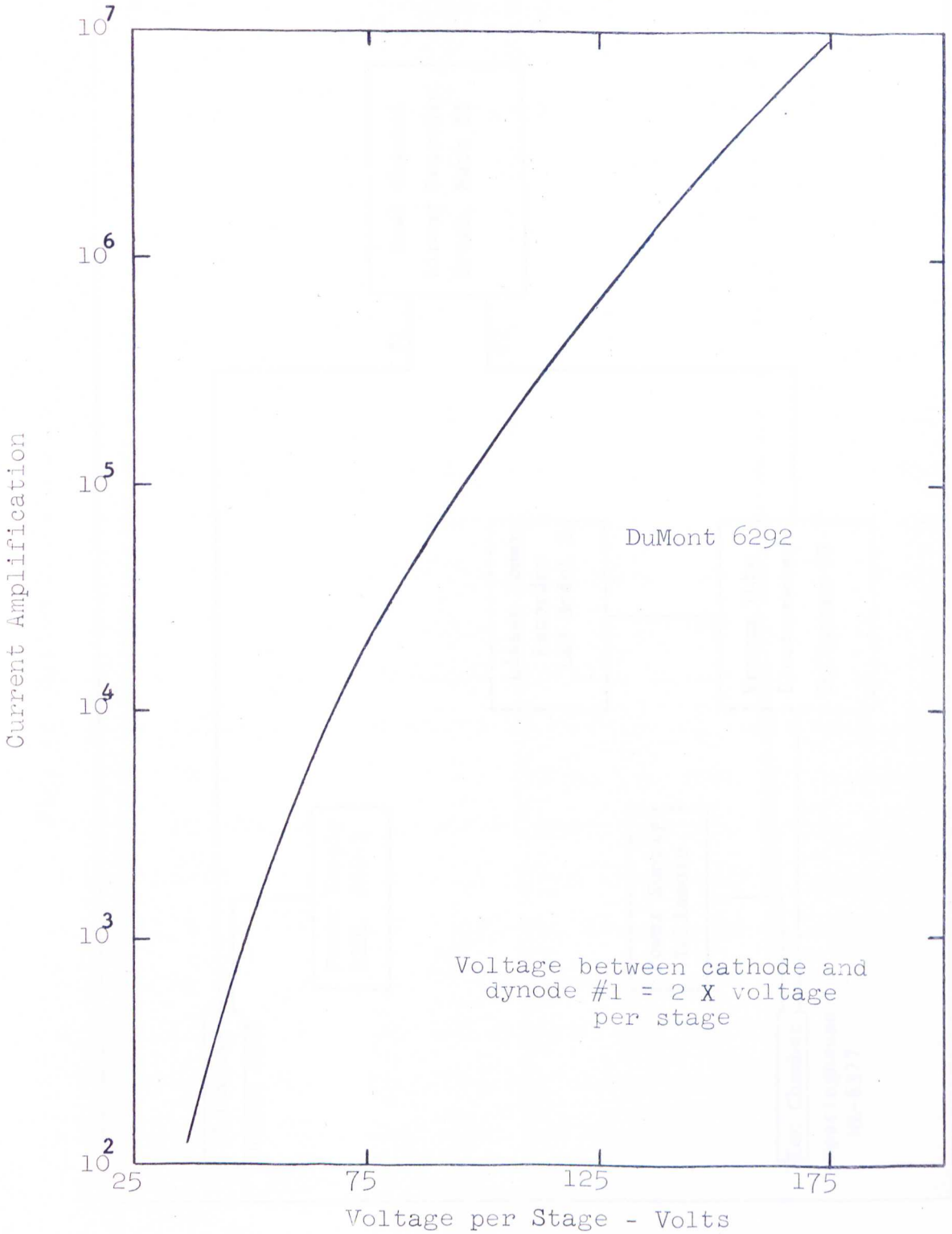

Fig. 13 System Block Diagram

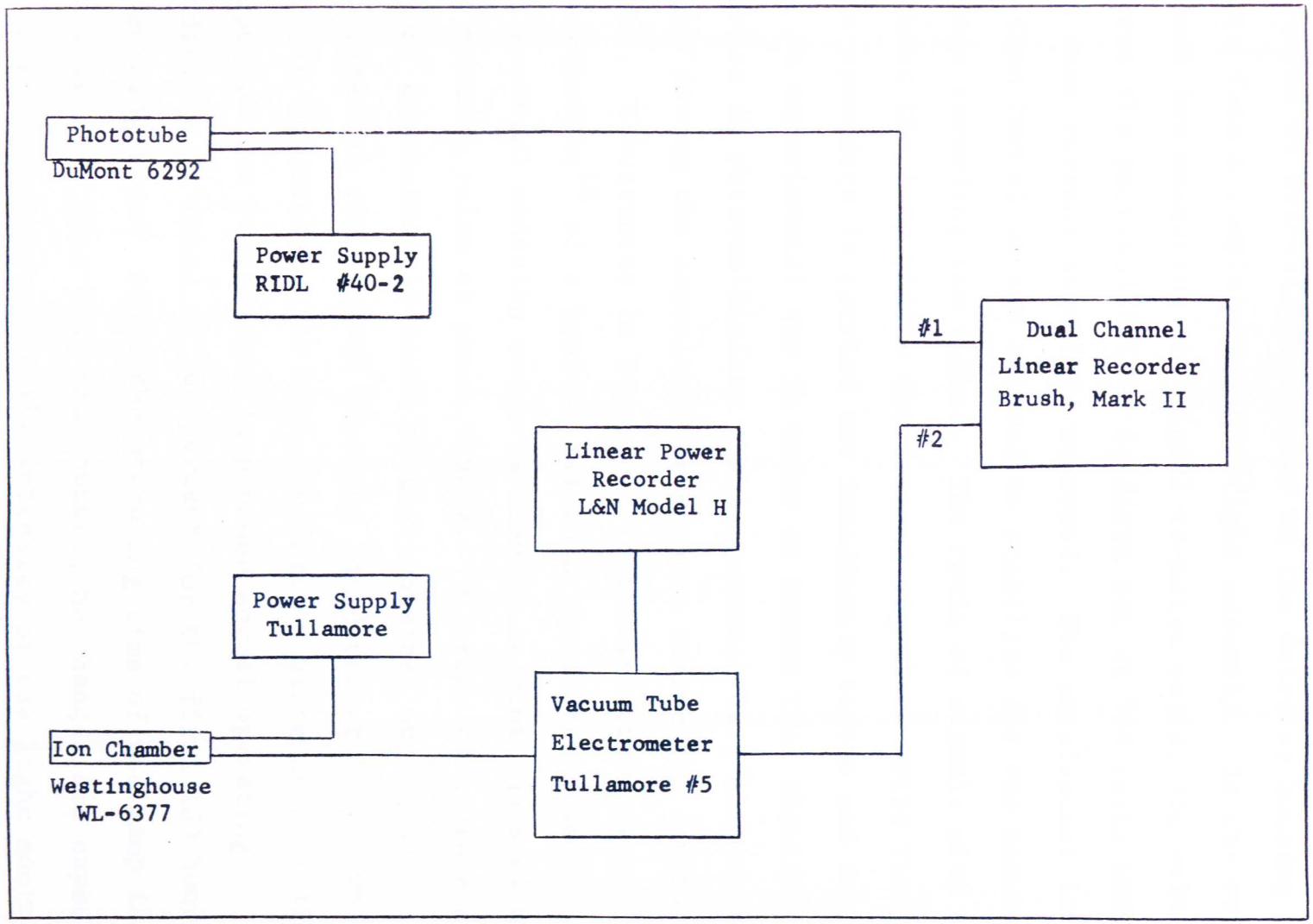

C. Detector Light Check Source

As a test source, a commercial panelescent lamp manufactured by Sylvania is coupled to the detector housing so as to form a completely light-tight assembly. In the procedure for measuring the signal-to-noise ratio, the voltage across the photomultiplier is first set at 900 volts and the dark current signal is measured. The panelescent lamp is then turned on and allowed to stabilize for one minute before recording the signal. The ratio of signals with and without the lamp yields the desired signal-to-noise ratio. This procedure is carried out immediately before and following an experimental run in order to insure that significant changes in photomultiplier characteristics have not taken place during the experiment or between succeeding experiments. Illustrated in Figure 14 is the spectral energy distribution[16] of a typical Sylvania panelescent lamp. The spectral emission curve is seen to be continuous with its maximum value at about 5100 Å. In order to achieve a signal approximately equal to that obtained during an experimental run without changing the detector supply voltage, it is necessary to mask the lamp. Maintenance of light output of the panelescent lamp under normal operating conditions is rated at 100 percent for the first 100 hours of burning time. Since the operating time of the lamp is significantly less than this number, no changes are expected and none are observed in the intensity of the light source.

Fig. 14 Spectral Energy Distribution of Typical Sylvania Panelescent Lamps at 60 cps.

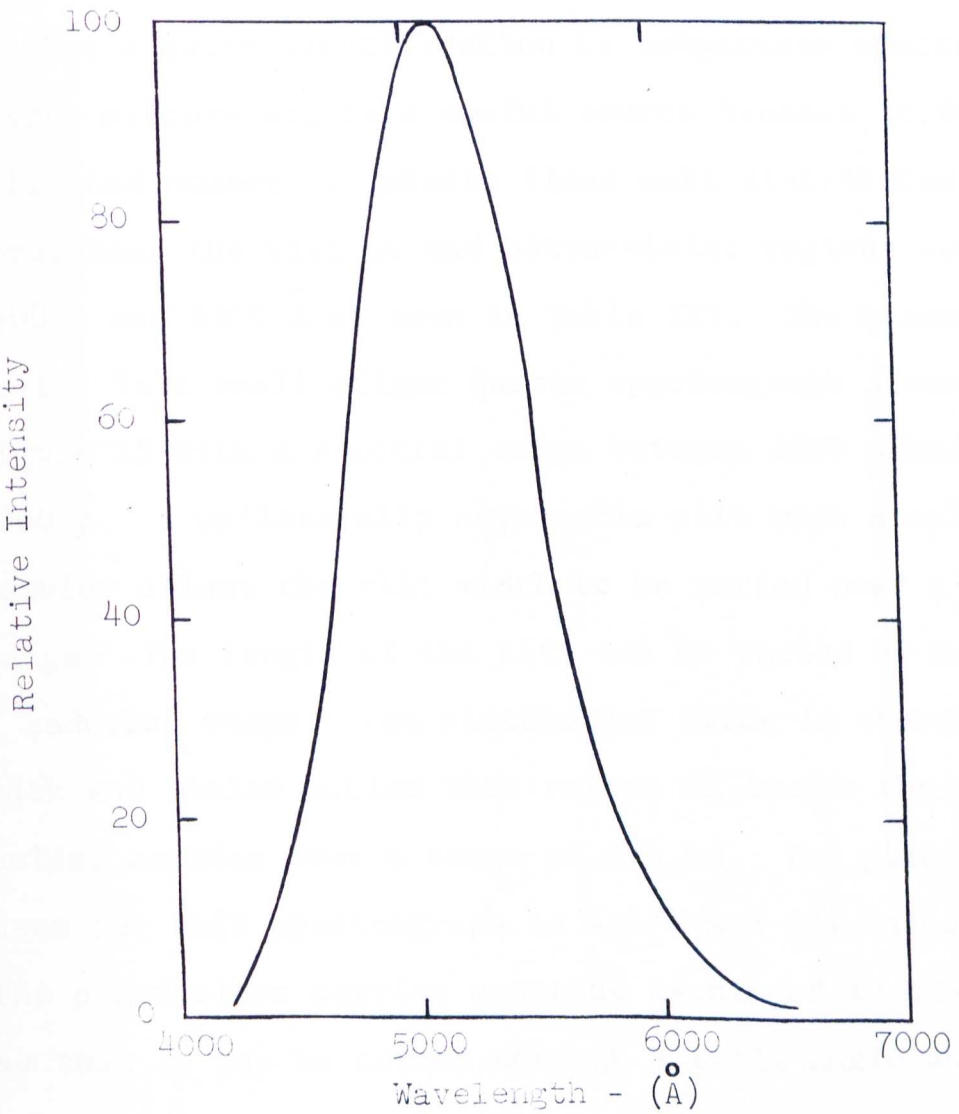

CHAPTER IV

SPECTROGRAPHIC STUDY OF THE LIGHT

The object of this study is to qualitatively determine the relative spectral distribution of the Cerenkov light as seen through approximately 16 feet of water and to compare this result with calculations in Appendix A.

For a quick identification by comparison spectra a quartz mercury arc is a useful source because it furnishes a limited number of intense lines well distributed throughout the visible and ultra-violet regions between 2300 Å and 6300 Å as seen in Table III. The measuring device is a small Hilger quartz spectrograph shown in Figure 15 with a spectral range between 1850 Å and 8000 Å. A unilaterally adjustable slit with a calibrated vernier allows the slit width to be varied over a wide range. The length of the slit can be varied by means of a reducing wedge. The plateholder slide is operated by a rack and pinion motion that raises or lowers the plate-holder carrier over a range of 6.5 cm. The plate size used for this spectrograph is 4-1/4 x 3-1/4 inches. The plateholder carrier mounting is hinged at the center so that it may be turned through a small angle about a vertical axis. Actual settings are read by counting the number of complete revolutions of the tilt screw from the minimum tilt position.

Prior to any measurement of the Cerenkov spectrum,

TABLE III

Groups of Mercury Lines Useful for Wavelength Identification[17]

Group	Color	Wavelengths (Å)	Approximate Intensity
1	Red	6234	10
		6152	20
2	Yellow	5790	50
		5770	50
3	Green	5461	100
4	Blue	4359-4348	20
5	Violet	4078	8
		4047	10
6	Ultraviolet	3663-3654-3650	70
7	Ultraviolet	3342	10
8	Ultraviolet	3132-3126	40
9	Ultraviolet	3026-3022	30
10	Ultraviolet	2967	10
11	Ultraviolet	2893	10
12	Ultraviolet	2804	20
13	Ultraviolet	2753	10
14	Ultraviolet	2652	8
15	Ultraviolet	2537	30
16	Ultraviolet	2482	5
17	Ultraviolet	2399-2378	3

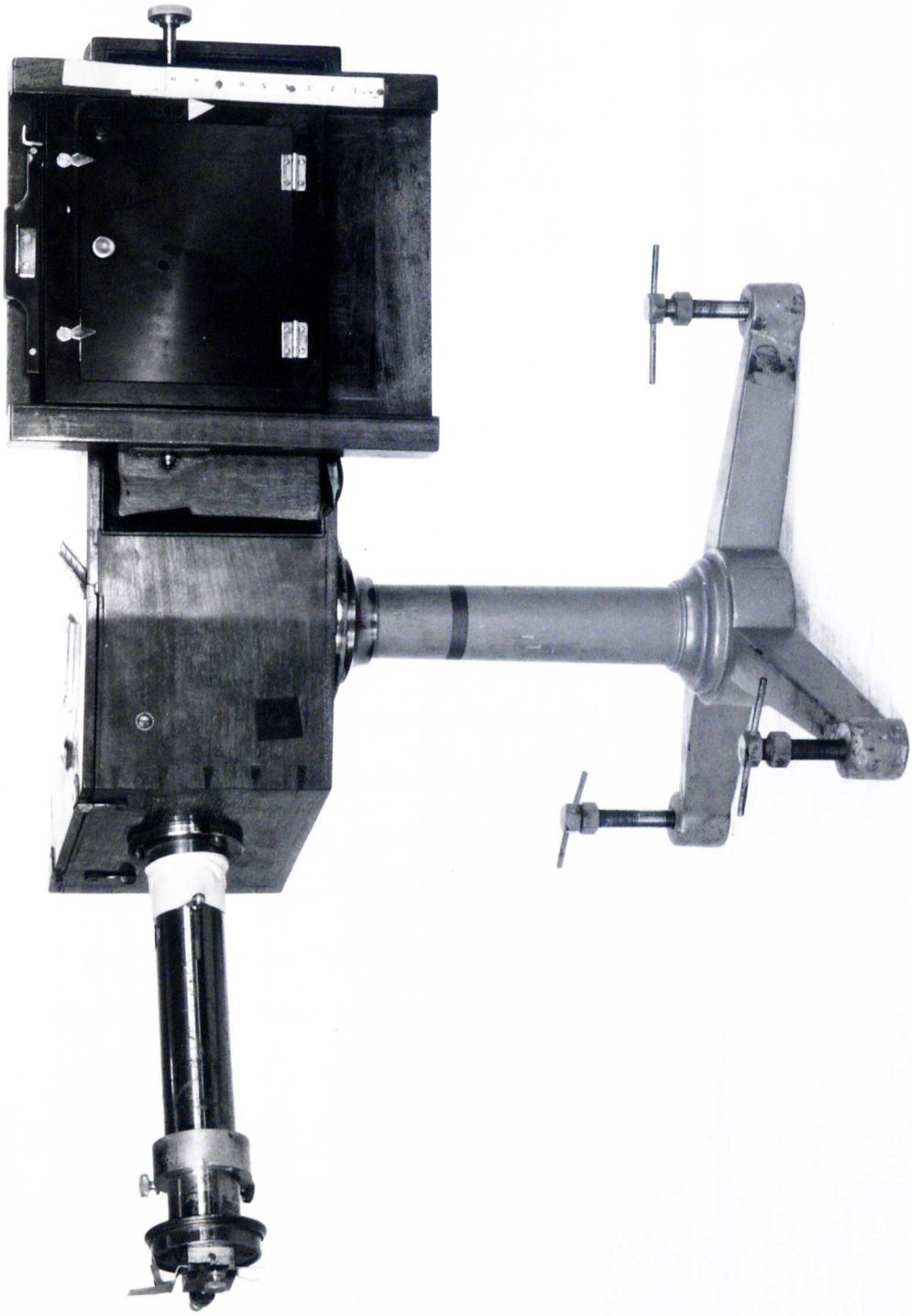

FIG. 15 HILGER QUARTZ SPECTROGRAPH

a series of test spectra for the mercury arc are photographed corresponding to variations in slit width, collimator setting and tilt. Slit openings vary from about 100 microns to full closure. During these exposures the full length of the slit is illuminated. The nominal optimum settings finally chosen which give the sharpest line images throughout the entire range are:

Slit setting:	8
Focus of collimating lens:	9
Tilt setting:	-7.5 (-22.5 is the arbitrary value denoting minimum tilt position)
Photographic plate exposure time:	3 seconds

The foregoing measurements are performed using Eastman Kodak, Type 103a-0, medium contrast photographic plates[18] having a sensitivity range between 2000 Å and 5500 Å as shown in Figure 16. Use of an emulsion of medium contrast gives a response which differentiates between weak and strong spectrum lines.

Measurement of the Cerenkov spectrum is performed by positioning the spectrograph on a support bar so that the collimator barrel looks directly down at the glory hole in the center of the reactor core (core configuration #2). Although spectrograms are taken while the reactor is at full power (10 kw), the light emitted from the core is relatively weak as compared to the mercury arc.

Fig. 16 Spectral Sensitivity (Kodak Spectroscopic Plate - Type 103a-0)

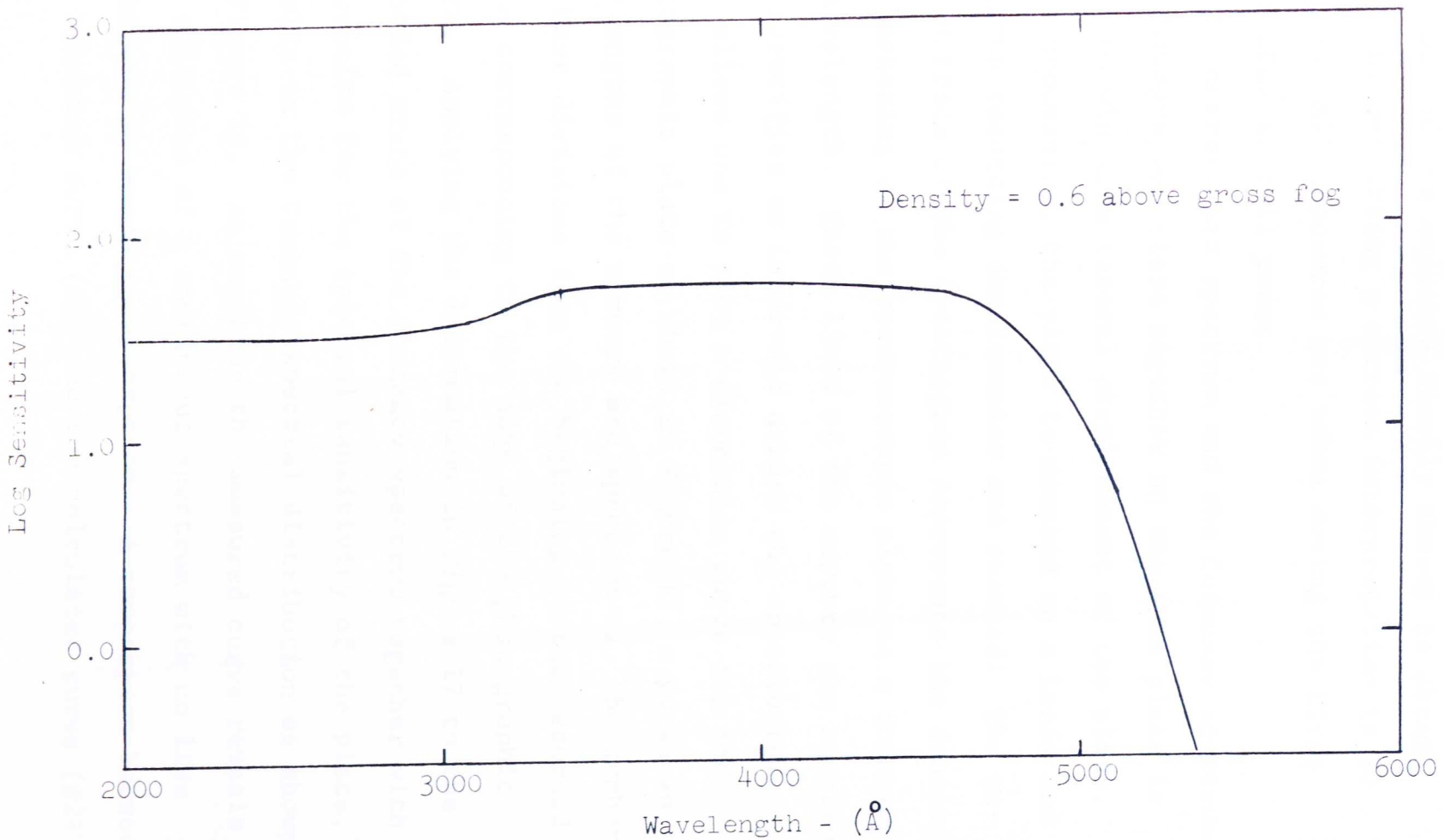

Consequently, three exposures for 2, 5, and 20 minutes are made and the exposure finally chosen to obtain a density permitting a correct interpretation is 20 minutes. All exposures are taken during the first 30 minutes at full power.

The mercury arc spectrum and the Cerenkov spectrum are photographed close together on the same plate in order to minimize lateral displacement of the plate. After processing, the plate is mounted on a Leeds and Northrup recording densitometer and scanned. The recorded trace of the spectrogram represents the density of blackening of the spectroscopic plate as a function of wavelength. Known lines of the mercury arc spectrum are identified at intervals across the spectrogram. This allows one to plot a dispersion curve for the photographic plate as shown in Figure 17, e.g. known wavelengths of the mercury arc spectrum vs. the number of chart divisions from the beginning of the recorded trace corresponding to the edge of the photographic plate. Applying the information in Figure 17 to the recorded trace of the Cerenkov spectrum together with a correction for the spectral sensitivity of the plate, results in the Cerenkov spectral distribution as shown in Figure 18. As expected the measured curve reveals the existence of a continuous spectrum with no line structure or bands of absorption. A comparison between the measured curve (#1) and the calculated curve (#2)

Fig. 17 Mercury Arc Spectrum Calibration Curve

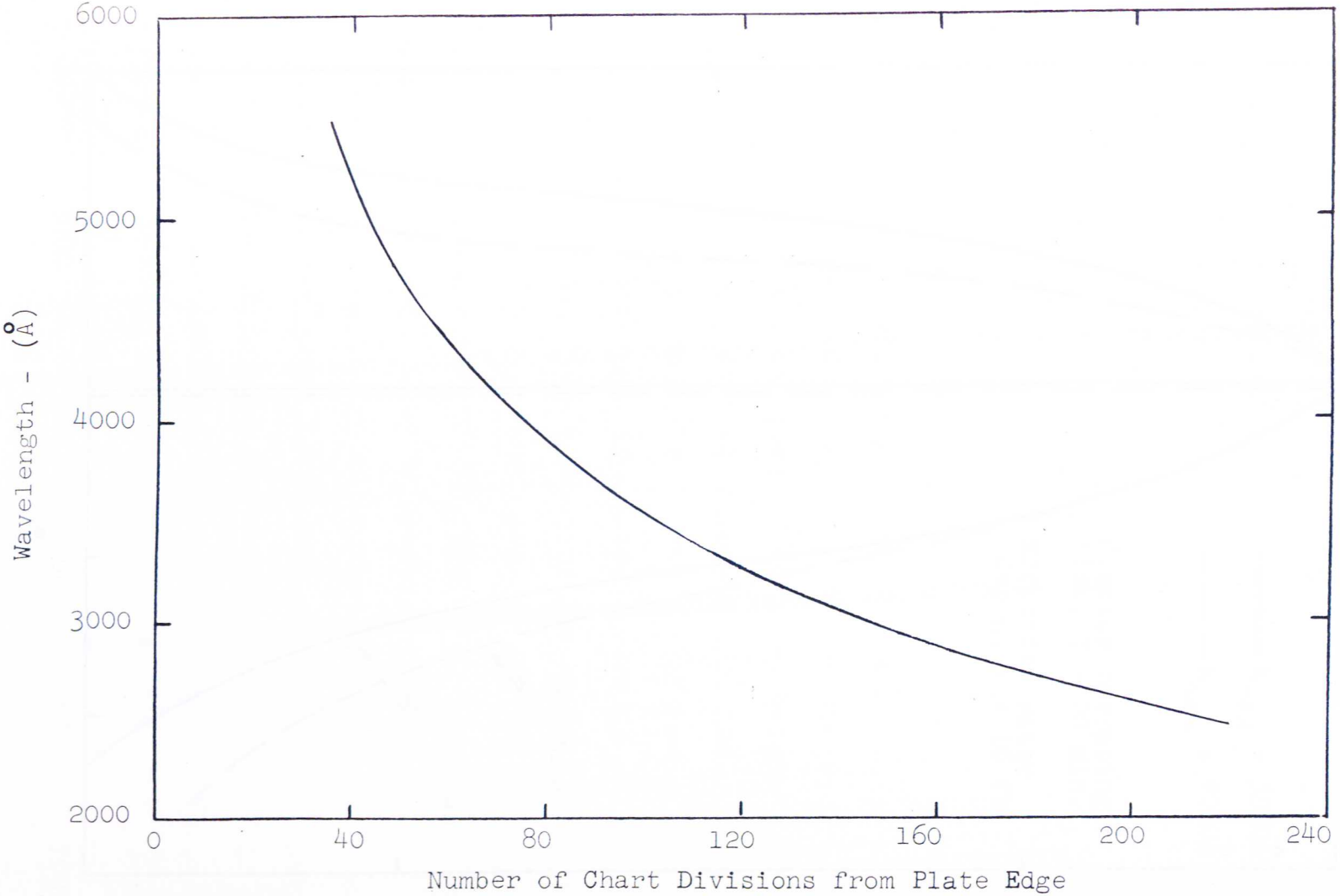

Fig. 18 Cerenkov Spectral Distribution

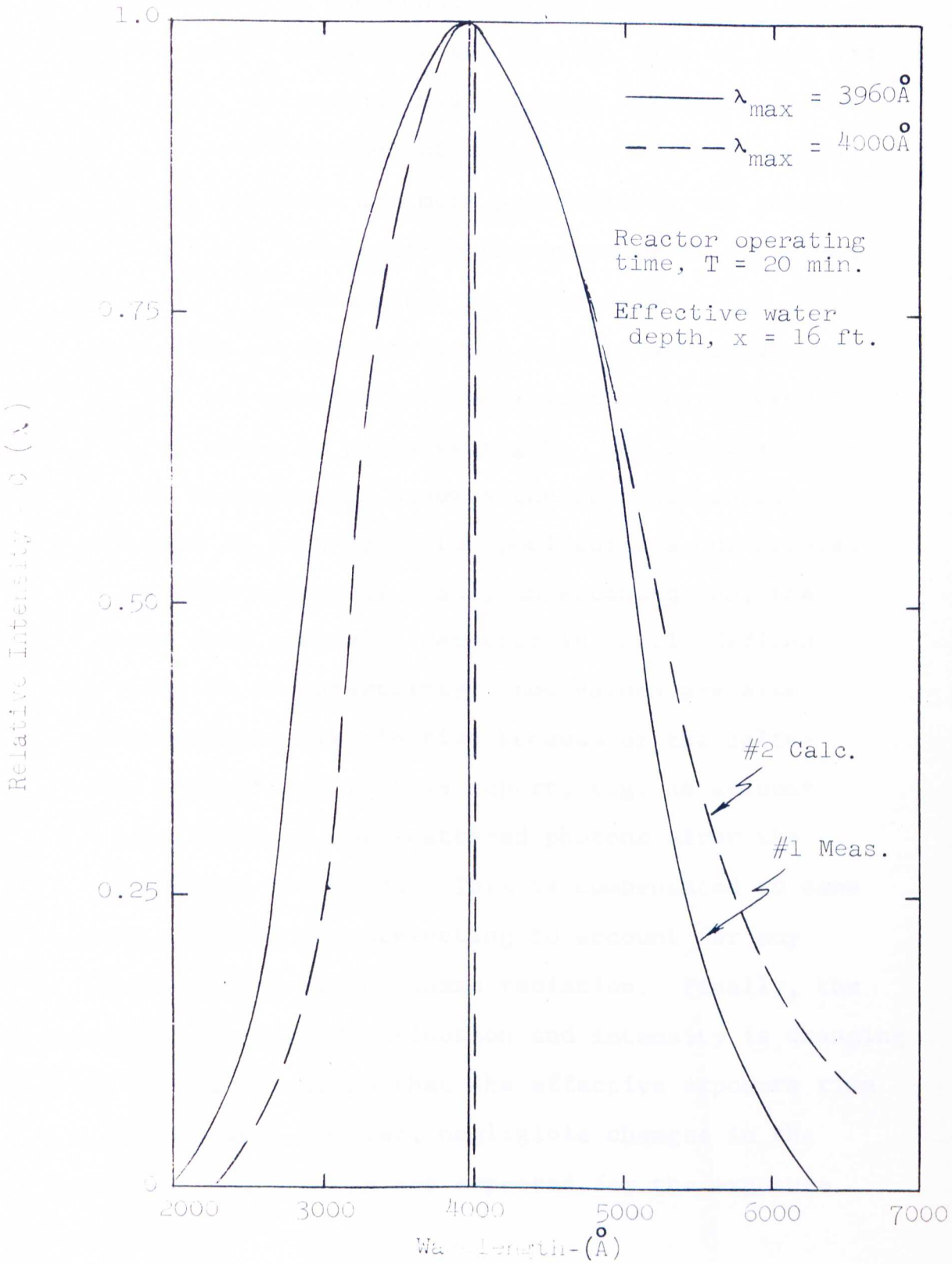

in Figure 18 for an operating time of 20 minutes shows fair agreement if one considers the assumptions and possible experimental errors, namely, lack of data and significant variations in absorption coefficients for distilled water throughout the entire spectral region under consideration and more particularly the region below 4000 Å. Furthermore, the presence of dissolved salts or of organic matter in water affects the transmission so that it is not safe to assume a value for the absorption coefficient of any given sample of water at any wavelength. The calculated spectral distribution assumes the Cerenkov source to be located 16 feet below the pool surface but because the Cerenkov source is really an extended one, the distance from source to detector is poorly defined and leads to an uncertainty. Low values are also expected in the distribution because of the calculation method used in this report, e.g. no account has been taken of the scattered photons after the first Compton collision. This is compensated to some extent, however, by neglecting to account for any self-absorption of the gamma radiation. Finally, the Cerenkov spectral distribution and intensity is changing with time which means that the effective exposure time is lengthened. However, negligible changes in the spectral distribution are expected for the exposure time used.

CHAPTER V

ANALYSIS OF THE LIGHT INTENSITY AS A FUNCTION OF REACTOR POWER

A. Introduction

To analyze the gamma emission rates of a reactor capable of producing Cerenkov radiation, it is necessary to examine the reactor operation cycles. Reactor operation may be divided into four phases with respect to power as shown in Figure 19. Phase one is the reactor state before startup where the power of the reactor is extremely low and is attributed mainly to the source multiplication and the delayed neutrons from previous operations. Phase two is the reactor startup period wherein the reactor rises to full power criticality. This is accomplished by adding reactivity to the system (e.g. removal of the shim and regulating rods). The interval designated as phase three is a period of constant power. Finally, phase four is the reactor shutdown period wherein the shim and regulating rods are inserted back into the core. The power curve for this latter interval is exponential in shape due to the gradual release of delayed neutrons. If delayed neutrons were not present, the power would drop as a function of rod movement to effectively zero power.

During all phases fission products are being

Fig. 19 Reactor Operational Phases; Power as a Function of Time

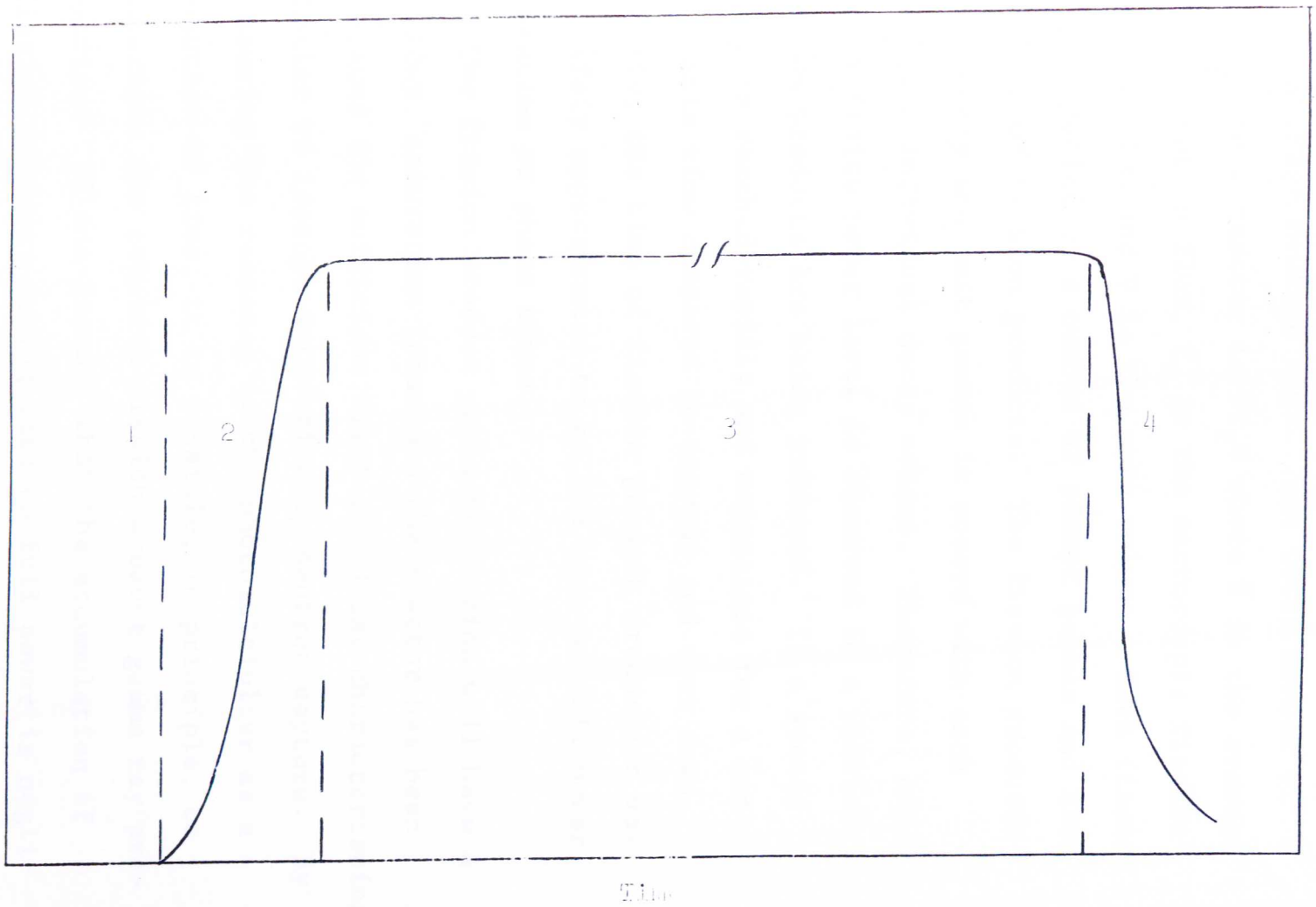

produced at a rate which is proportional to the power or the average neutron flux. The total number of fissions in a reactor is $\bar{\emptyset}\Sigma_f V$ where $\bar{\emptyset}$ is the average thermal neutron flux, Σ_f is the macroscopic fission cross-section and V is the core volume. Each fission is accompanied by a number of prompt gammas and also a number of fission products. The fission products later decay and emit gammas in accord with each product's individual decay scheme. Therefore, any time a finite power level is observed in a reactor, fission products are being produced. If a steady power is reached rapidly and maintained for a considerable time compared to startup and shut down quickly, the time of fission product production may be safely approximated to be the time of full power operation or phase three.

The fission product gamma production will have a buildup, saturation (provided the reactor has been operated for sufficient time) and decay characteristics similar to isotope activation by neutron capture. By measuring the response of the photomultiplier as a function of time, it is possible, in principle, to determine the relative fission product gamma ray production. If one assumes that the accumulation of fission products during rise to full power is negligible, the fission product gamma buildup during steady state reactor operation may be approximated by normalizing

curves of the Cerenkov light signal at the point full steady power is achieved. Similarly, the gamma decay after shutdown may be approximated by normalizing the Cerenkov light signal at the point where the reactor is shut down by rapid insertion of the control rods. Two factors which complicate the analysis, namely, the activation of the aluminum and its subsequent decay emitting both betas and gammas capable of producing Cerenkov light, and the delayed neutron contribution to the light signal immediately following shutdown, are considered in further detail in the analysis of the data.

B. Signal Response

1. Theoretical

Among the gamma rays emitted by the reactor, it is convenient to classify them into two categories:

(a) those which are emitted instantaneously and whose number is proportional to the power of the reactor

(b) those which are emitted in the course of radioactive product decay and whose number depends upon the integrated flux received by these products and their decay rates.

Referring to group (a), this is the case of the gamma rays emitted by the fissioning of the uranium, the inelastic collisions, and the radiative captures. They disappear when the reactor is shutdown. For group (b), these are the gamma rays emitted by the fission products

and by induced radioactivity in the core and structural materials and which have half lives ranging from seconds to years.

For the subsequent analysis, it is convenient to define the following terms:

V_o - the electrical signal produced by the compensated ion chamber

V_t - the electrical signal produced by the photomultiplier tube detecting the light emitted in the water in and around the reactor core.

V_p - the electrical signal proportional to the number of prompt fission gamma rays produced in the reactor and resulting in the fast electrons emitting the Cerenkov light in the water

V_c - the electrical signal proportional to the number of gamma rays produced by the radiative capture of the neutrons by the aluminum cladding, structural materials and the water moderator and causing the electrons to emit the Cerenkov light in the water

V_a^{Al} - the electrical signal proportional to the number of beta particles and gamma rays created through the activation of the aluminum cladding and structural materials

V_f - the electrical signal proportional to the number of gamma rays emitted in the process of fission product decay

V_t - the sum of four terms: $V_t = V_p + V_c + V_a^{Al} + V_f$

During an increase in the reactor power, the terms V_p and V_c increase exponentially with the same period as that corresponding to the increase in thermal neutron flux density throughout the reactor. The signal V_a^{Al} varies in a less apparent manner. Under the influence of the neutron flux irradiating the cladding and structural materials, the aluminum is activated and disintegrates by emitting beta particles having a maximum energy of 2.86 Mev and gamma rays of 1.80 Mev which are able to produce fast electrons.

Because of the complexity of the signal V_f, the following analysis is performed by assuming that the contribution of V_f to the total signal, V_t is negligible initially. Such an assumption is justified because it is found empirically that the fission product buildup is relatively slow.

If one assumes as a first approximation that each disintegration of the activated aluminum yields a beta particle capable of producing light, then

$$\frac{dN}{dt} = V\Sigma_a\emptyset - \lambda N \tag{5}$$

where N = the number of Al-28 nuclei

Σ_a = macroscopic cross-section of Al-27 for thermal neutrons

λ = decay constant of Al-28

$\emptyset$ = thermal neutron flux

V = volume of aluminum in the core

Hence

$$N = V\Sigma_a e^{-\lambda t} \int \phi e^{\lambda t} dt \tag{6}$$

The number of beta particles created per second is equal to

$$N' = \lambda V\Sigma_a e^{-\lambda t} \int \phi e^{\lambda t} dt \tag{7}$$

where $N' = \lambda N$. During an excursion of the reactor, the neutron flux varies according to the expression

$$\phi = \phi_o e^{\alpha t} \tag{8}$$

ϕ_o being the initial value of the flux and $\alpha = \frac{1}{\omega}$, where ω is the reactor period defined as the time required for the neutron flux to change by a factor e = 2.718. The expression in equation (7) then becomes

$$N' = V\Sigma_a \lambda \phi_o e^{-\lambda t} \int e^{(\alpha + \lambda)t} dt \tag{9}$$

Integrating equation (9) yields the following

$$N' = V\Sigma_a \lambda \phi_o e^{-\lambda t} \left[\frac{e^{(\alpha + \lambda)t}}{\alpha + \lambda} + C_1 \right] \tag{10}$$

The integration constant C_1 is evaluated by imposing the initial condition at t = 0, namely

$$N' = V\Sigma_a \phi_o \tag{11}$$

Hence

$$C_1 = \frac{\alpha}{\lambda(\alpha + \lambda)} \tag{12}$$

Substituting the expression for C_1 into equation (10) and simplifying gives

$$N' = \frac{V\Sigma_a\emptyset_o}{\alpha + \lambda}\left[\lambda e^{\alpha t} + \alpha e^{-\lambda t}\right] \tag{13}$$

For aluminum $\lambda = 4.95 \times 10^{-3}$ sec $^{-1}$ and the above expression rapidly approaches

$$N' = \frac{V\Sigma_a\emptyset_o\lambda e^{\alpha t}}{\alpha + \lambda} \tag{14}$$

Therefore

$$V_a^{Al} \backsim N = ke^{\alpha t} \tag{15}$$

where k is a proportionality constant. For a reactor excursion on a period:

$$V_t(t) = Ke^{\alpha t} \tag{16}$$

The signal produced by the photomultiplier and consequently the number of photons produced by the Cerenkov effect increases exponentially as a function of time with a period equal to that of the reactor. The signal produced by an ionization chamber indicates thermal neutrons just as the photomultiplier detects the light intensity produced by the Cerenkov effect. In both cases the signal is exponential and has the same

period.

When the reactor is stabilized at a power P_o, the term V_a^{Al} rapidly arrives at a state of equilibrium while the signal V_f due to the fission product gamma rays continues to increase slowly as a function of the integrated flux received by the uranium fuel. The term V_t, consequently, depends upon the previous history of the reactor so that V_t is not strictly proportional to the power of the reactor. The proportionality between the signal V_t and the power of the reactor is, therefore, valid only during an excursion of the reactor. In effect, the number of fission product gamma rays does not appreciably increase in time during a rise in power, whereas, on the contrary, the number of instantaneous gamma rays increase exponentially. If, after operation at a stable power P_o for a time t_o, the reactor is first shut down for a time interval $t_1 - t_o$ and then the power is increased to $2P_o$, the value of the signal V_t depends upon the time interval $t_1 - t_o$, corresponding to a decrease in fission products formed during the previous run, as shown in Figure 20.

When the control rods are dropped, the power decreases very rapidly from the value P_o, corresponding to a state of stable power, to a considerably lower power level associated with the delayed neutrons. The terms V_p and V_c which are proportional to the number of instantaneous gamma rays present in the reactor decreases rapidly during

Fig. 20 Delayed Gamma Effect on Cerenkov Signal Response for a Shift in Reactor Power

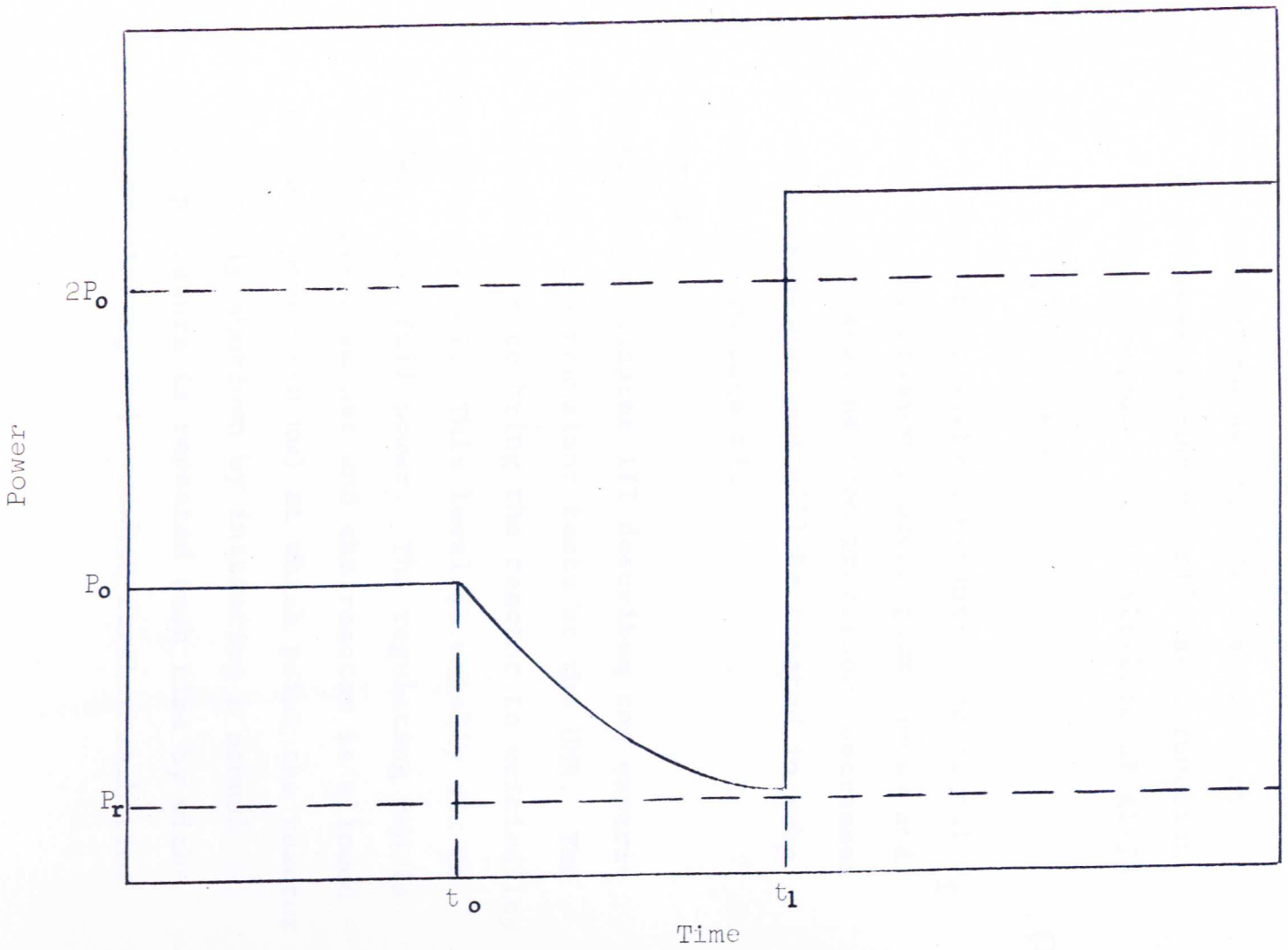

the time corresponding to the drop of the rods. The subsequent decrease in gamma ray intensity is much more slow. This decrease corresponds to the decay of the fission product gamma rays, the decay of the delayed neutron precursors and the decay activities of the aluminum which are formed during the operation at power P_o. V_a^{Al} decreases exponentially as a function of time with a period equal to the half-life of Al-28

$$V_a^{Al}(t) = k'e^{-\lambda t} \tag{17}$$

where k' is a proportionality constant. The signal V_f corresponding to the fission product gamma decay and the decay of the delayed neutron precursors decreases in a more complex manner and will be treated in subsequent paragraphs on page 81.

2. Experimental

a. Transient - Chapter III describes the experimental setup for the transient tests at the UMR. The general procedure is to bring the reactor to criticality at a lower power level. This level is usually six to seven decades below full power. The regulating rod is then removed a fixed amount and the reactor is allowed to rise to full power (10 kw) at which point the reactor is instantaneously shutdown by initiating a manual scram. This procedure is repeated each time by withdrawing the regulating rod somewhat further each time

until the reactor period becomes undesirably short, say 20 seconds. Each time the period is observed on the console period recorder and also by timing the movement of the Brush recorder galvanometer deflection over a decade. Examination of the experimental curves for variations of the signal as a function of time justifies equation (16). In the course of a divergence, the curves of Figures 21 through 26 show that signal V_t follows the neutron signal recorded by the ion chamber for periods as short as 20 seconds. For longer periods the effects of Al-28 activation and fission product buildup is evident from the steeper slope of the curves. The data are summarized in Table IV.

These results are augmented by a series of tests performed in a General Atomics TRIGA Mark F reactor designed for pulsing. Parameters which are measured to determine the pulse characteristics are the peak power and the pulse width at half maximum. The transient behavior of the reactor is monitored using the same photomultiplier tube as in previous tests on the UMR. The Cerenkov detector is positioned about 18 inches above the surface of the pool overlooking the core. A collimator, attached to the photomultiplier assembly to minimize background light, extends down to within 2 inches of the pool surface. The first step in performing the transient

Fig. 21 Cerenkov Signal vs Neutron Power Level

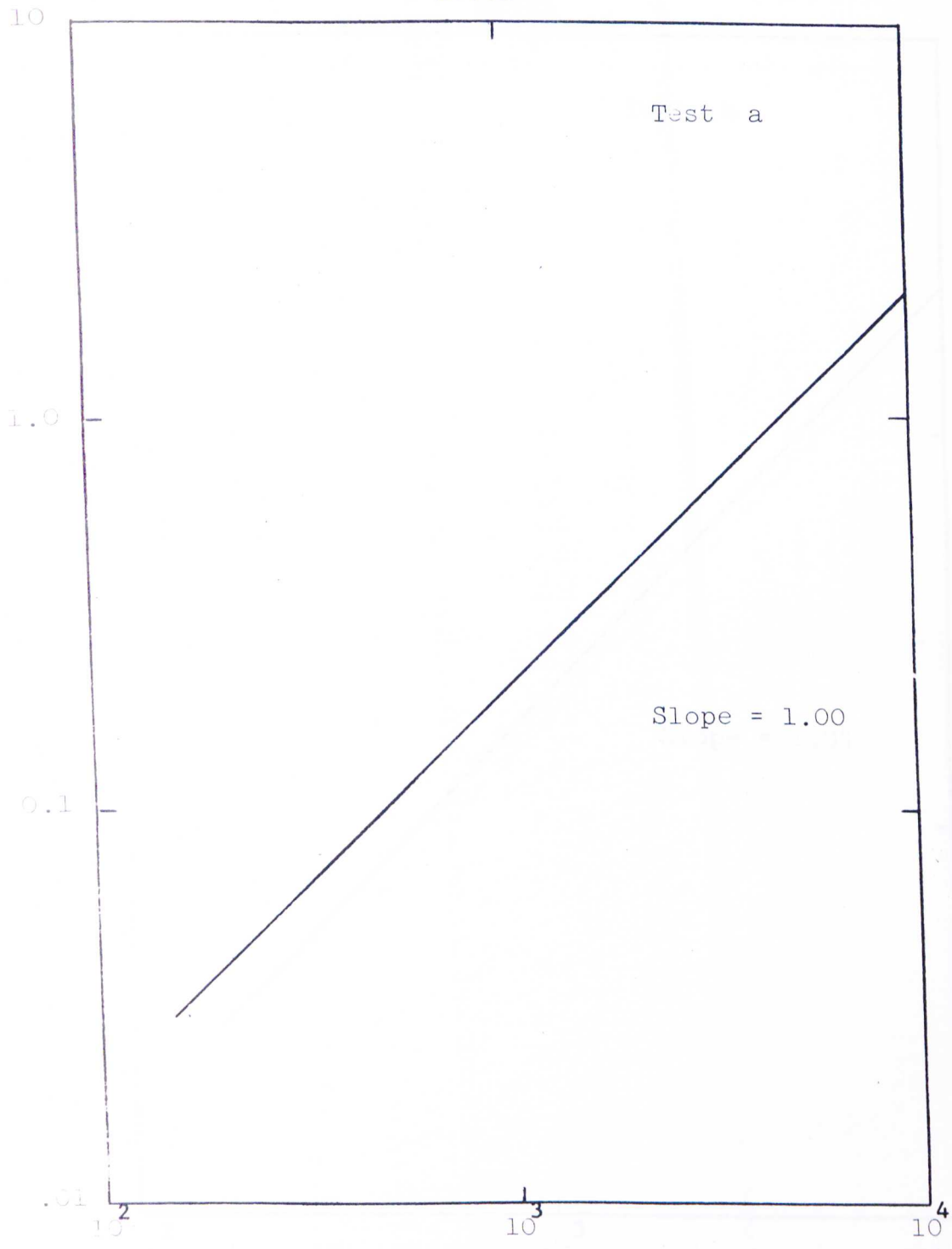

Fig. 22 Cerenkov Signal vs Neutron Power Level

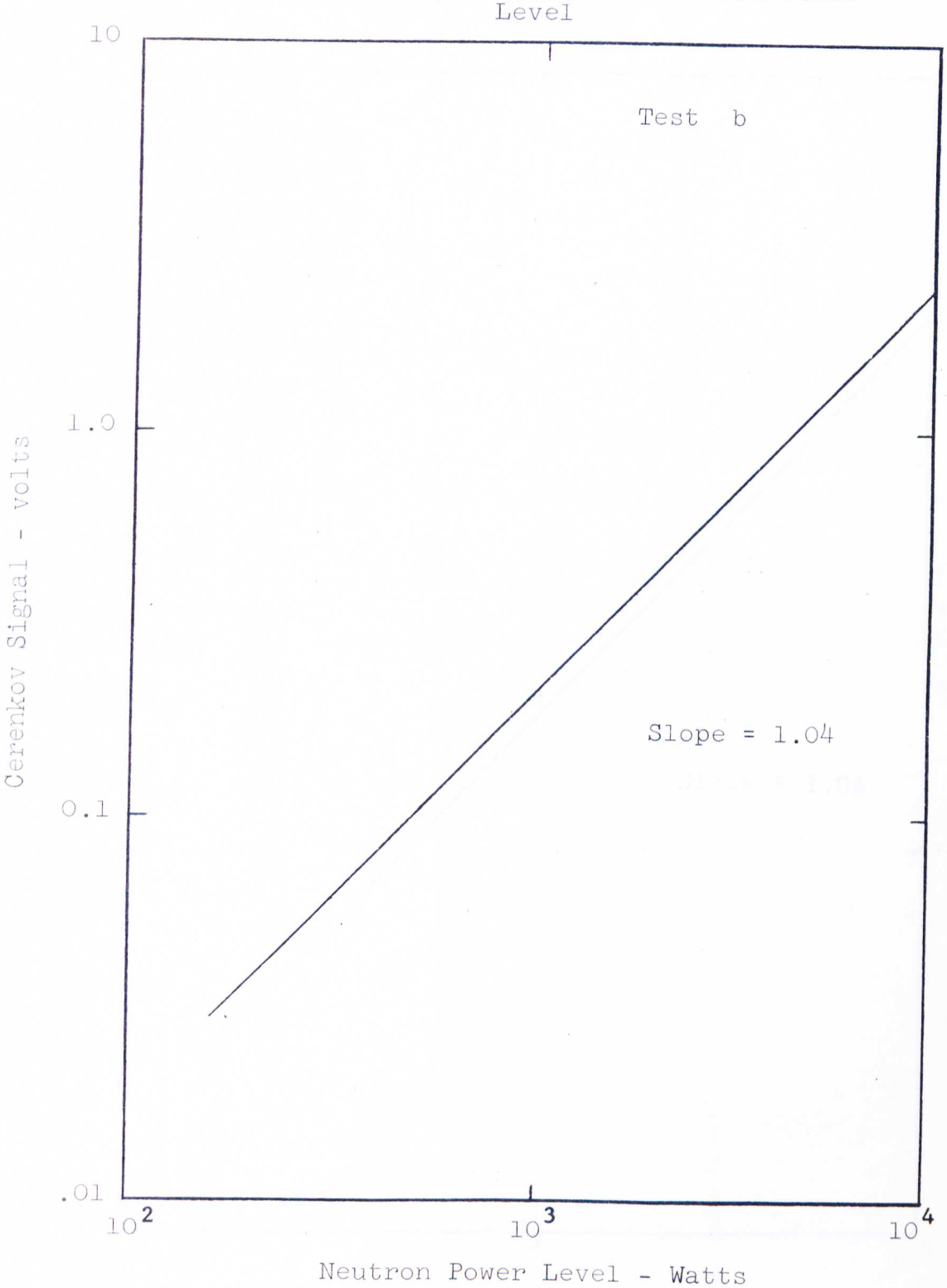

Fig. 23 Cerenkov Signal vs Neutron Power Level

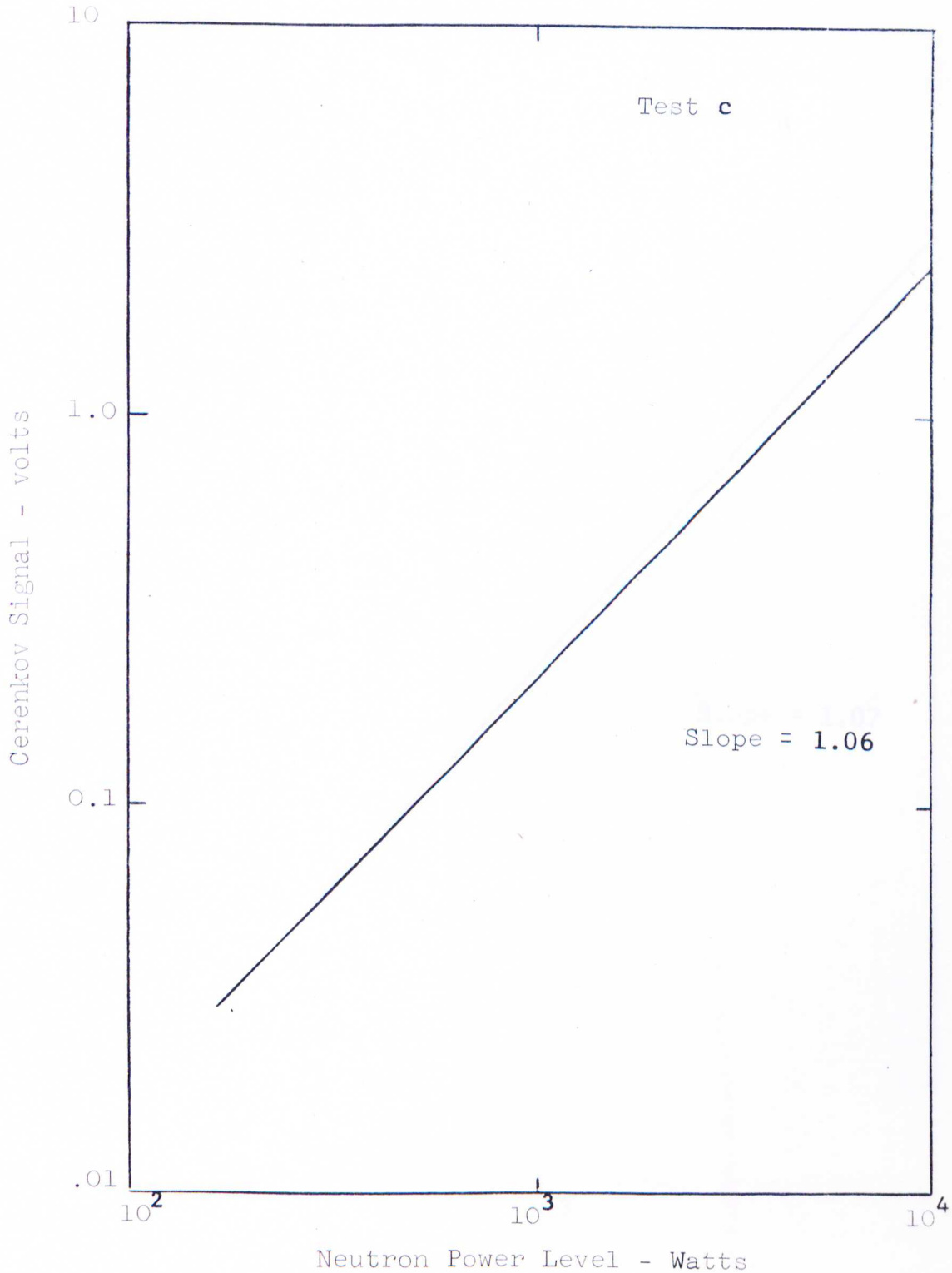

Fig. 24 Cerenkov Signal vs Neutron Power Level

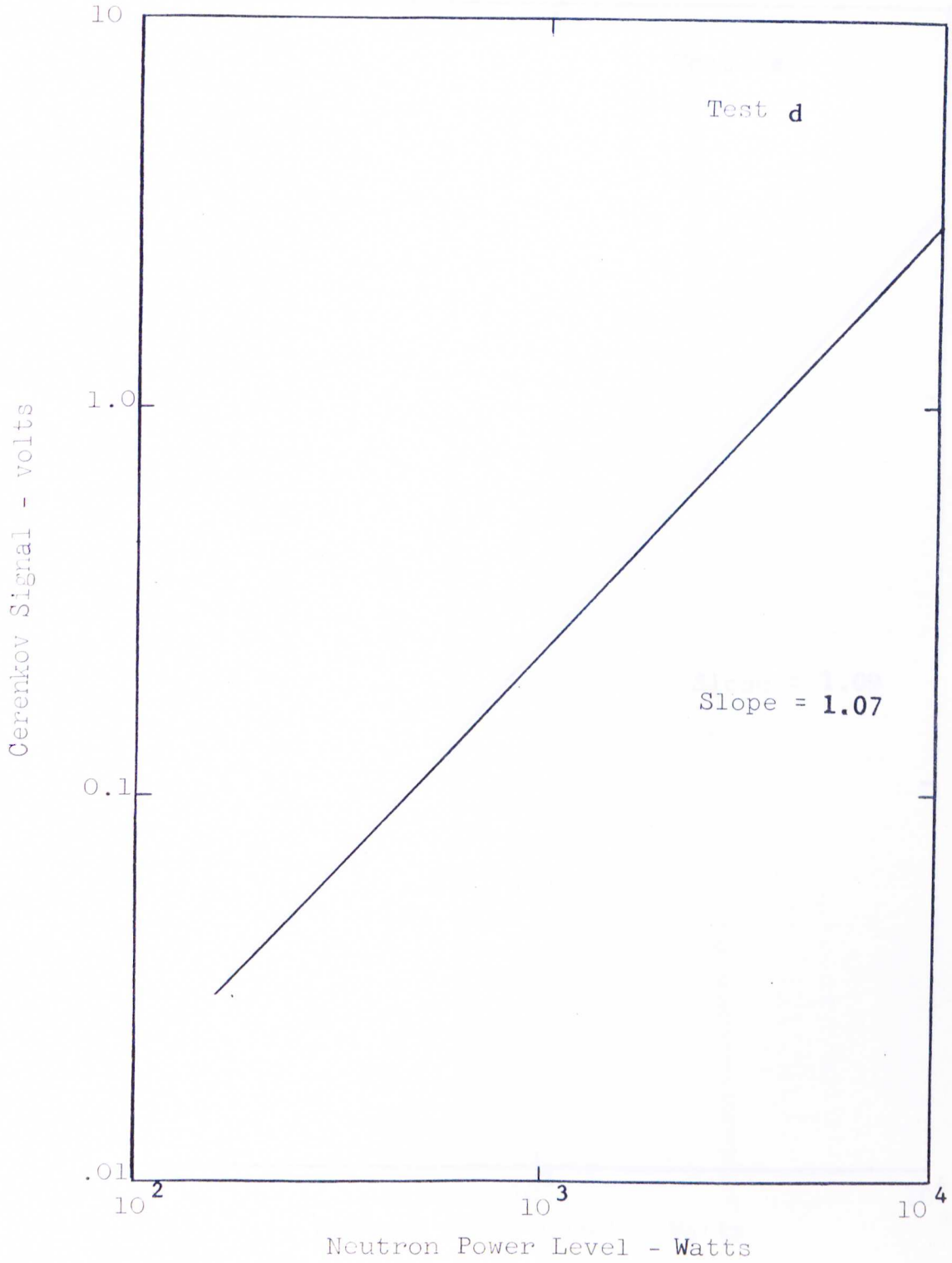

Fig. 25 Cerenkov Signal vs Neutron Power Level

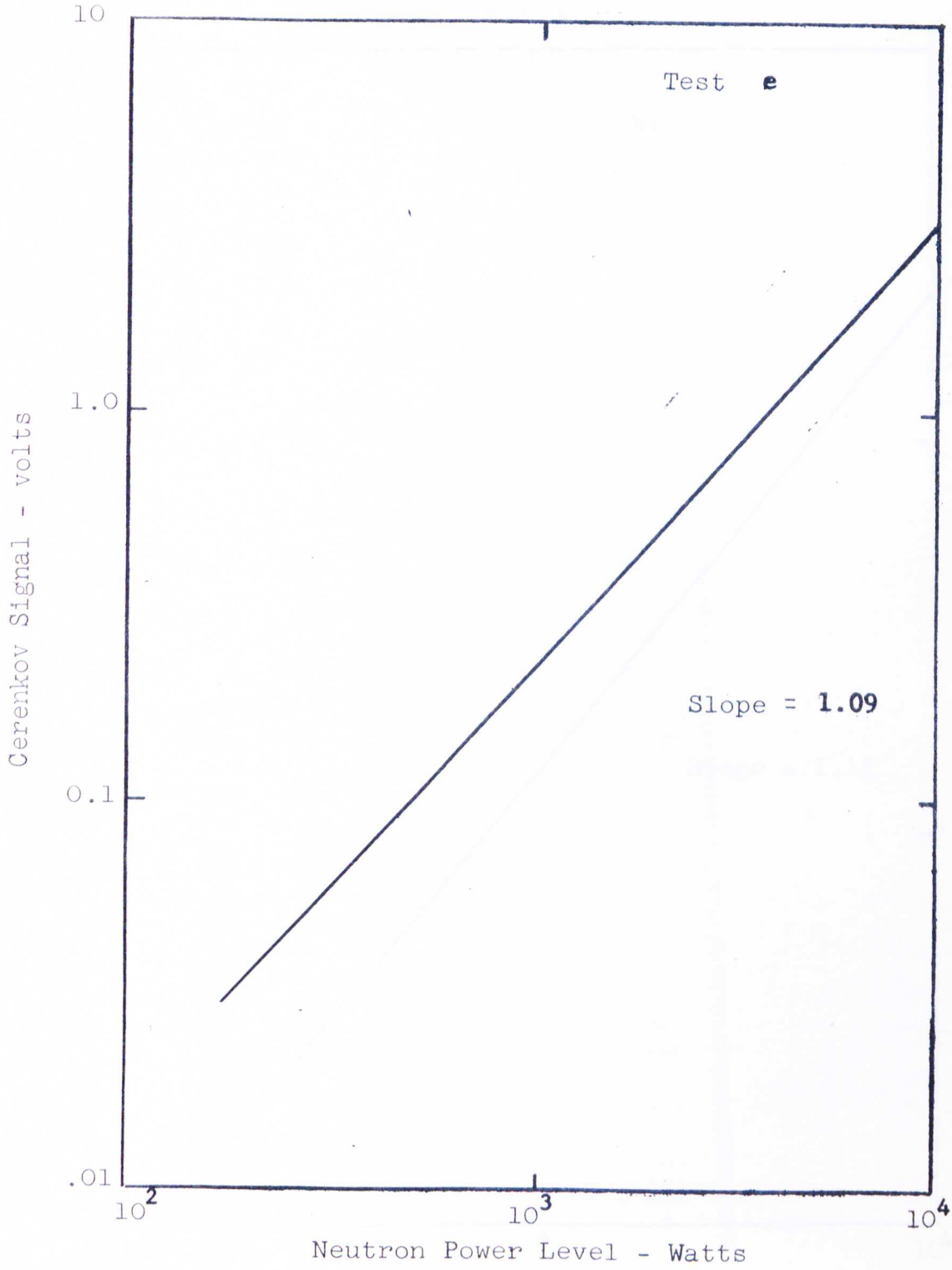

Fig. 26 Cerenkov Signal vs Neutron Power Level

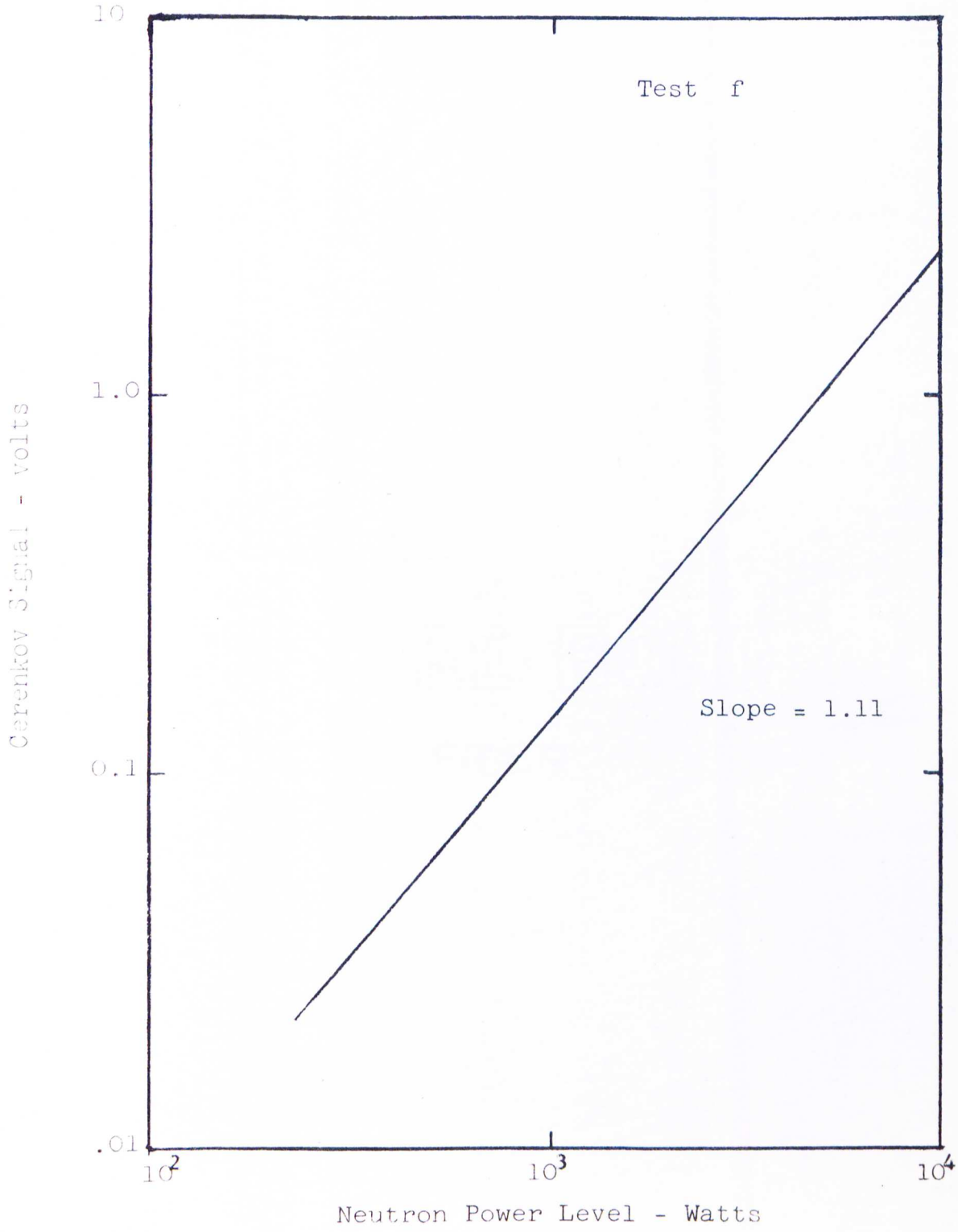

TABLE IV

Cerenkov Transient Data

Test	ω(sec)	δ	$P = P_o^{\delta}$	% Diff.
a.	20	1.00	10	0
b.	29	1.04	10.9	9.0
c.	34.8	1.06	11.5	15.0
d.	44.5	1.07	11.7	17.0
e.	70	1.09	12.3	23.0
f.	110	1.11	12.8	28.0

P = apparent power from Cerenkov detector
P_o = 10 kw - indicated by linear level channel
ω = Measured period averaged over upper two decades (100 w - 10 kw) from linear level neutron channel
δ = Slope of curves in Figures 21 through 26

tests is to calibrate the Cerenkov detector. The ionization chamber had been previously calibrated at a known steady power by measuring the chamber current and obtaining a calibration constant in amperes per megawatt (MW) and linearly extrapolating to higher powers. For the transient tests a chamber signal lead is connected through a galvanometer amplifier to a Minneapolis Honeywell Model 1012 fast recorder which contains a Heiland Type M1650 galvanometer. The maximum peak to peak deflection of the galvanometer is 8 inches with $\pm 2\%$ linearity. The recorder trace is adjusted by means of the gain control on the galvanometer amplifier so as to obtain a maximum deflection of 4 inches at 1200 MW. The Cerenkov detector is connected to the recorder in a similar manner through another channel on the galvanometer amplifier and the trace again adjusted for a maximum deflection of 4 inches at 1200 MW. Because of the strong light intensity at 1200 MW the photomultiplier is masked. The amount of masking is optimized with the supply voltage to the photomultiplier so as to obtain a strong signal and still prevent damaging the detector. Final adjustments result in a maximum signal of 2.8 volts at 1200 MW.

The measurement of width at half-maximum is straight forward and one of the most accurately measurable parameters. It can be used as a substitute for the period since the relation between period and half width is linear, e.g.

the Fuchs theoretical model relationship between τ and $W_{1/2}$ is given by[19]

$$W_{1/2} = 3.5\,\tau \tag{18}$$

The empirical relationship is[19]

$$W_{1/2} = 3.3\,\tau \tag{19}$$

In general, it is more difficult to measure τ than $W_{1/2}$ from a complete pulse trace. In order to obtain good period data, it is necessary to increase the recorder sensitivity so as to obtain a larger spread during the initial exponential power rise during a pulse. This would be at the expense of P_{max} and $W_{1/2}$ data since the recorder would go off scale. Since $W_{1/2}$ is more readily measured, a plot of P_{max} vs τ may be obtained by measuring the half width $W_{1/2}$ and using the relation $W_{1/2} = 3.3\,\tau$. Comparison of the pulse shape as produced by the photomultiplier with that produced by an uncompensated ion chamber shows very good agreement as is evident from the data given in Figures 27 and 28. The data in Figure 27 represents Cerenkov detector and ion chamber outputs recorded simultaneously on a Minneapolis Honeywell Visicorder for the same pulse. Within the limits of accuracy of these measurements no difference exists between the two detector systems. In the case of the ion chamber, the question arises as to whether the linear

Fig. 27 Peak Power vs Pulse Half Width

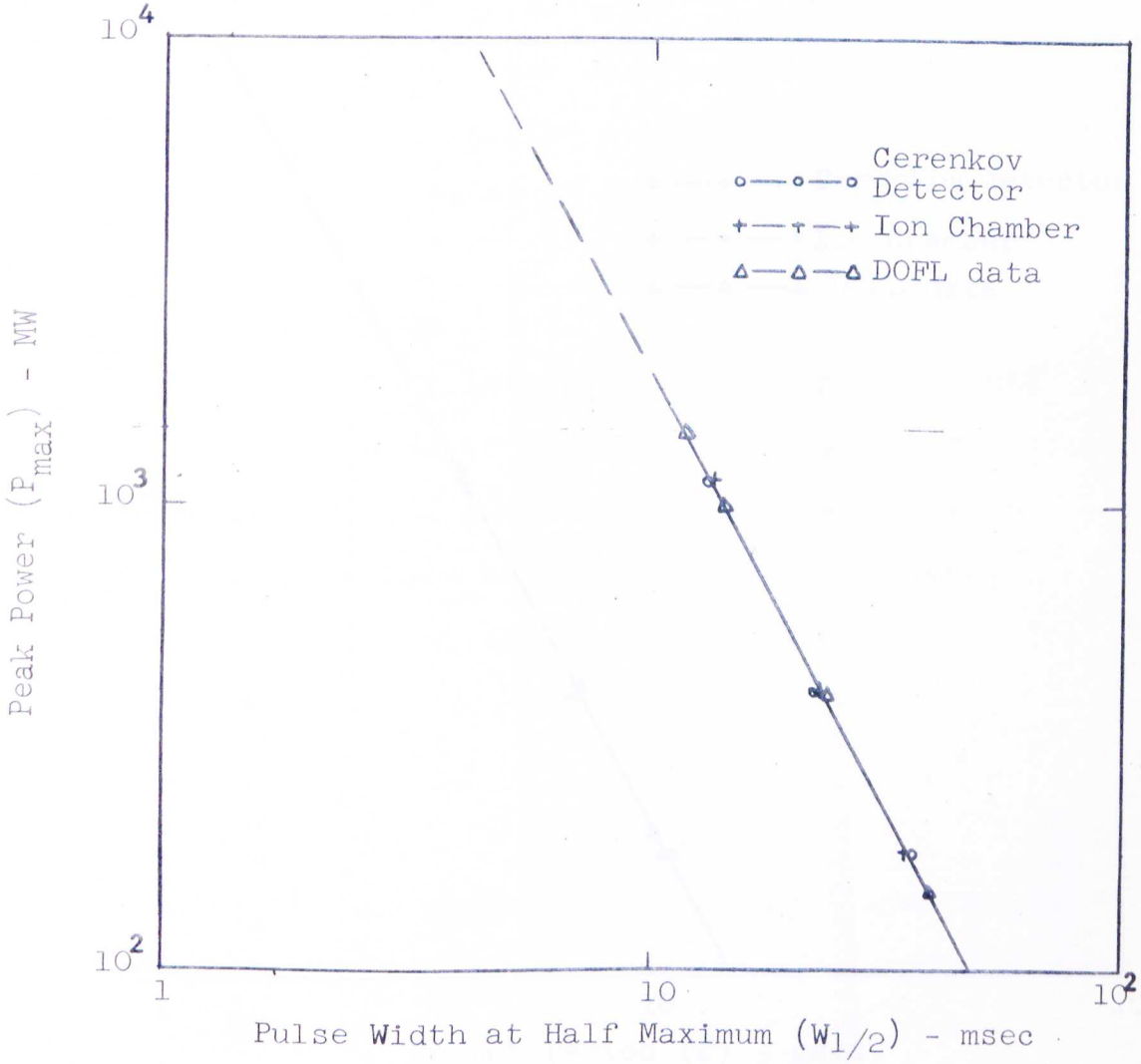

Fig. 28 Peak Power vs Prompt Period

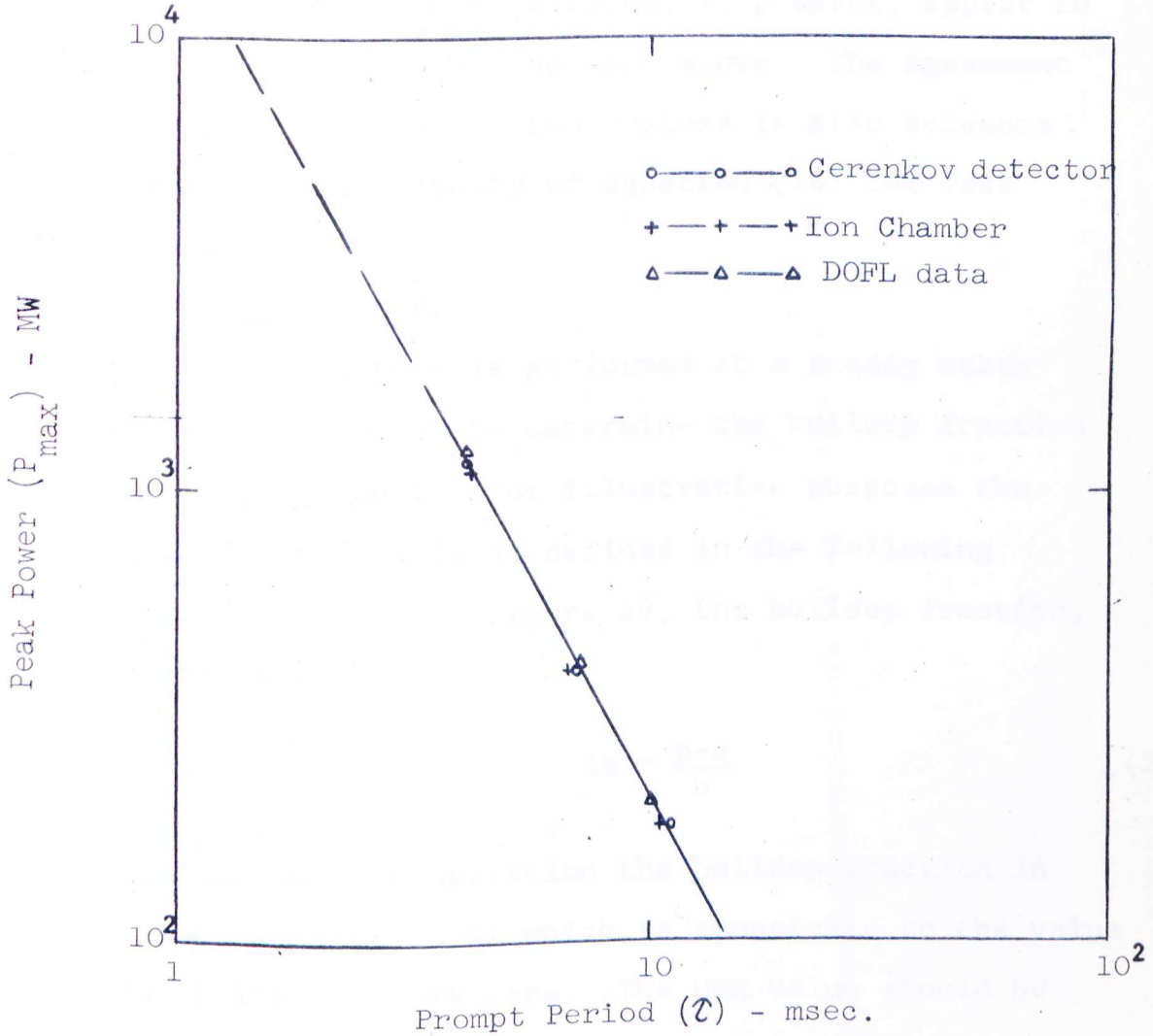

extrapolation of the steady state calibration constant is strictly true. More specifically, a change in the neutron to gamma ratio from steady state to pulse operation could affect the measured peak power. Furthermore, high gamma and neutron radiation fields experienced by an ion chamber and its connecting cables may cause appreciable signal pickup due to momentary breakdown of cable insulator. These effects, if present, appear to be negligible based on the data above. The agreement between the data of the two systems is also evidence in favor of the validity of equation (16) for fast transients.

b. Steady State

A TRIGA test is performed at a steady state power level of 50 kw to determine the buildup fraction of the light signal. For illustrative purposes the buildup fraction will be defined in the following manner. Referring to Figure 29, the buildup fraction, B, is given by:

$$\%B = \frac{b-a}{b} \qquad (20)$$

After four minutes operation the buildup fraction in the TRIGA reached 13.4% which is comparable to the value of 14.5% from the UMR core. The UMR value should be somewhat higher since the startup time from source level to power in the TRIGA and UMR is $\backsim$ 250 seconds and $\backsim$1000 seconds respectively. Therefore, some fission

Fig. 29 Illustrative Definition of Relative Buildup Fraction

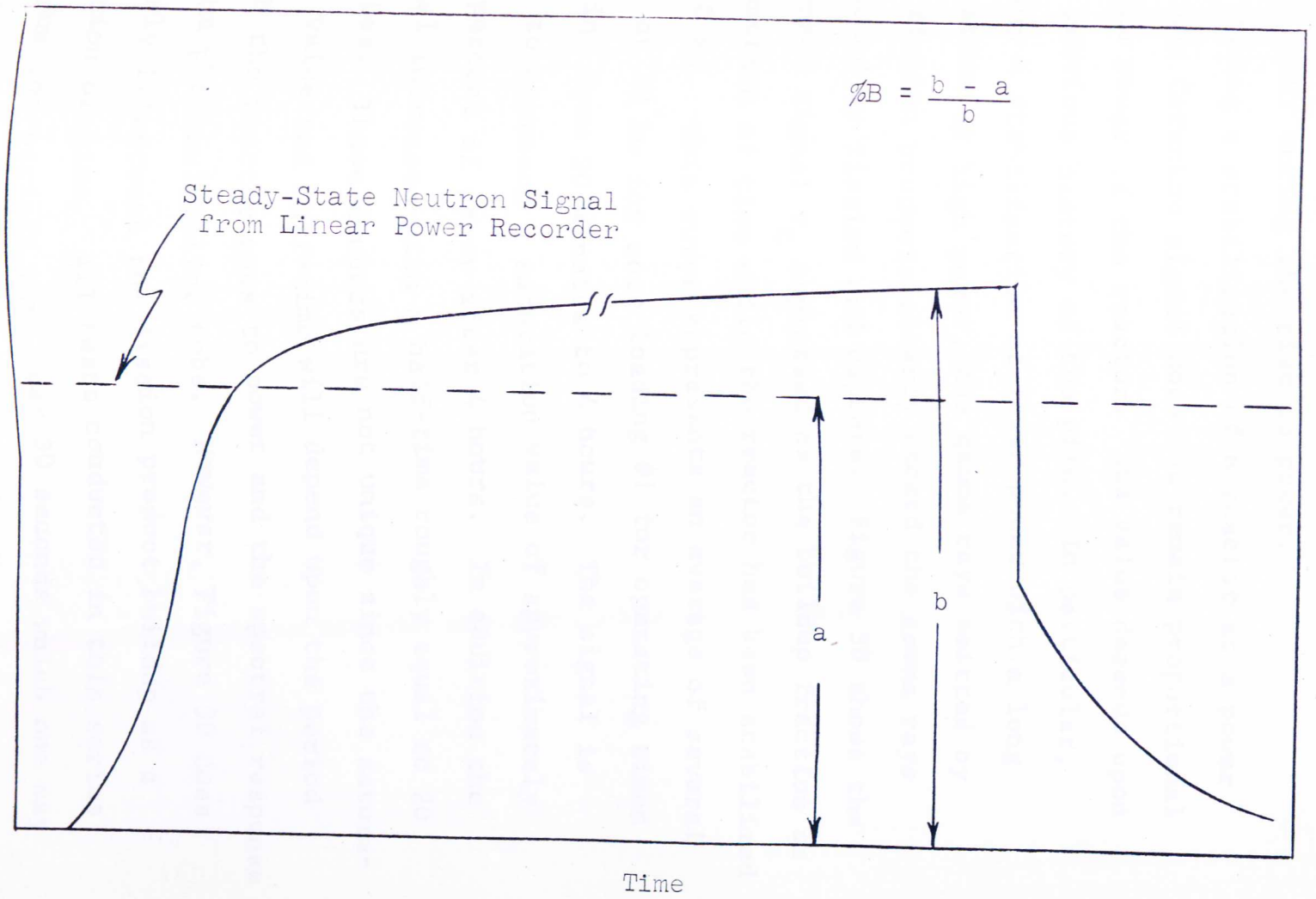

product buildup and hence increase in Cerenkov light does occur during the rise to power.

During a stabilization of a reactor at a power P_o, the Cerenkov signal does not remain proportional to the power of the reactor. Its value depends upon the previous history of the pile. In particular, during a stabilization at lower power with a long operation at high power, the gamma rays emitted by the fission products clearly exceed the gamma rays produced by fission and capture. Figure 30 shows the Cerenkov signal V_t expressed as the buildup fraction as a function of time while the reactor has been stabilized at 10 kw. This curve represents an average of several runs at 10 kw for core loading #1 for operating times ranging from 20 minutes to 4 hours. The signal is seen to approach a saturation value of approximately 160 percent of power after 4 hours. In addition the signal increases with a half-time roughly equal to 20 minutes. These numbers are not unique since the saturation value and half-time will depend upon the period which the reactor goes to power and the spectral response of the photomultiplier tube. However, Figure 30 does clearly illustrate the fission product buildup as a function of time. All tests conducted in this series are run for periods very near 30 seconds which one may consider typical for startup. A further consideration in noting the fission product buildup is the effect of

Fig. 30 Cerenkov Signal Buildup Fraction vs Reactor Operating Time

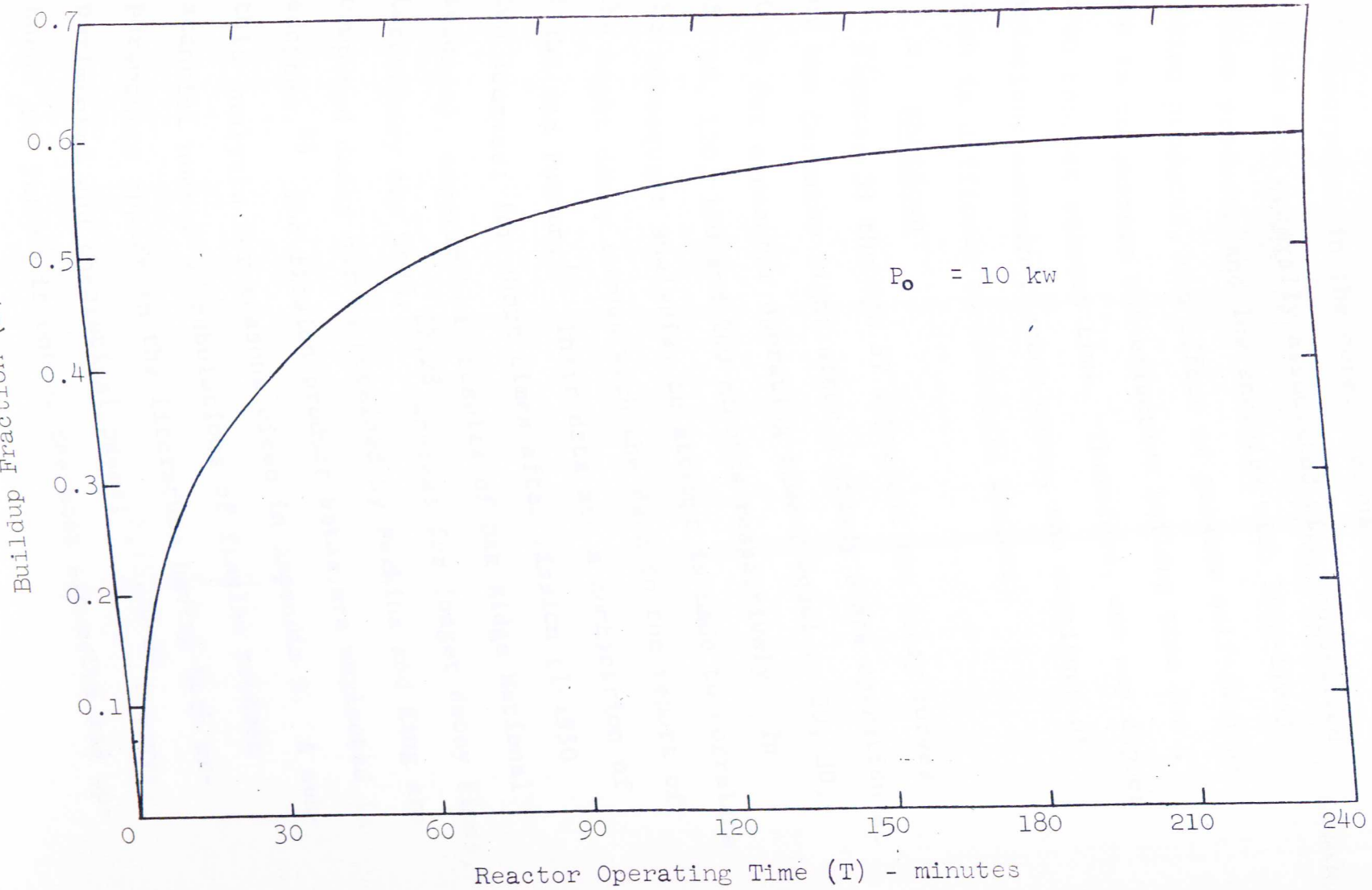

self-absorption in the core. Because high gamma ray energies are generally associated with short-lived fission products and low energies with long-lived fission products, the effect of greater self-absorption is to shorten the effective buildup time for a given reactor startup time. Therefore, one may expect variations between reactor cores, the magnitude of which is difficult to ascertain apriori.

c. Shutdown

Figures 31 through 37 represent the decay curves for the Cerenkov light after a steady state operation at 10 kw for a reactor operating time T equal to 20, 30, 45, 60, 120, 180 and 240 minutes respectively. In the subsequent analysis, an attempt is made to correlate the light decay curves with the data in the report of Knabe and Putnam.[13] Their data are a combination of two sources; for short times after fission (1-1550 seconds), experimental results of Oak Ridge National Laboratory are used,[27,28] whereas for longer decay times, computed decay curves obtained by Perkins and King are adopted.[25] The fission product betas are neglected in this analysis for reasons cited in Appendix A. A substantial number of tabulations of fission product parameters appear in the literature having both experimental and theoretical bases;[7,13,20-29] however, Knabe and Putnam is one of the most extensive and up-

Fig. 31 Cerenkov Light Decay as a Function of Shutdown Time

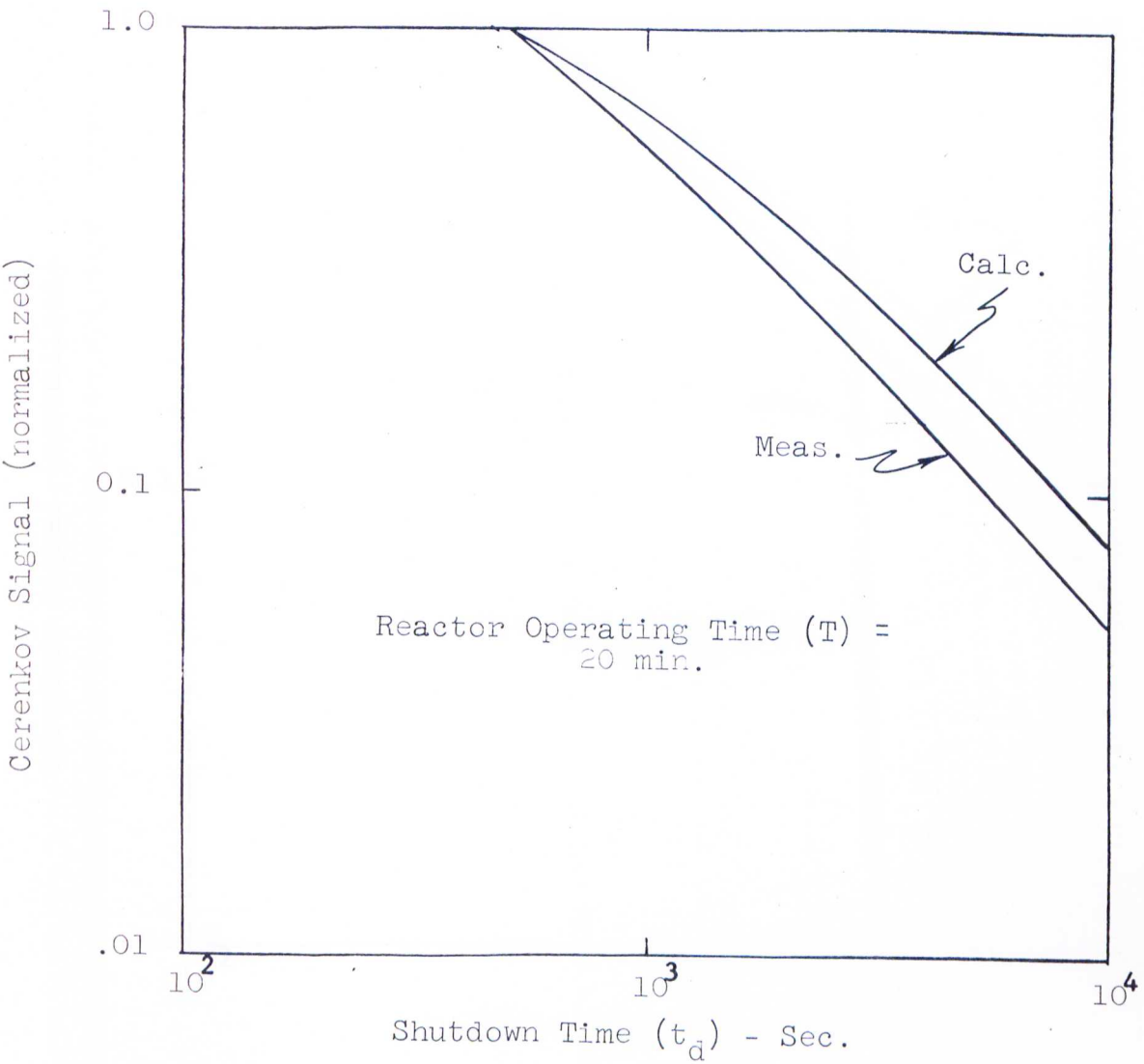

Fig. 32 Cerenkov Light Decay as a Function of Shutdown Time

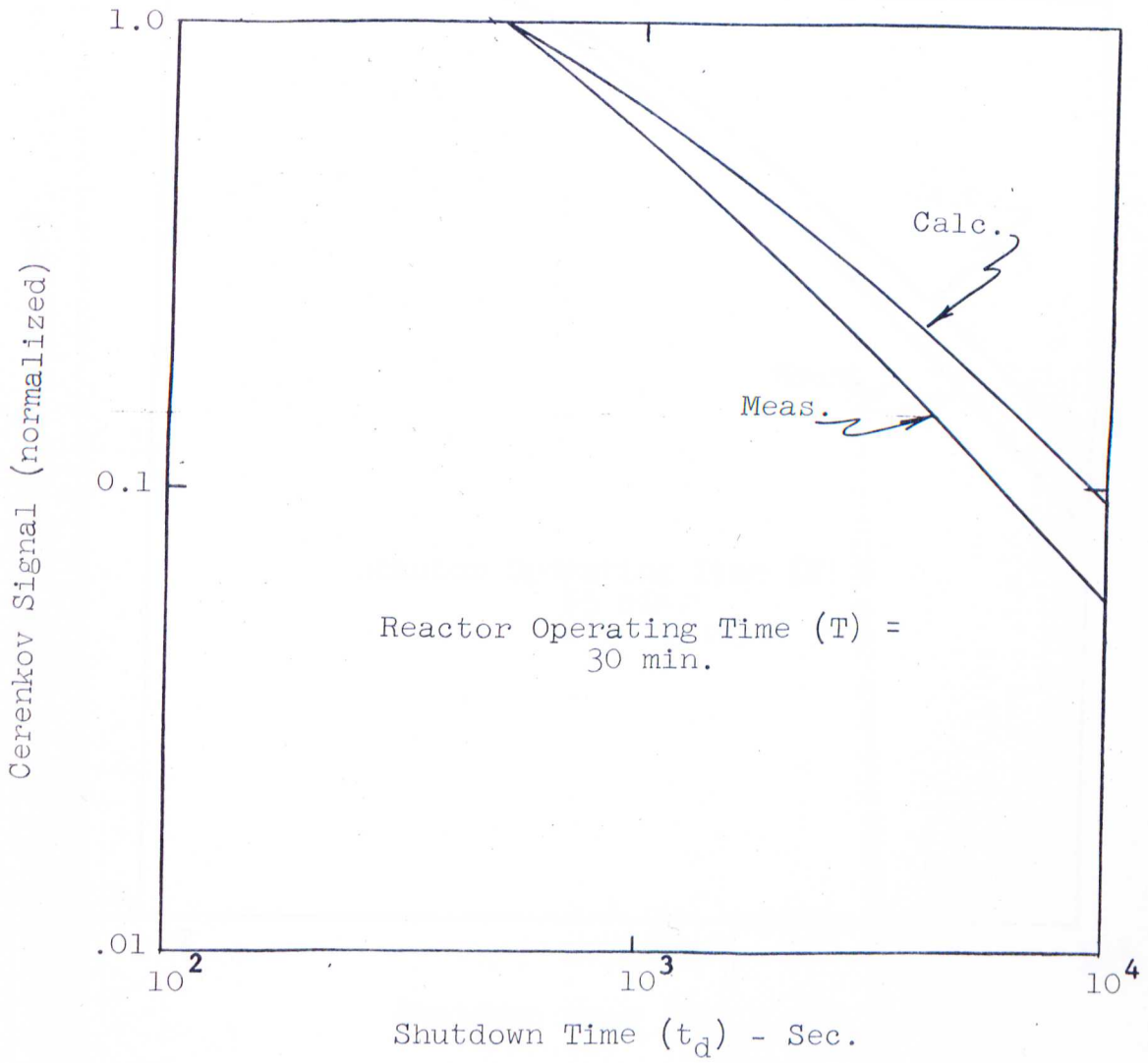

Fig. 33 Cerenkov Light Decay as a Function of Shutdown Time

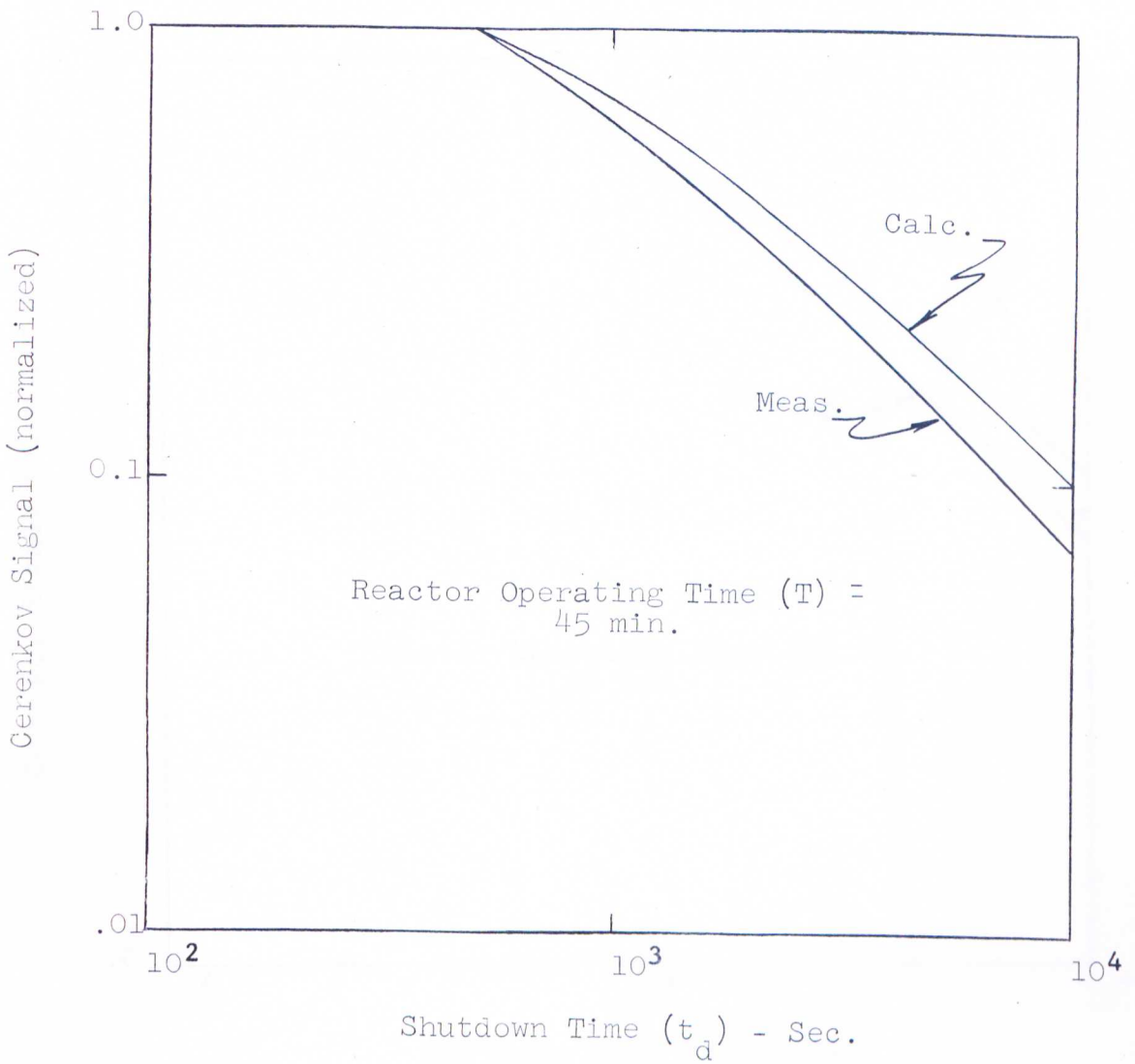

Fig. 34 Cerenkov Light Decay as a Function of Shutdown Time

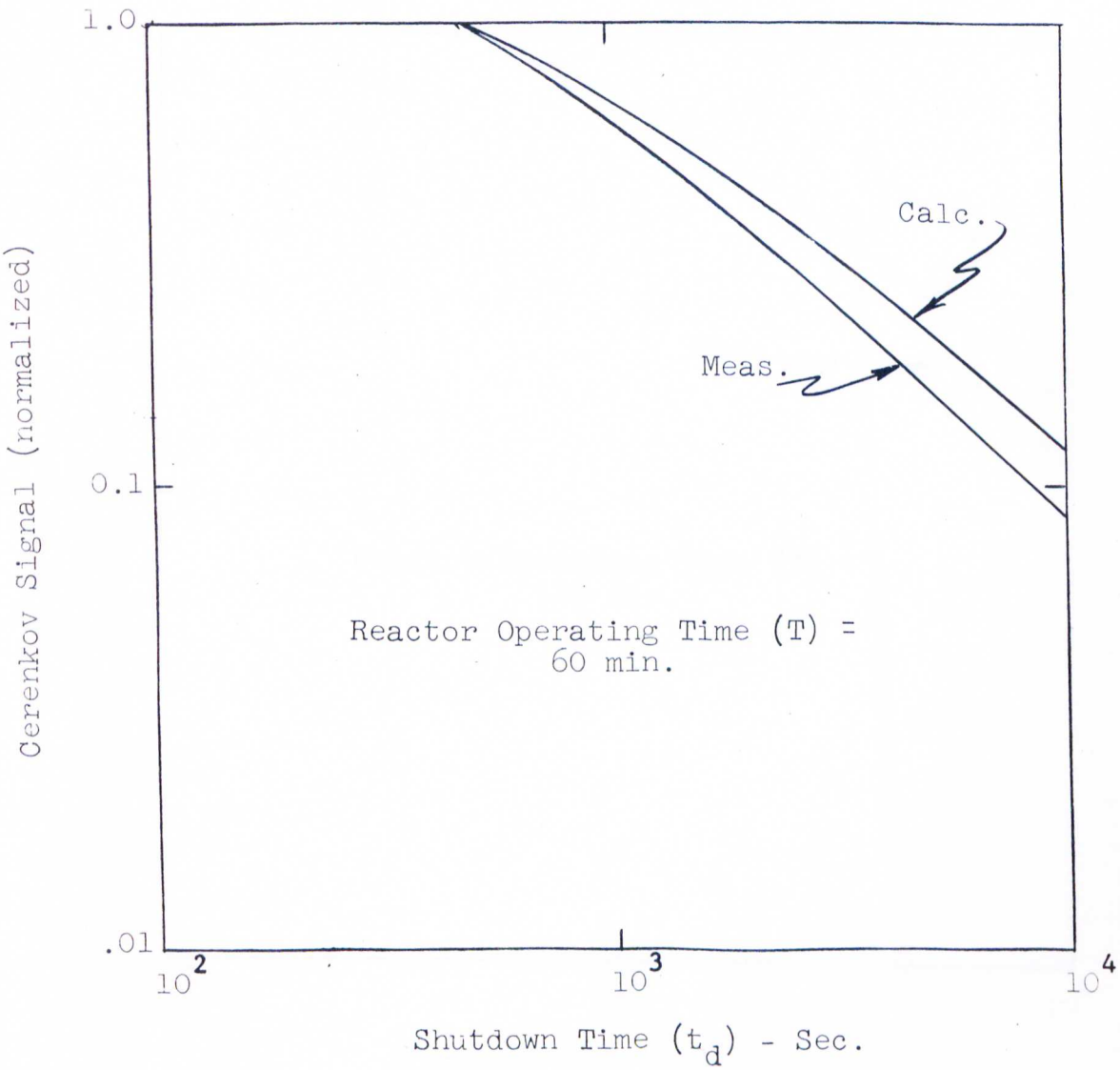

Fig. 35 Cerenkov Light Decay as a Function of Shutdown Time

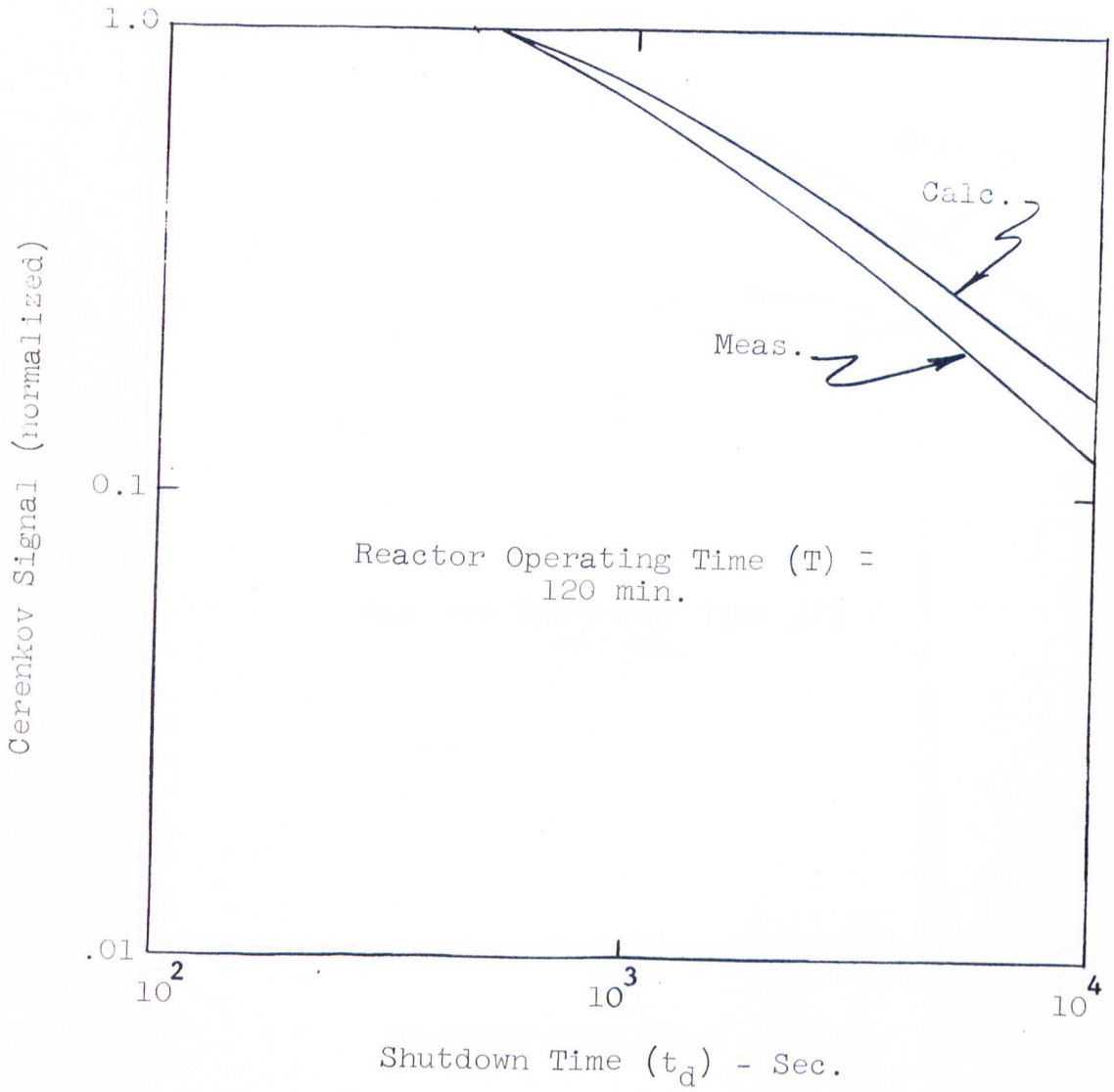

Fig. 36 Cerenkov Light Decay as a Function of Shutdown Time

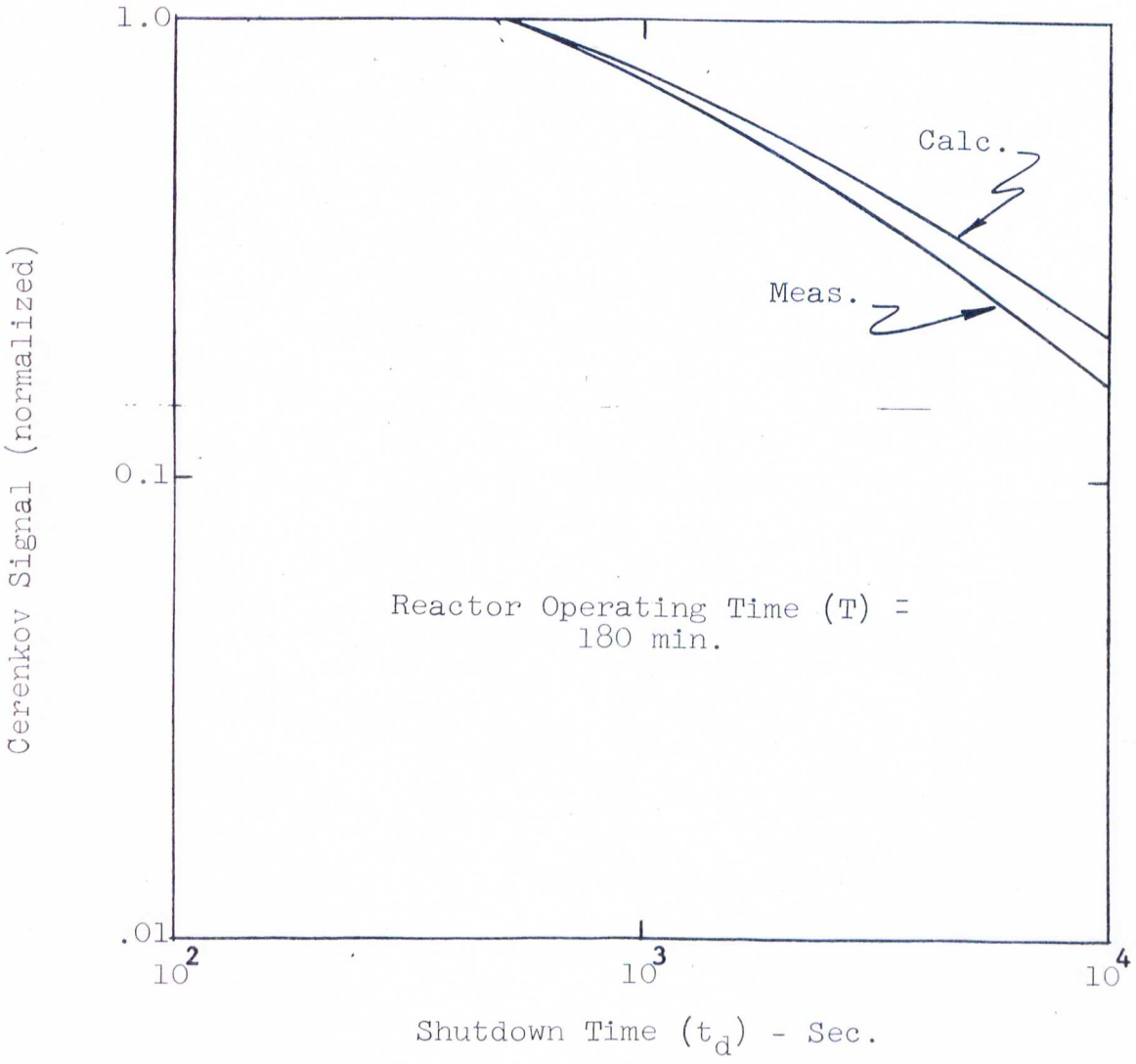

Fig. 37 Cerenkov Light Decay as a Function of Shutdown Time

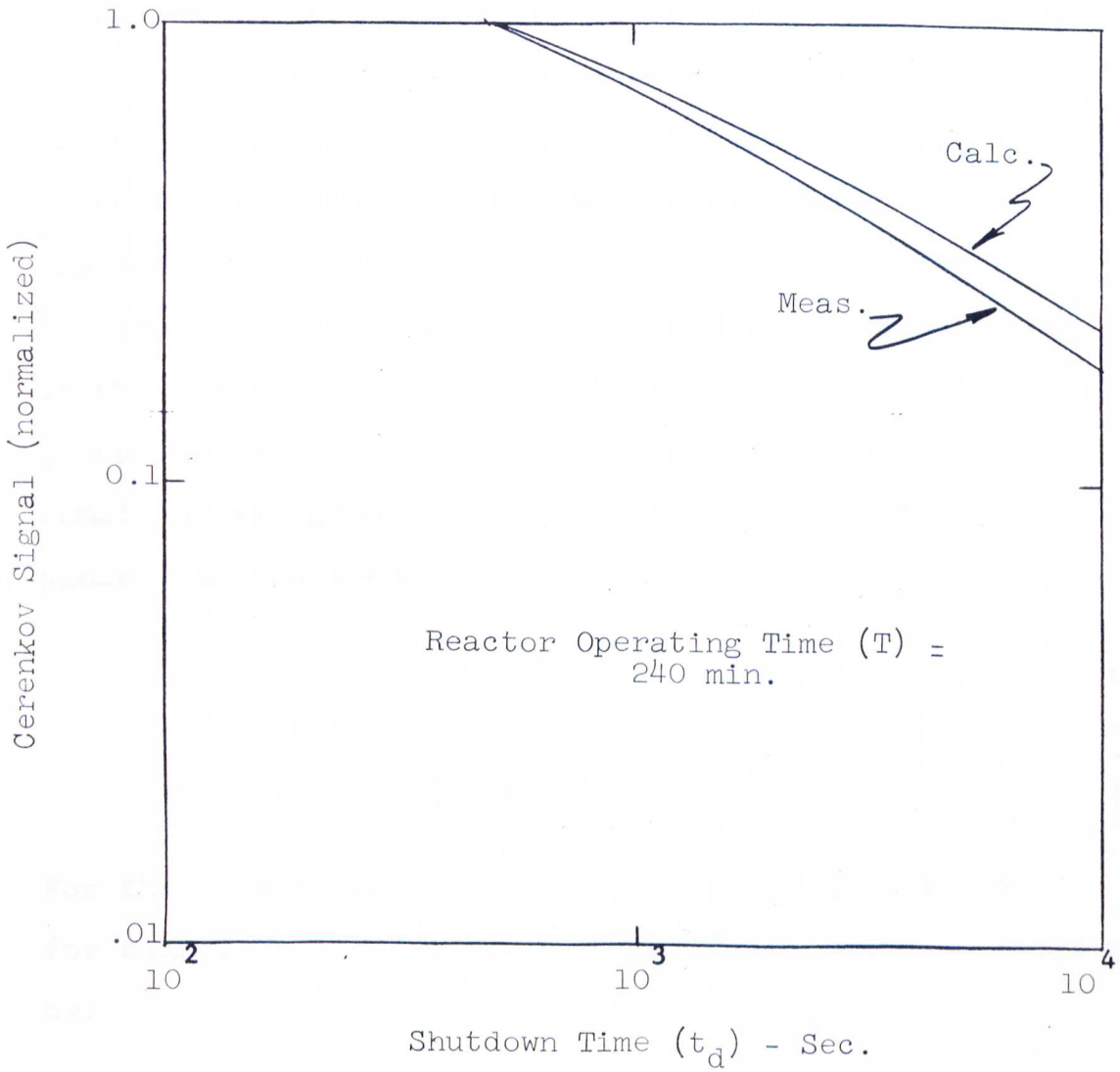

to-date references found and will be used as a basis for the calculations on fission products which follow.

The rate of energy release from fission products, as a function of time after fission, can be represented by the following expression:

$$\Gamma(t) = a_o t^{-s} \text{ Mev/fiss-sec} \tag{21}$$

where t is the time after fission in seconds and a_o and s are constants. In the report of Knabe and Putnam the photons are classified into seven energy groups covering the energy range between 0.1 and 5.5 Mev (see Table VII, Appendix A). Since the minimum photon energy which can produce a 0.260 Mev Compton electron (Cerenkov threshold in water) is 0.407 Mev and the average energy of the first group is 0.30 Mev, if we neglect this group the rate of energy release per fission for the remaining six groups is represented by the following piece-wise continuous function:

$$\Gamma(t) = \begin{cases} 0.364t^{-0.70} & 1 \leq t \leq 10 \text{ sec} \quad (22a) \\ 0.829t^{-1.06} & 10 \leq t \leq 10^3 \quad (22b) \\ 4.62t^{-1.31} & 10^3 \leq t \leq 10^5 \quad (22c) \end{cases}$$

For the reactor that operates at a power P(μ) watts for time T, the decay of fission product power is represented by:

$$P(t,T) = K \int_{1}^{T} d\mu \cdot \Gamma(t + \mu) P(\mu) \quad \text{watts} \tag{23}$$

where $K = 5.12 \times 10^{-3}$ fissions per Mev and μ is an arbitrary time during operation. For the case of constant power level operation $P(\mu) = P_o$, and equation (23) becomes

$$\frac{P(t,T)}{P_o} = K \int_{1}^{T} a_i (t + T)^{-s_i} d\mu \tag{24}$$

where

$$\Gamma(t + \mu) = a_i (t + \mu)^{-s_i} \tag{25}$$

Applying equations (22a), (22b), and (22c) to equation (24) results in the following expression:

$$\frac{P(t,T)}{P_o} = K \left[\int_{1}^{10} 0.364(t + \mu)^{-0.70} d\mu + \int_{10}^{10^3} 0.829(t + \mu)^{-1.06} d\mu + \int_{10^3}^{T} 4.62(t + \mu)^{-1.31} d\mu \right] \tag{26}$$

Integrating equation (26) yields the desired relation, namely

$$\frac{P(t,T)}{P_o} = 5.12 \times 10^{-3} \left\{ 1.21 \left[(t + 10)^{0.30} - (t + 1)^{0.30} \right] + 14.5 \left[(t + 10)^{-0.06} - (t + 10^3)^{-0.06} \right] + 15.1 \left[(t + 10)^{-0.31} - (t + T)^{-0.31} \right] \right\} \tag{27}$$

A reasonable fit between calculated and measured decay curves is possible if a comparison is made for a normalization at t = 500 seconds instead of at t = 1 second for the following reasons. If one considers the contributions of the Al-28 ($t_{1/2}$ = 2.3 minutes) decay betas and gammas to

the Cerenkov light, then after approximately 3.5 half-lives most of the aluminum has decayed. In addition, the analysis is complicated to some extent by the emission of delayed neutrons. The formula for the gamma decay rate due to fission products in a reactor applies to a reactor of operating interval T seconds, during which the reactor power or fission rate is not zero. Reactor shutdown refers to the instant at which the fission rate rapidly drops due to control rod insertion, however, fission products continue to generate delayed neutrons after shutdown. The delayed neutrons maintain the neutron flux at a level of the order of 1% of the pre-shutdown flux for times up to a minute or so, and this keeps the fission rate at a similar fraction of the operating power level. When this occurs, terminating the operating time, T, at the point where shutdown only begins to occur must obviously be avoided in order to be able to evaluate and compare the calculated and measured decay curves.

Normalizing the calculated and measured curves at t = 500 seconds then indeed seems reasonable as a basis for comparison. The normalized data is shown in Figures 31 through 37. Figure 38 is a plot of the percent difference between the calculated and measured curves vs operating time. These values are calculated for a decay time of 10^4 seconds at which point a maximum difference occurs. It can be seen from Figure 38

Fig. 38 % Difference Between Measured and Calculated Decay Curves

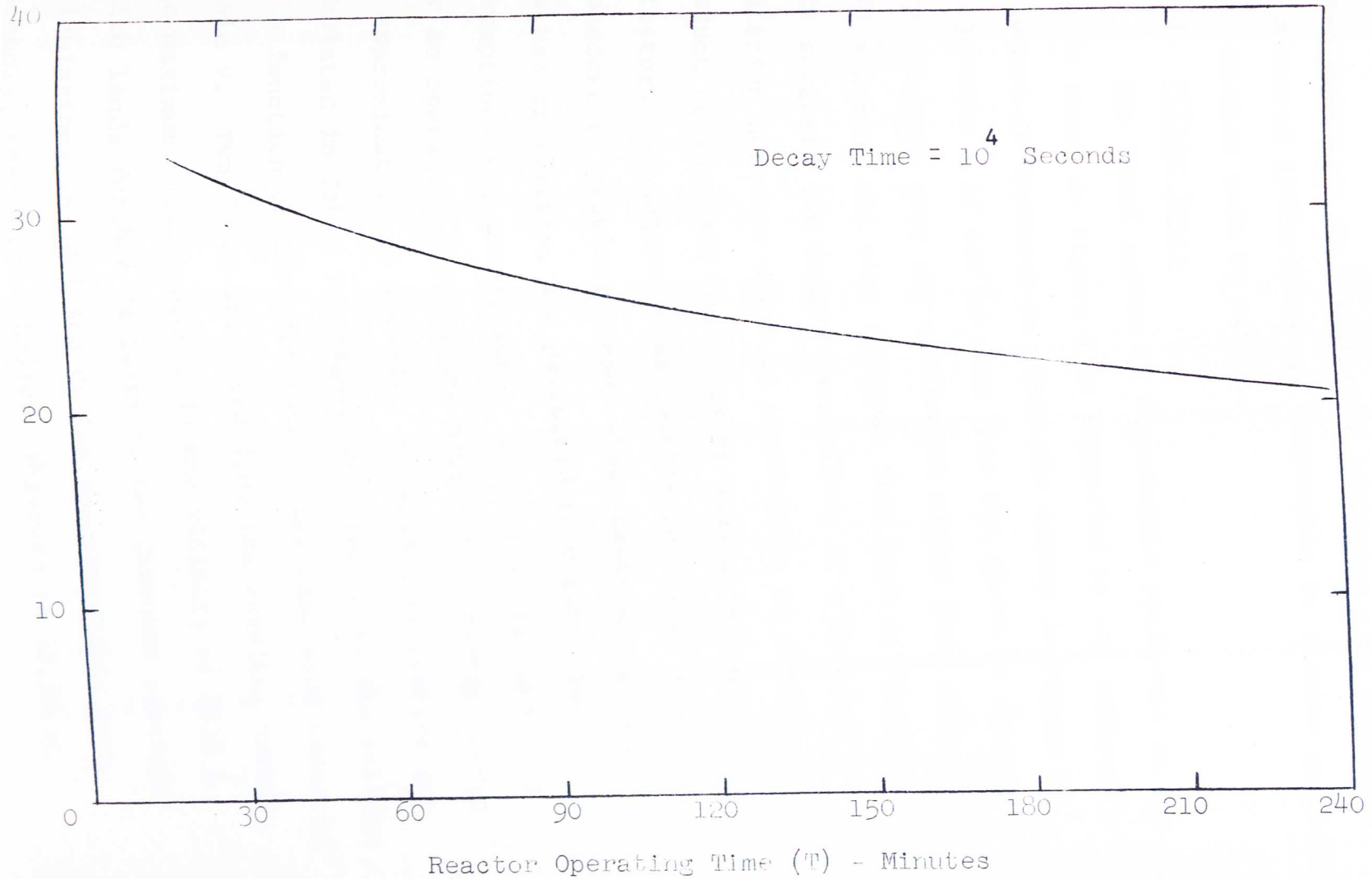

that the difference between the analytical and empirical curves decreases as the reactor operating time increases. The observed differences are comparable to fission product decay studies made by others.

d. Filter Tests

The final series of experiments performed on the core as shown in Figure 5 is suggested by the analysis performed in Appendix A. From the curves in Figure 49 in Appendix A it can be seen that the spectrum changes very slightly over the wavelength region from 2500 Å to 3400 Å during the time interval from zero to four hours. This suggests the unique possibility of a Cerenkov radiation detector which is insensitive to fission product buildup and hence may be used as a power level detector. Subsequent measurements identical in procedure to previous steady state tests except for the use of filters, are performed to verify these assumptions and conclusions. All tests are conducted for an operating time of one hour and a startup period of approximately 40 seconds. Experimental results are tabulated in Table V. Figure 39 illustrates the buildup as a function of time for each of the tabulated cases in Table V. Two facts are noted from the results, namely, the maximum buildup occurs in the vicinity of 3920 Å which lends further validity to the Cerenkov spectrum calculations in addition to the spectrographic data. Secondly, the minimum buildup observed is 18.3% at

TABLE V

Fractional Buildup of Cerenkov Signal After a Reactor Operating Time of One Hour

Wavelength at T_{max} (Å)	T_{max} (%)	Half Width (Å)	Fractional Buildup
3500	31.6	235	0.204
3920	30	110	0.284
4450	30	80	0.263
4700	35	90	0.242
4980	47	120	0.224
5530	44	120	0.183
No Filter	--	---	0.442

Fig. 39 Buildup Fraction vs Reactor Operating Time (Filter Tests)

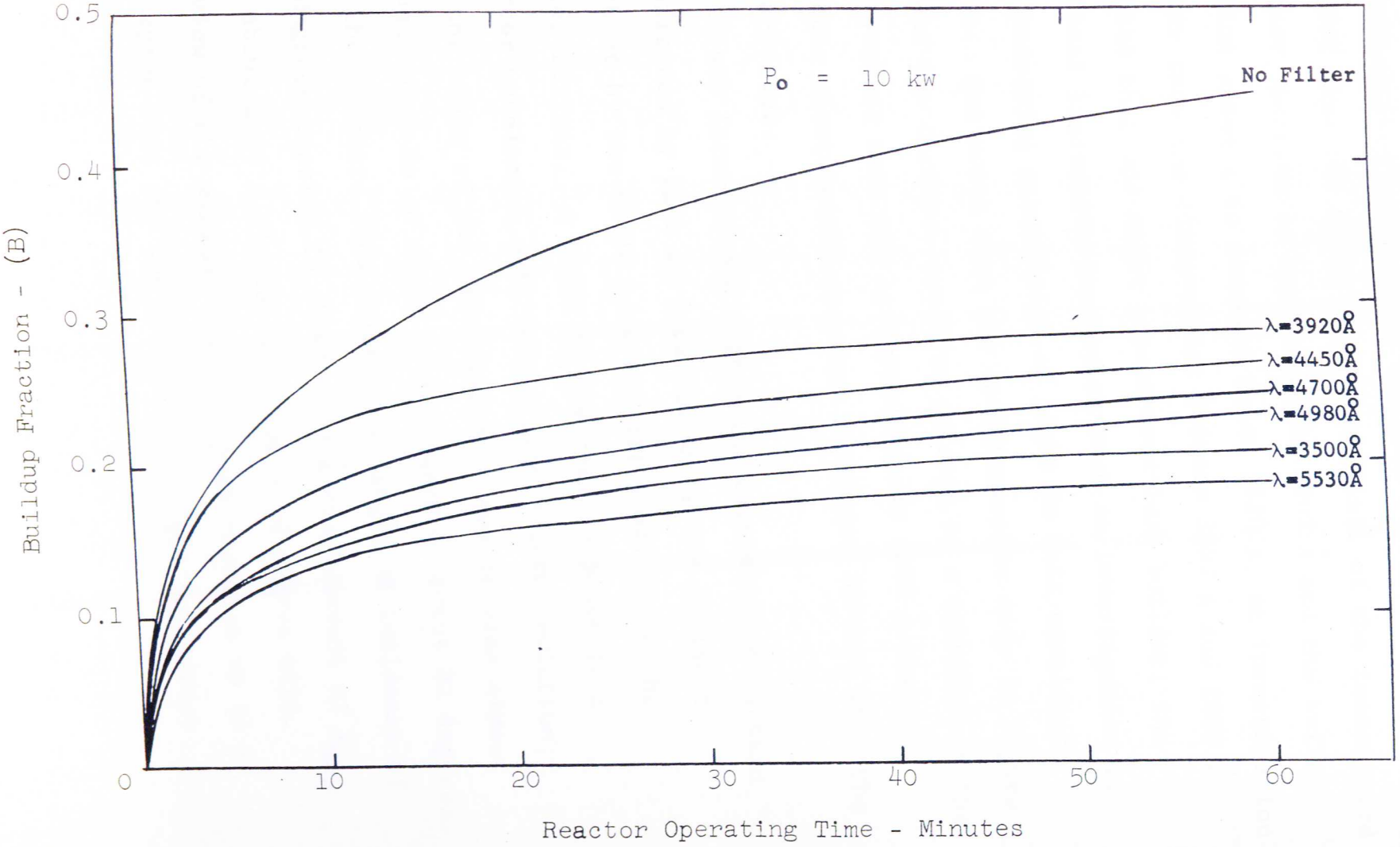

5530 Å which is essentially the long wavelength limit of the transmitted spectrum at the pool surface. In view of the fact that the short wavelength limit of the transmitted Cerenkov spectrum is approximately 2000 Å and the buildup fraction appears to decrease below 3920 Å, an investigation further into the ultra-violet between 3500 Å and 2000 Å suggests that one might expect even less buildup; the practical limitation imposed on such an investigation is the increasing attenuation of light in this wavelength region. One notes from the spectrographic data in Figure 18 that the Cerenkov spectrum as seen by a detector at the pool surface cuts off at approximately 2000 Å whereas the true unattenuated spectrum continues further into the ultra-violet.

In any interference filter the transmission pattern is affected by lack of parallelism in the incident light or by the whole beam not being normal to the filter surface. A shift in the peak response to a shorter wavelength will result from either deviation, but the shape of the transmission curve remains almost unchanged up to an angle of incidence of about 20 degrees. For the standard Jena filters, an angle of incidence of 10 degrees results in about a 20 Å displacement of λ_{max} and about a 30 Å displacement for a 20 degree tilt. In view of the minimal shift in peak response up to a 20 degree tilt and the fact that a light collimator

is used, any errors due to lack of parallelism of the incident light is considered negligible.

Up until now, no mention has been made of any possible variations in the Cerenkov spectrum due to temperature effects or dispersion. Referring to Table I, less than a 2% change in the index of refraction occurs over a wavelength region extending from 3034 Å to 6438 Å for a temperature of 20°C. Moreover, the negative temperature coefficient of n equal to -1.00×10^{-4} per °C results in less than a 2% change over a temperature range 20 to 60°C for the same wavelength region. Consequently, no observable effects are expected in the measured data.

It should also be noted that gamma ray activities from previous operation at power levels in excess of 1 kw produce a residual Cerenkov light signal at shutdown which lingers for several hours or more. Hence, in order to minimize any measurement errors, at least one day is allowed to elapse between reactor operation at power levels greater than 1 kw and an experimental run. Each startup therefore is effectively equivalent to startup with a cold clean core.

CHAPTER VI

SUMMARY

A relatively simple, single instrument for the measurement of reactor power does not yet exist. The most common means of measuring power level in a reactor is to utilize neutron detectors which give a direct indication of the neutron population density. Both the reactor power and the neutron flux are directly related to the neutron density in the reactor, but the neutron flux is also dependent on the neutron attenuation between the reactor and the detector. Measurement of the neutron flux then provides a useful signal for operation and control of reactors. However, because the presently used neutron detectors are located outside the reactor lattice, they are sensitive to perturbations in core leakage and shielding due to control rod configuration and changes in attenuation characteristics of the intervening material.

It is possible, in principle, to use the signal from a Cerenkov detector for reactor control, but because the gamma ray intensity is not simply related to the reactor power the problem is more complicated. For example, a short time after reactor shutdown from long operation at high power the delayed gamma ray activity from fission products might obscure a dangerously rapid increase in neutron population.

Moreover, even after several hours shutdown, Cerenkov measurements might be inaccurate during startup at low power levels because the signal is due partly to gamma ray activities from previous operation at high power.

The attempt to use interference filters as a means of optically biasing out the fission product contribution to the Cerenkov signal met with limited success insofar as the range of filter wavelengths used and the physical situation permitted, namely, the attenuation characteristics of water as a function of wavelength.

In spite of these limitations, the good agreement between the Cerenkov detector and the ion chamber response in the transient tests has a number of interesting and significant implications. The Cerenkov detector affords an excellent means of monitoring pulsed pool reactors or the power variation during an over-power surge, and without exposure to high neutron and gamma fluxes which could destroy normal neutron detectors. Furthermore, since it can be remotely located, the Cerenkov detector, by integrating the total light intensity produced by the reactor, is relatively insensitive to core perturbations and shielding.

The fact that the Cerenkov light decay follows the empirical equations for fission product gamma decay suggests the possibility of using this technique

for remote monitoring of spent-fuel-element activities or mixtures of radioisotopes. A Cerenkov light calibration source of well defined geometry could be fabricated and placed in a material of high refractive index and low absorption coefficient such as water and used as a standard.

One obvious area open to additional investigation is the measurement of the Cerenkov light further into the ultra-violet region to determine with certainty whether or not a region exists which essentially is unaffected by fission product contributions. In line with this discussion, mention might be made of the fact that pressurized water systems (e.g. power reactors) operating at higher temperatures than those encountered in research type reactors have an inherent fission product biasing factor, although small. This factor occurs as a result of the negative temperature coefficient of index of refraction. Thus, at temperatures in the neighborhood of, say, 280°C the effective threshold for the production of Cerenkov light is approximately 0.340 Mev; the minimum gamma ray energy for the production of a Compton electron having this energy being 0.551 Mev. Although this has the effect of reducing the light signal from both the fission product and "prompt" gamma radiations, it is more pronounced in the case of the fission products because of the fact that very few fission products have

energies greater than 3 Mev[13] whereas the "prompt" gamma spectrum extends beyond this up to about 7 Mev.[7,30]

Since the instantaneous gammas follow the reactor power, a gamma detector biased around 3 Mev affords a means of eliminating fission product gamma rays and thus obtaining a "pure" signal proportional to power. Using a Cerenkov detector, one could take advantage of the index of refraction of the medium to set the energy bias. In this connection gaseous media appear to have the greatest potential since the refractive indices of gases are so much lower than those of solids and liquids. Moreover, the refractive index may be varied over a wide range by simply varying the pressure. Borkowski and Kerr,[31] in a preliminary experiment, demonstrated the effect of biasing out all gammas below 3 Mev by using CO_2 and SF_6 under high pressure to achieve the required index of refraction. Their detector consisted of a gas filled tube and as a result was only able to measure the local power density and hence is subject to local perturbations. In order to realize the full benefits of a gaseous Cerenkov detector and yet retain simplicity, it is desirable to utilize such a detector where, first of all, as much of the core as possible can be viewed in order to minimize any geometry effects and secondly, a minimum amount of equipment is necessary. The

obvious choice is a gas cooled reactor wherein typical coolants such as He and CO_2 are already under high pressure ranging from 500 to 2000 psia. The only necessary equipment would be a light sensor judiciously located so as to minimize or eliminate completely any gamma rays streaming towards the viewing window and photomultiplier. These would produce Cerenkov radiation not properly biased since their refractive indices are high compared to gases. It appears that, for any simple and practical scheme, the Cerenkov detector at present is limited to water type systems. A water system provides a highly transparent medium for the production and transmission of Cerenkov light which is chemically stable, non-scintillating and acts as its own shield. The refractive indices and corresponding kinetic energy thresholds for electrons for some common gases at normal temperature and pressure (N.T.P.) is given in Table VI. Figure 40 shows how the threshold energy for these gases varies with pressure.

Another appropriate area for further work is the extension of the detector operating range to possibly four or five decades. Nuclear reactors operate at power levels ranging from milliwatts to megawatts. In order to measure the Cerenkov signal over all or most of this range without range switching it is necessary for the detector to have a logarithmic response. In addition, since the reactor period is a

TABLE VI

Threshold Kinetic Energies for Electrons in Some Common Gases at N.T.P.[1]

Gas	n	E_t(Mev)
Helium	1.000035	61
Argon	1.000284	21
Air	1.000293	21
Nitrogen	1.000297	20
Carbon Dioxide	1.000450	16

Fig. 40 Variation of Threshold Energy, E_t as a Function of Pressure for Some Common Gases

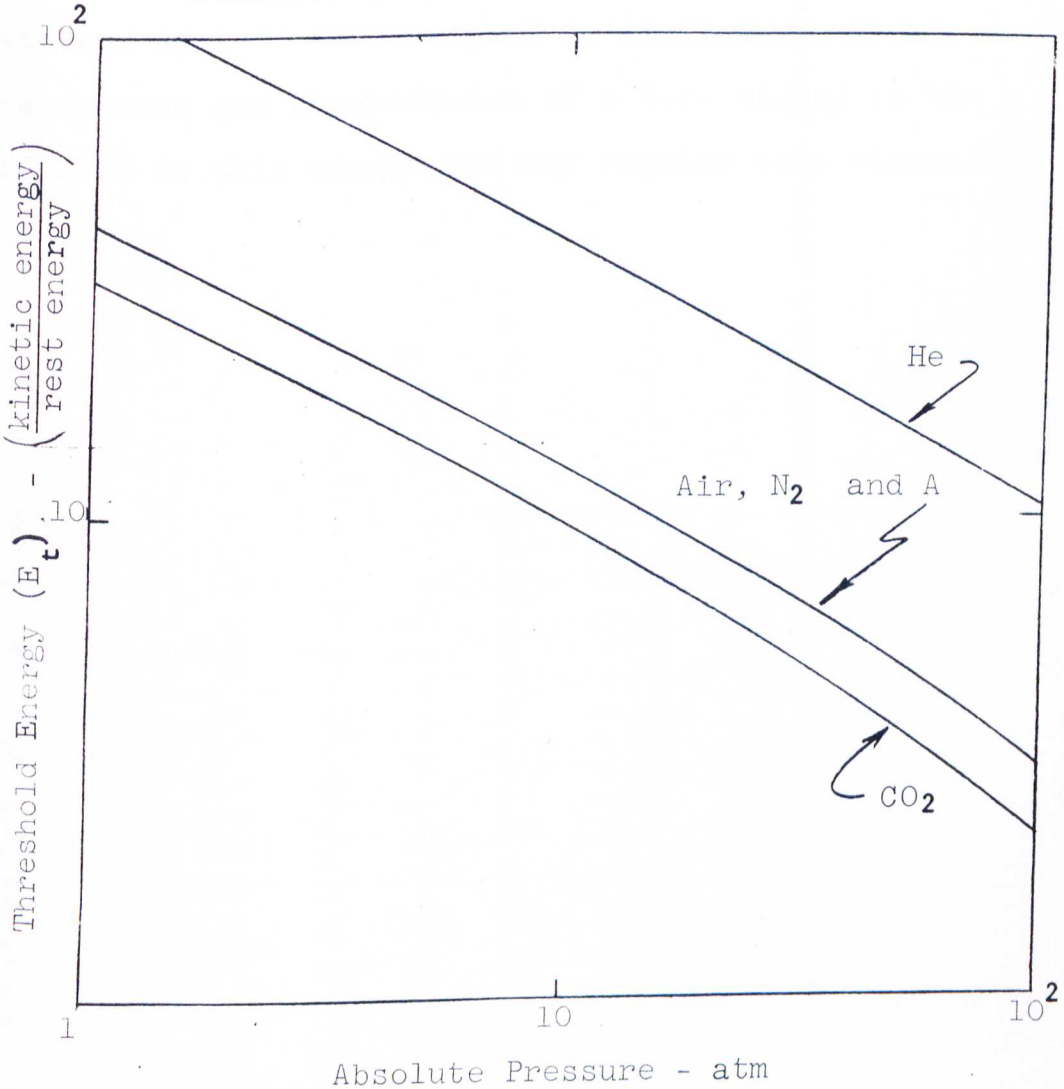

logarithmic function, signals which are proportional to reactor period may be used to control the reactor and to limit the rate of power level rise to safe values. Advantage might be taken of the logarithmic relationship between the gain and applied voltage inherent in photomultipliers which has been investigated by Sweet,[32] Bell et al[33] and others.[34] Contrary to pulse-type detector systems whose signal is limited by noise, measurement and transmission of a d.c. signal is unaffected in this manner and may require less circuitry.

APPENDIX A

The object of this section is to present the relations necessary to calculate for any known initial electron energy distribution the Cerenkov radiation spectrum for any medium of known refractive index. In the case of gamma rays penetrating a refractive substance, it is necessary first to determine the initial electron energy distribution. These distributions have been tabulated for a wide range of gamma energies.[35,36]

The electrons may be related to a number of Cerenkov light quanta by

$$N_{pj} = \frac{4\pi^2 e^2}{hc} N_j \left(\frac{\Delta\lambda}{\lambda^2}\right)_{avg} \int_{\beta max}^{1/n} \left(1 - \frac{1}{\beta^2 n^2}\right) dx \qquad (1)$$

where N_{pj} is the number of light quanta in the wavelength interval $\Delta\lambda$ about λ_{avg} generated in unit time by N_j electrons of specified initial energy coming to rest in the medium.

e is the charge of the particle

h is Planck's constant

c is the speed of light in vacuo

x is the total range of the particle within the medium

β_{max} is the initial velocity of the electrons

$\frac{1}{n}$ is the limiting velocity for the Cerenkov effect

The integral in equation (1) may be evaluated graphically from a plot of $(1 - \frac{1}{\beta^2 n^2})$ vs x.[38] Figure 41 is such a plot made for water (n = 1.333). It is assumed here that n is wavelength independent (see Table I, Chapter II). Figure 42 is a plot of electron range as a function of energy for electrons in water for establishing values of x corresponding to specified initial electron energies.[35] Integration up to each range corresponding to abscissa midpoint values of selected initial electron energy groups may be carried out and the values of the integral so obtained used in equation (1). Each N_j may be substituted into equation (1) and N_{pj} evaluated for each initial electron energy group over the wavelength range of interest. From this, N_{pt}, the total number of light quanta generated in unit time at a wavelength λ_{avg} may be obtained by summation according to

$$N_{pt} = \sum_j N_{pj} \qquad (2)$$

where the sum is taken over all the j initial electron energy groups. The number of light quanta at each wavelength may then be plotted vs wavelength λ_{avg} to obtain the spectral distribution.

Data tabulated by Johns et al make it possible to calculate initial electron energy distributions when the incident radiation is gamma rays.[35,36] To obtain the radiant energy emitted per unit time in the wavelength interval $\Delta\lambda$ about λ_{avg} use is made of the relation

Fig. 41 Range of Electrons in Water as a Function of $\left(1 - \frac{1}{\beta^2 n^2}\right)$

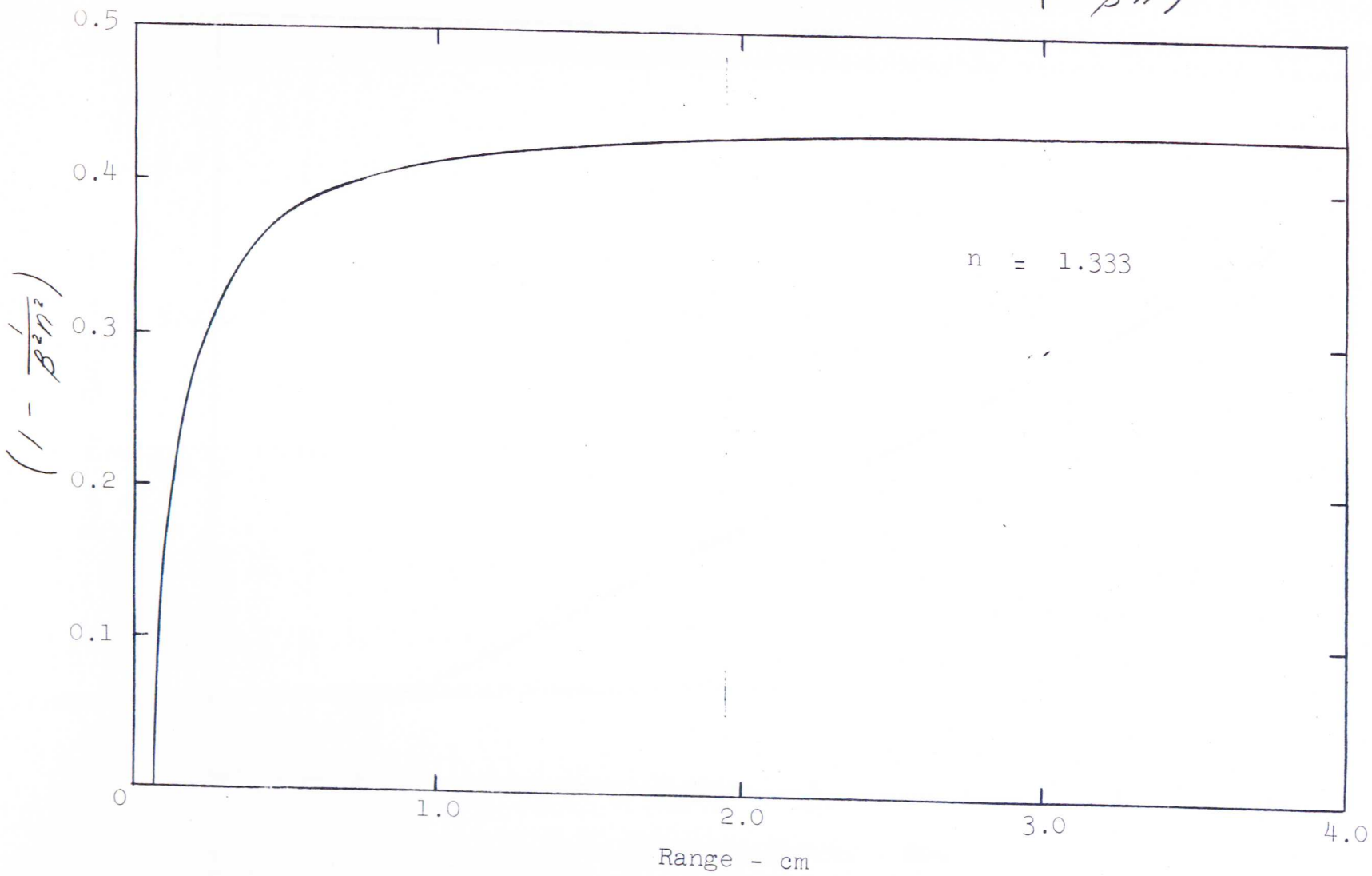

Fig. 42 Range of Electrons in Water vs Electron Energy

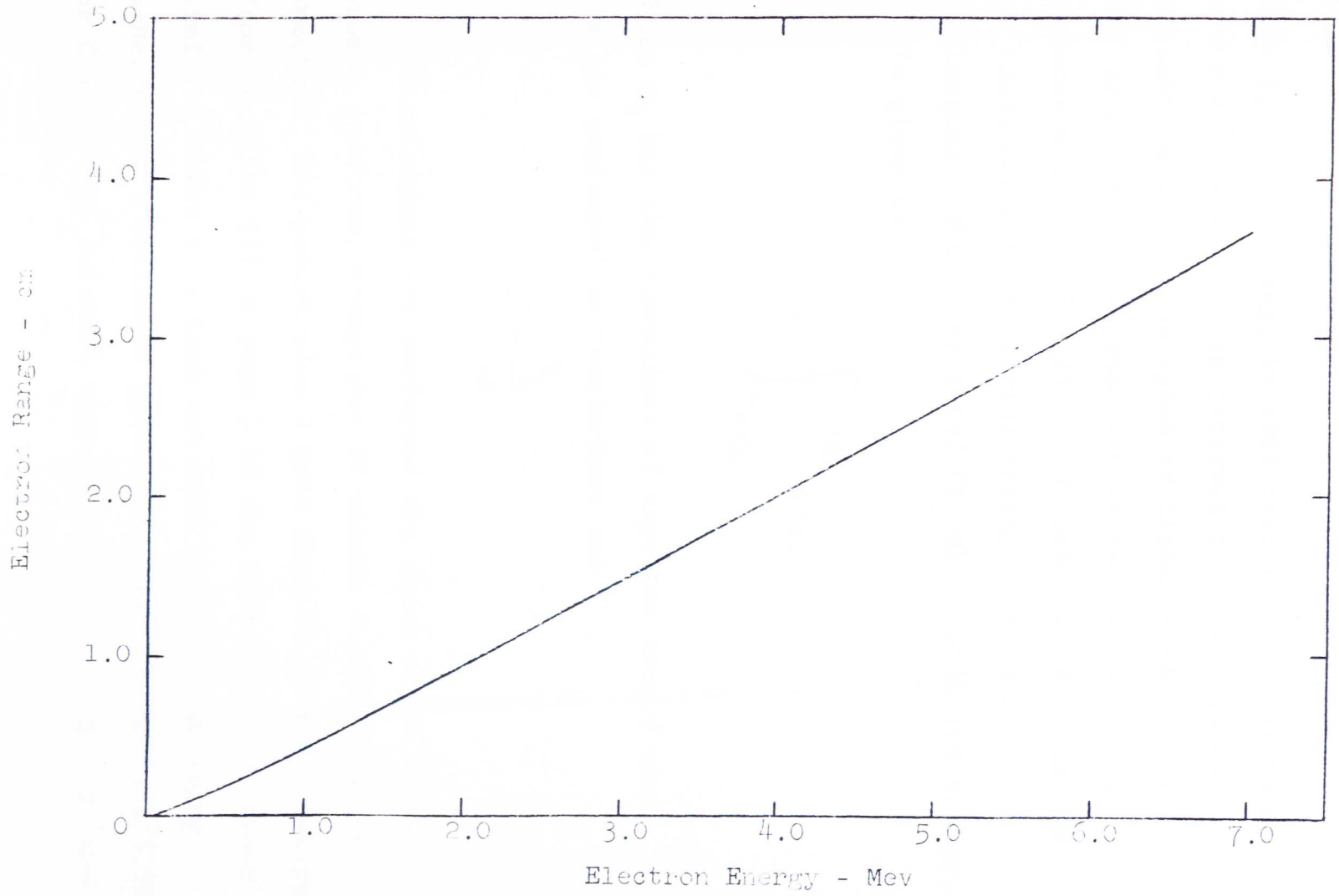

$$E_k = N_{pt} \cdot \frac{hc}{\lambda_{avg}} \tag{3}$$

where E_k is the energy in ergs radiated in unit time at the k^{th} wavelength in interval $\Delta\lambda$, h is Planck's constant, and c is the speed of light in vacuo. A plot of E_k vs λ_{avg} between wavelengths of interest produces a curve which bounds an area proportional to the total Cerenkov radiation energy between those wavelengths. Thus, the total Cerenkov radiation energy, E_t, is given by

$$E_t = \int_{\lambda_{avg_1}}^{\lambda_{avg_2}} E' d\lambda \tag{4}$$

where E_t has the dimensions of ergs per second when λ's are expressed in centimeters and

$$E' = \frac{E_k}{\Delta\lambda} \tag{5}$$

Calculations are performed for three cases, namely, prompt spectrum, prompt plus 20 minute fission product spectrum, and prompt plus 4 hour fission product spectrum. From equation (1) on page 2 of the main text, the lower limiting value of β that can make Cerenkov radiation coherent in a medium of refractive index 1.333 is 1/1.333, or 0.750. The relation between particle energy, E, and

β is

$$E = m_o c^2 \left[\frac{1}{\sqrt{1 - \beta^2}} - 1 \right] \qquad (6)$$

where m_o is the rest mass of the particle. From equation (6) the limiting value of E for production of Cerenkov radiation electrons in water is 0.260 Mev.

Figure 43 is a plot of the calculated gamma spectrum in the core of the UMR for the following cases: prompt spectrum, prompt + 20 minute fission product spectrum, and prompt + 4 hour fission product spectrum. The subsequent calculations assume that only the Compton electrons are of consequence in the production of Cerenkov radiation (both pair production and photoelectric effect are negligible in comparison). Calculation of the fission product gamma spectrum is based on data reported by Knabe and Putnam. In this report the photons are classified first into seven energy groups covering the energy range between 0.1 and 5.5 Mev. The group limits are the same as given by Perkins and King.[25] In addition, group VII of the Perkins and King data is split up into six individual sub-groups so that actually twelve energy groups are considered. The group limits are listed in Table VII. It is found that the average energies of each of the twelve groups are effectively constant in time up to about 10^6 seconds. The calculation of the fission product gamma spectrum presented herein includes all

Fig. 43 Calculated UMR Gamma Spectrum

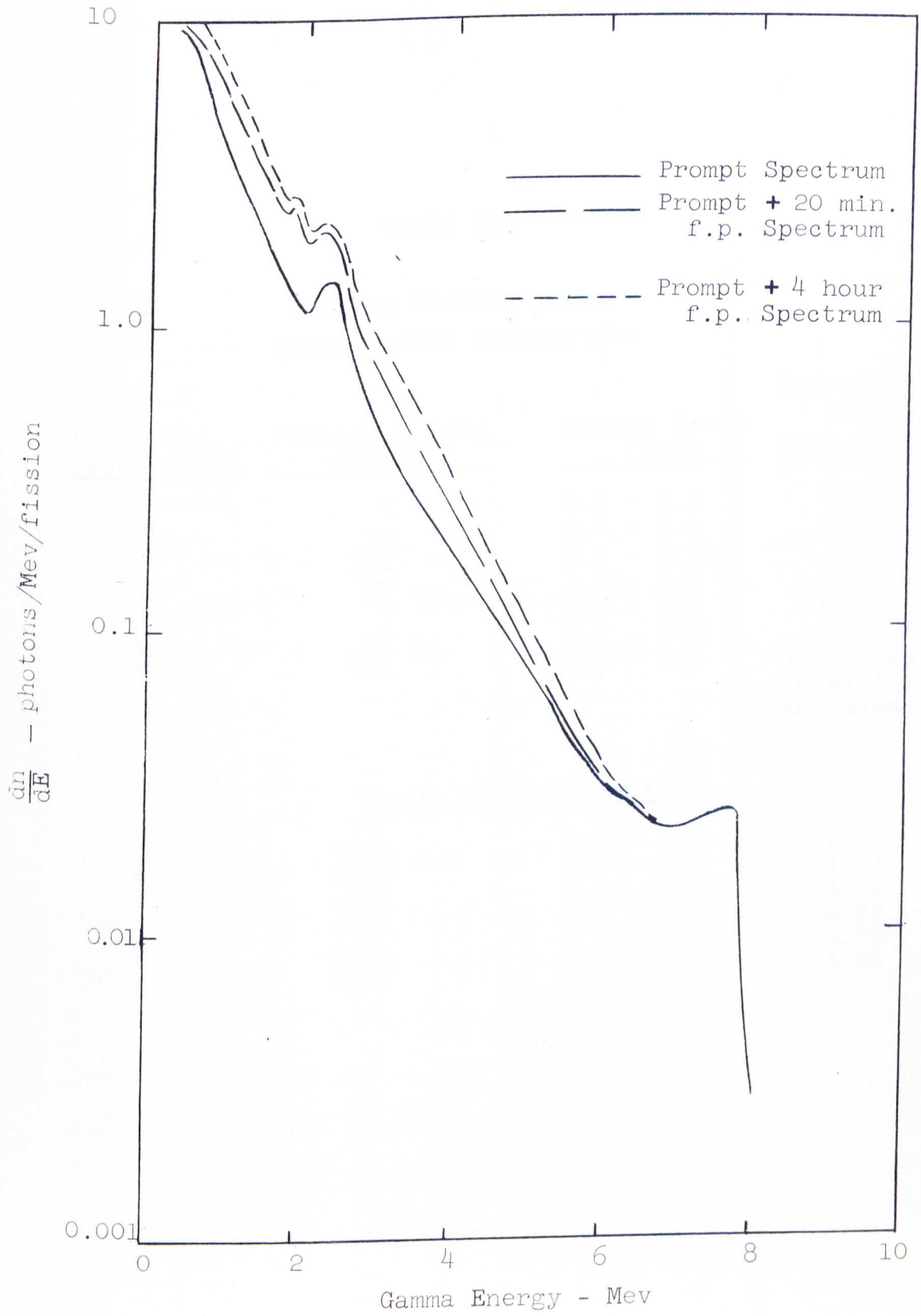

TABLE VII

FISSION PRODUCT GAMMA
ENERGY GROUP DEFINITIONS

12 Groups Subdivision	Perkins & King Groups	Energy Range (Mev)	Reported Avg. Energy (Mev)
1	I	0.1 - 0.4	0.30
2	II	0.4 - 0.9	0.63
3	III	0.9 - 1.35	1.10
4	IV	1.35- 1.8	1.55
5	V	1.8 - 2.2	1.99
6	VI	2.2 - 2.6	2.38
7-12	VII	2.5 - 5.5	Varies between 3.5 and about 3.1
		Group VII Subgroups	
7	VIIa	2.6 - 3.0	2.75
8	VIIb	3.0 - 3.5	3.25
9	VIIc	3.5 - 4.0	3.70
10	VIId	4.0 - 4.5	4.22
11	VIIe	4.5 - 5.0	4.70
12	VIIf	5.0 - 5.5	5.25

groups except group I since the gamma energy which can produce a 0.260 Mev Compton electron (Cerenkov threshold in water) is 0.407 Mev. The appropriately weighted Compton electron energy spectra for the three cases mentioned are calculated from information in the reference by Johns et al and are plotted in Figures 44 through 46 respectively. These curves represent the initial energy distribution of Compton electrons produced in water by the important gamma ray sources as mentioned in Chapter II for a reactor power equal to 10 kw. The number of electrons produced with energies in each energy interval is determined for discrete photon energies ranging from 0.6 Mev to 8.0 Mev and they are added together to give the multi-peaked curves shown in Figures 44 through 46. It is assumed in each case that the entire source is homogeneously distributed throughout a volume of water so large that only a negligible fraction of the core gamma rays escape without producing a Compton electron. In addition, beta particles from fission products of U-235 are neglected as mentioned earlier in Chapter II.

If $f \cdot dE$ is the fraction of recoil Compton electron with energies between E and E + dE then the area obtained by graphical integration of the curves in Figures 44 through 46 may be identified with the total number of Compton electrons produced in each case.

Fig. 44a Distribution of Compton Recoil Electron Energies

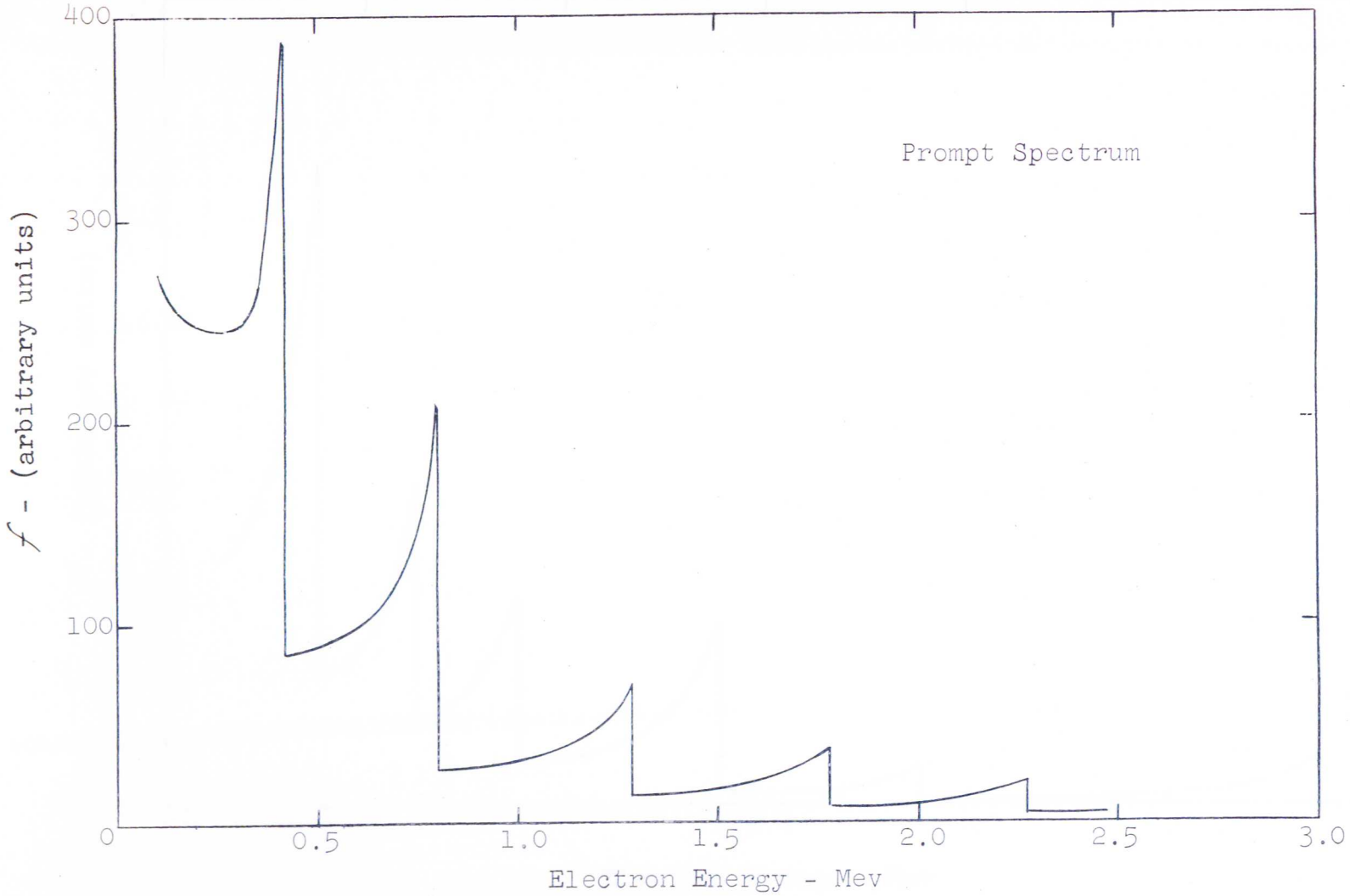

Fig. 44b Distribution of Compton Recoil Electron Energies

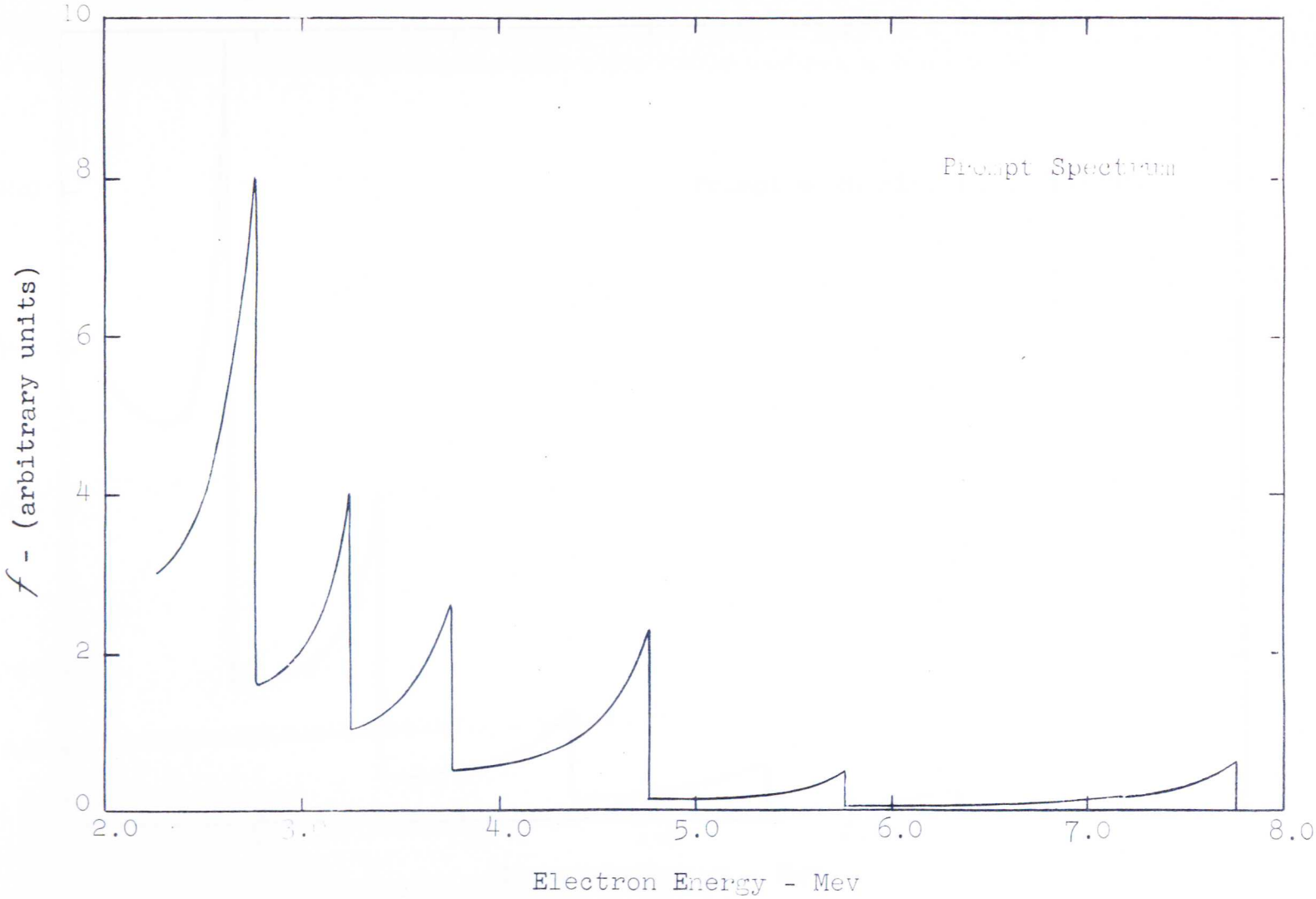

Fig. 45a Distribution of Compton Recoil Electron Energies

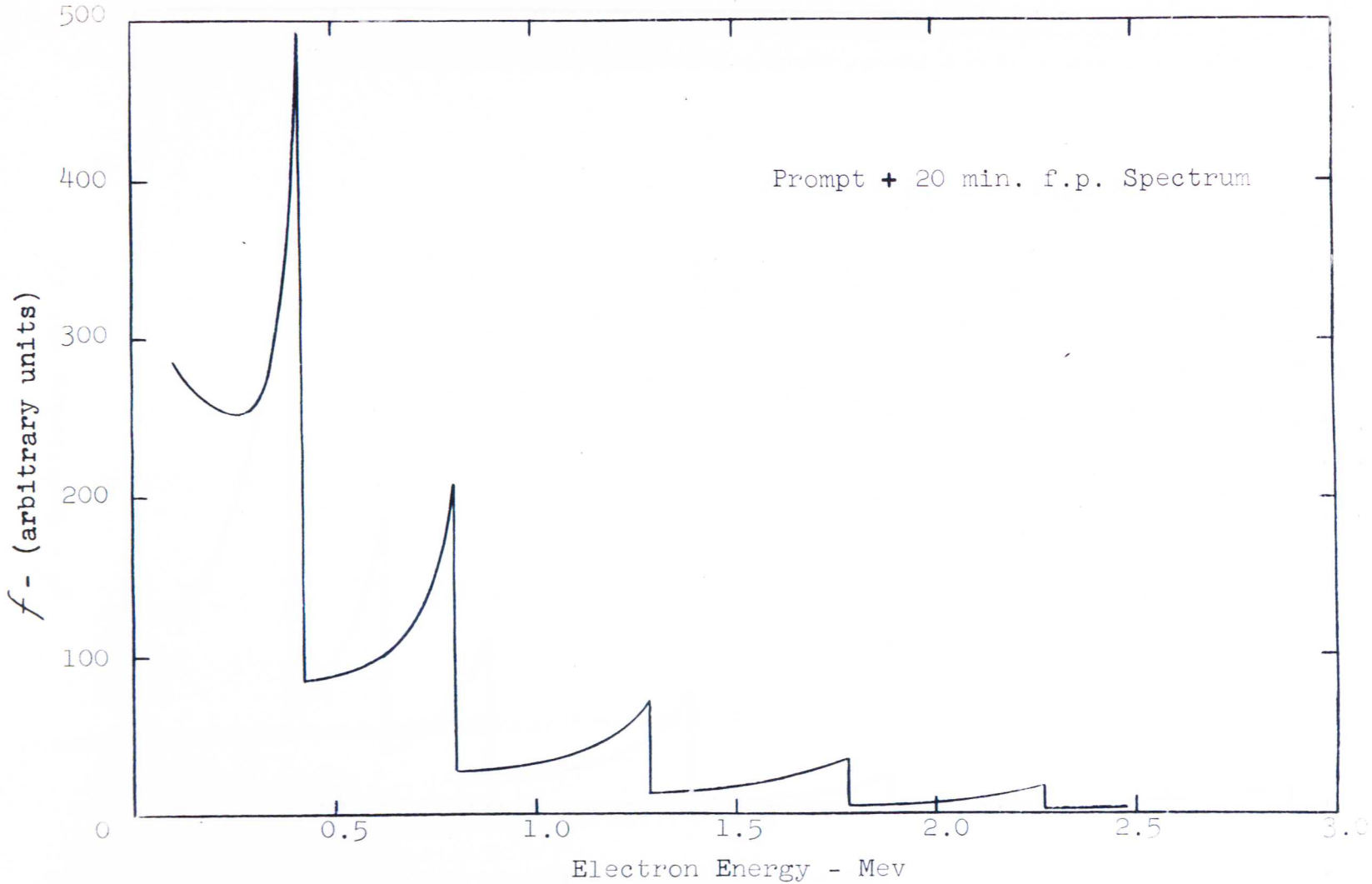

Fig. 45b Distribution of Compton Recoil Electron Energies

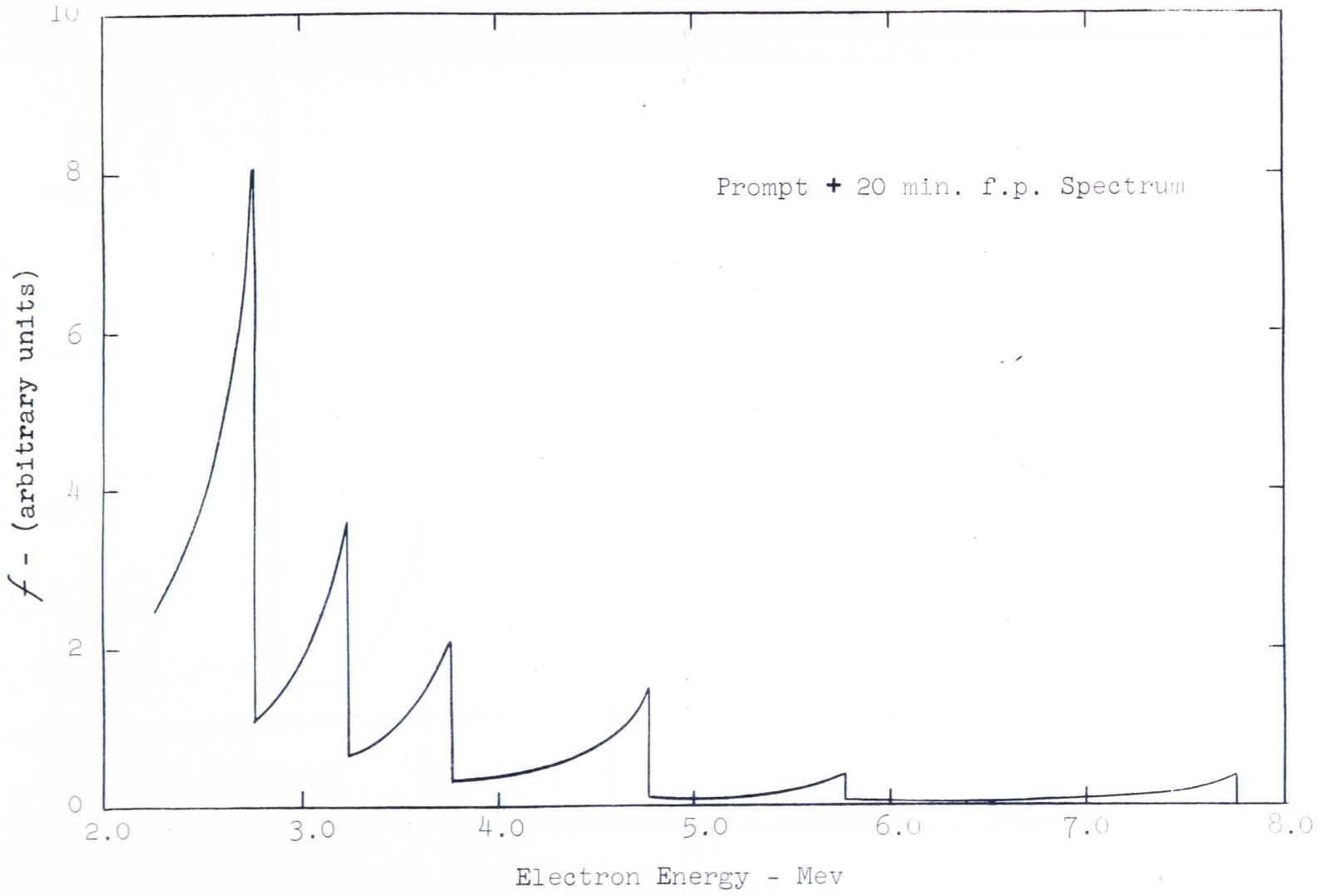

Fig. 46a Distribution of Compton Recoil Electron Energies

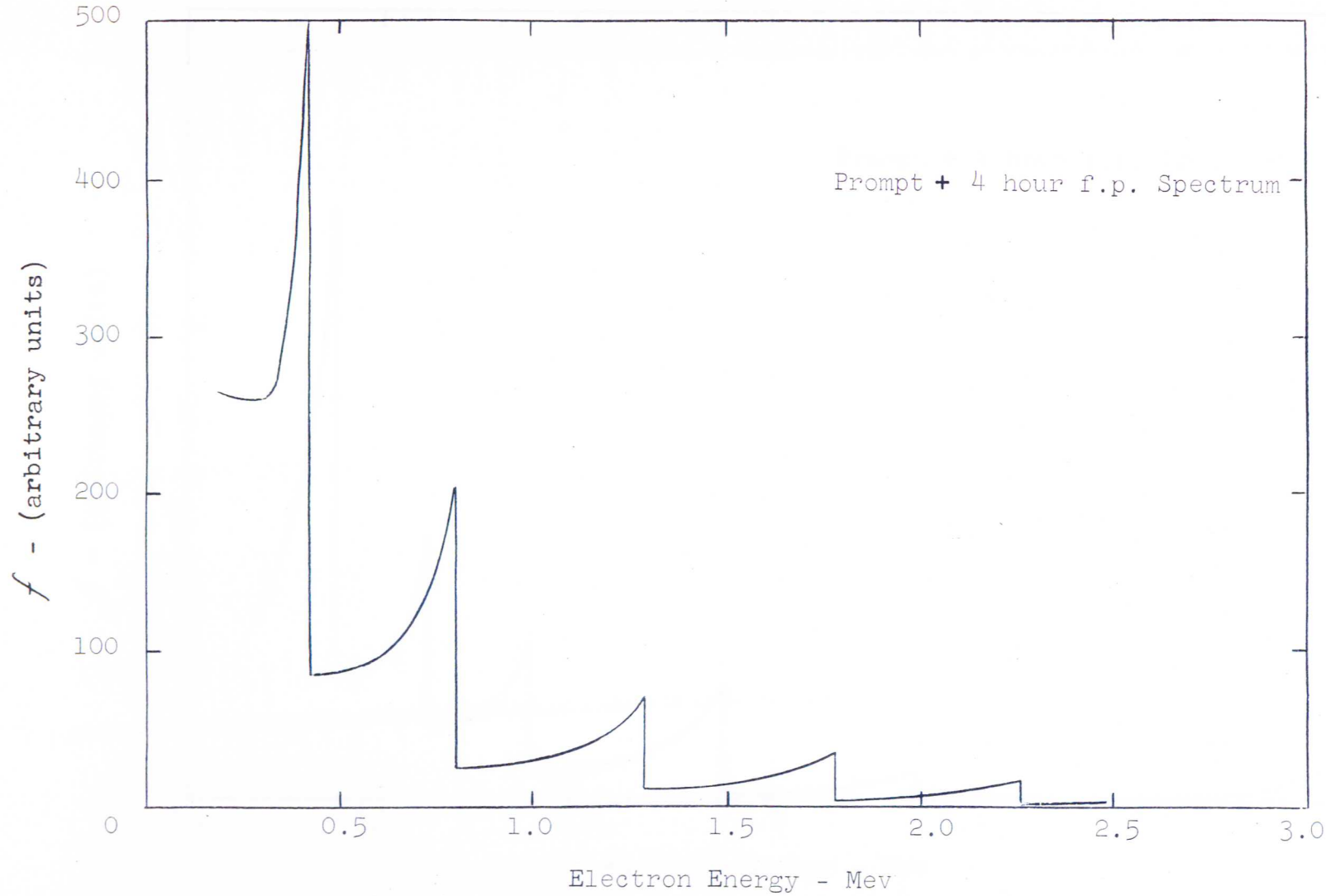

Fig. 46b Distribution of Compton Recoil Electron Energies

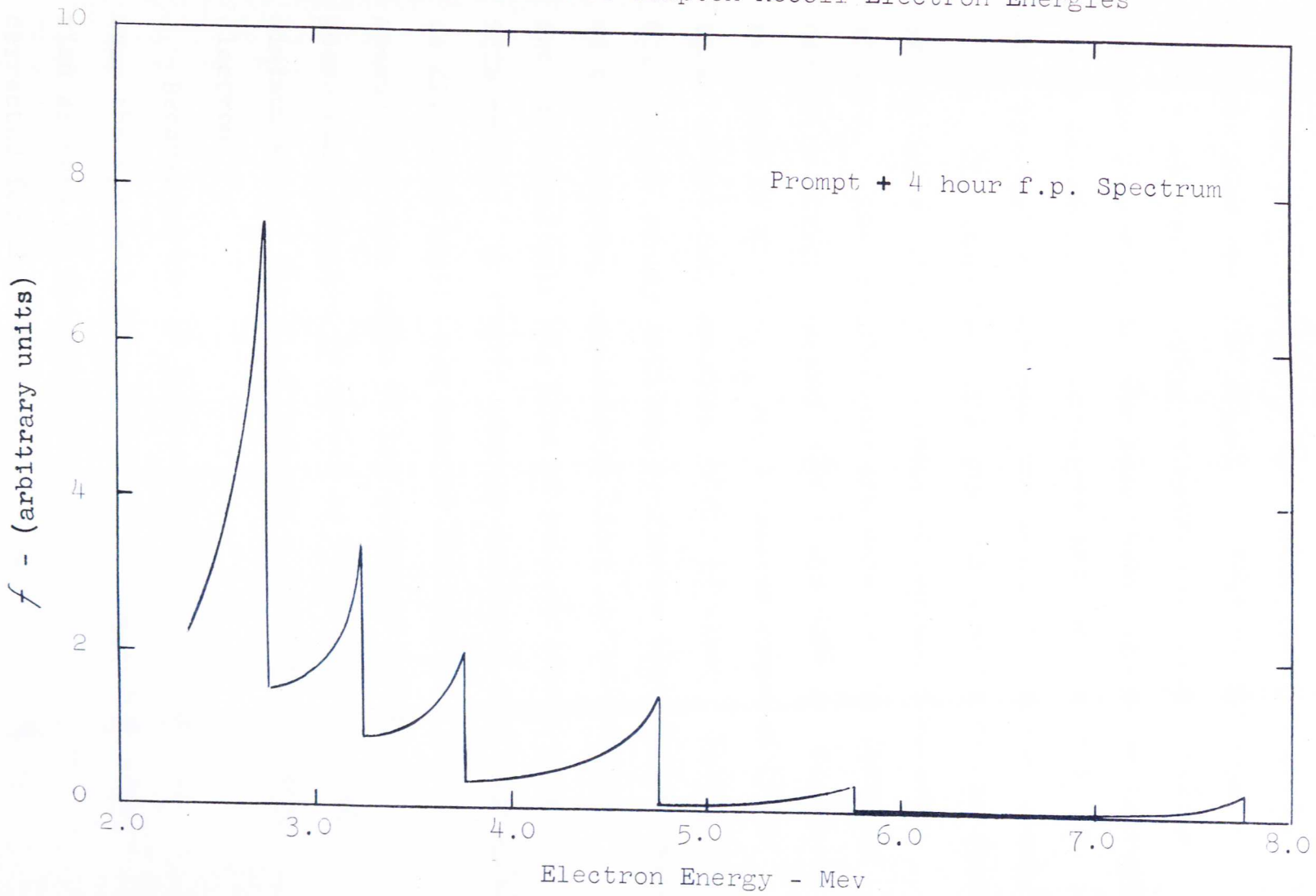

This must equal the number of gamma rays produced in the same time interval in the steady state since it is specified that the volume is large enough that only a negligible number of gamma rays escape before Compton interaction. The area under Figures 44 through 46 is divided into 19 sub-areas and the electrons in each sub-area are assigned the abscissa midpoint energy value. The fraction which each sub-area is of the total multiplied by the total number of Compton electrons, gives N_j. The calculations are made for the Cerenkov radiation emitted between 2000 Å and 8000 Å. Figure 47 is a plot of E' vs λ_{avg} for a reactor power of 10 kw in an effectively infinite volume of water. In all cases, the effects of any self-absorption are neglected because of the resulting complexities since the calculations are performed with the idea of only obtaining qualitative information. It should also be mentioned that the method as described herein may lead to low answers, since no account has been taken of the scattered gamma rays possessing energies in excess of 0.407 Mev, e.g. the minimum energy which can produce a 0.260 Mev Compton electron.

Because of the 17 foot depth of water over the core the spectral distribution of the Cerenkov radiation as seen by the photomultiplier tube must be corrected for the transmission characteristics of water. The attenuation is expressed in terms of the

Fig. 47 Calculated Cerenkov Spectral Distribution

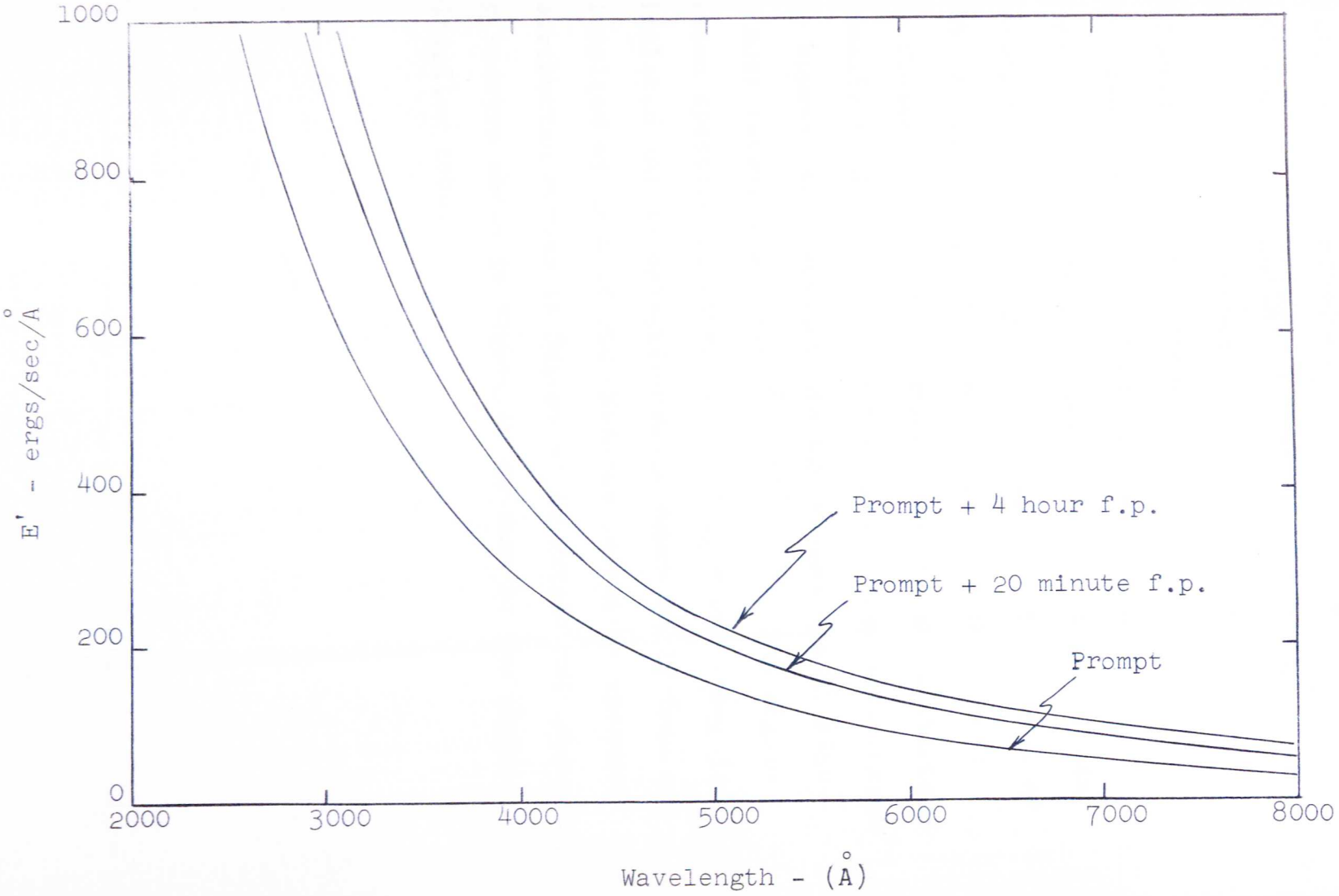

quantity k in the equation $I = I_o \exp(-kx)$. I represents the intensity of a parallel beam of light with initial intensity I_o, after passing through a depth of x centimeters of water. Figure 48 is a plot of k vs λ for distilled water. Large variations exist in the reported literature values of k vs λ over certain wavelength regions especially below 4000 Å. Distilled water, as used in these studies, is very far from a pure substance and the different results are attributed basically to differences in the water. The data chosen here appears to represent average values and is also the most recent available.[40,41,42,43,44] The transmission spectrum of water $H(\lambda) = I/I_o = \exp(-kx)$ is calculated for an effective water depth of 16 feet and multiplied by each of the Cerenkov radiation spectral distribution curves in Figure 47 to obtain the corresponding spectra shown in Figure 49 as seen by the photomultiplier tube.

Fig. 48 Attenuation Coefficient of Distilled Water vs Wavelength

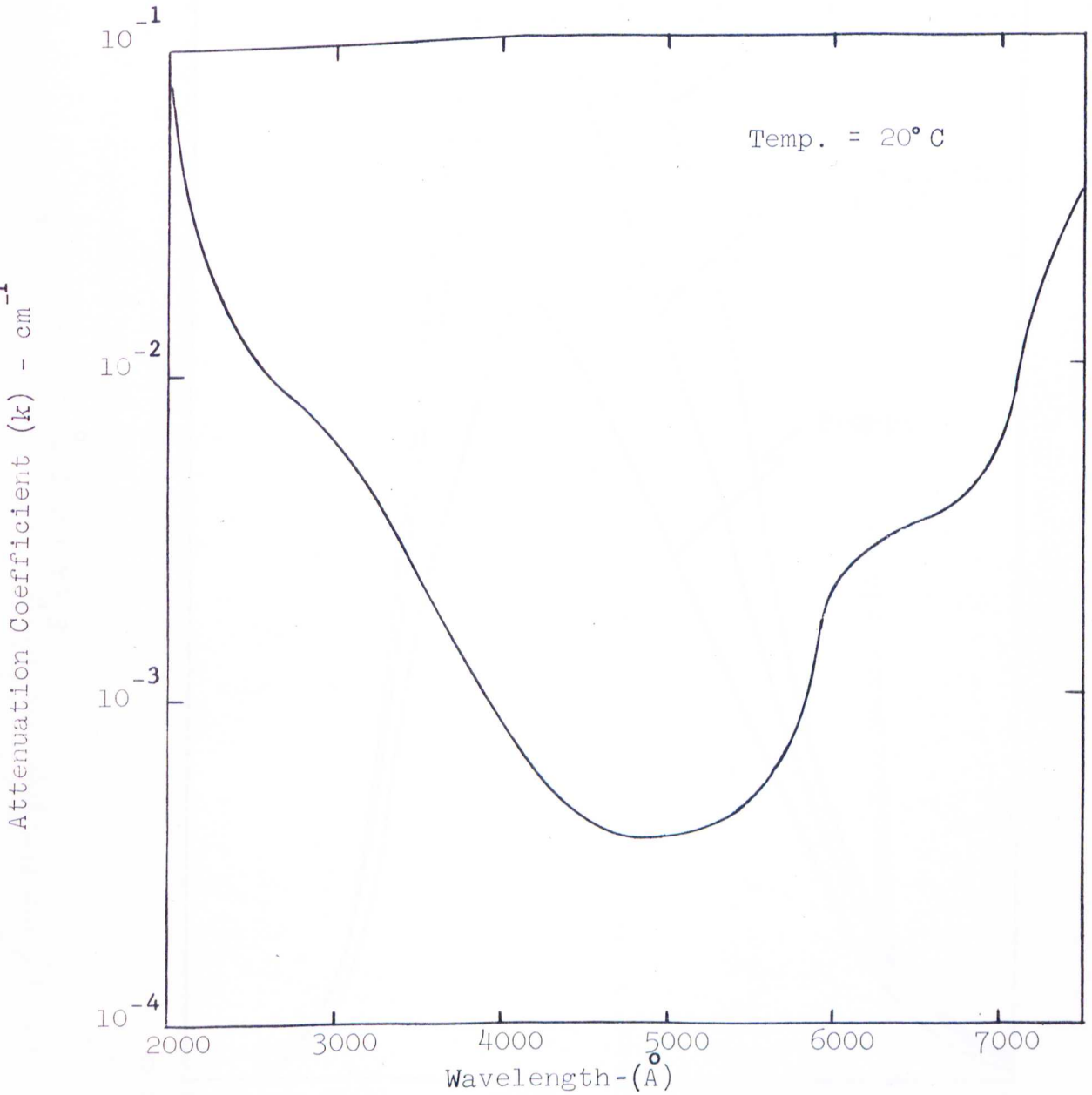

Fig. 49. Calculated Cerenkov Spectral Distribution Through 16 Feet of Water

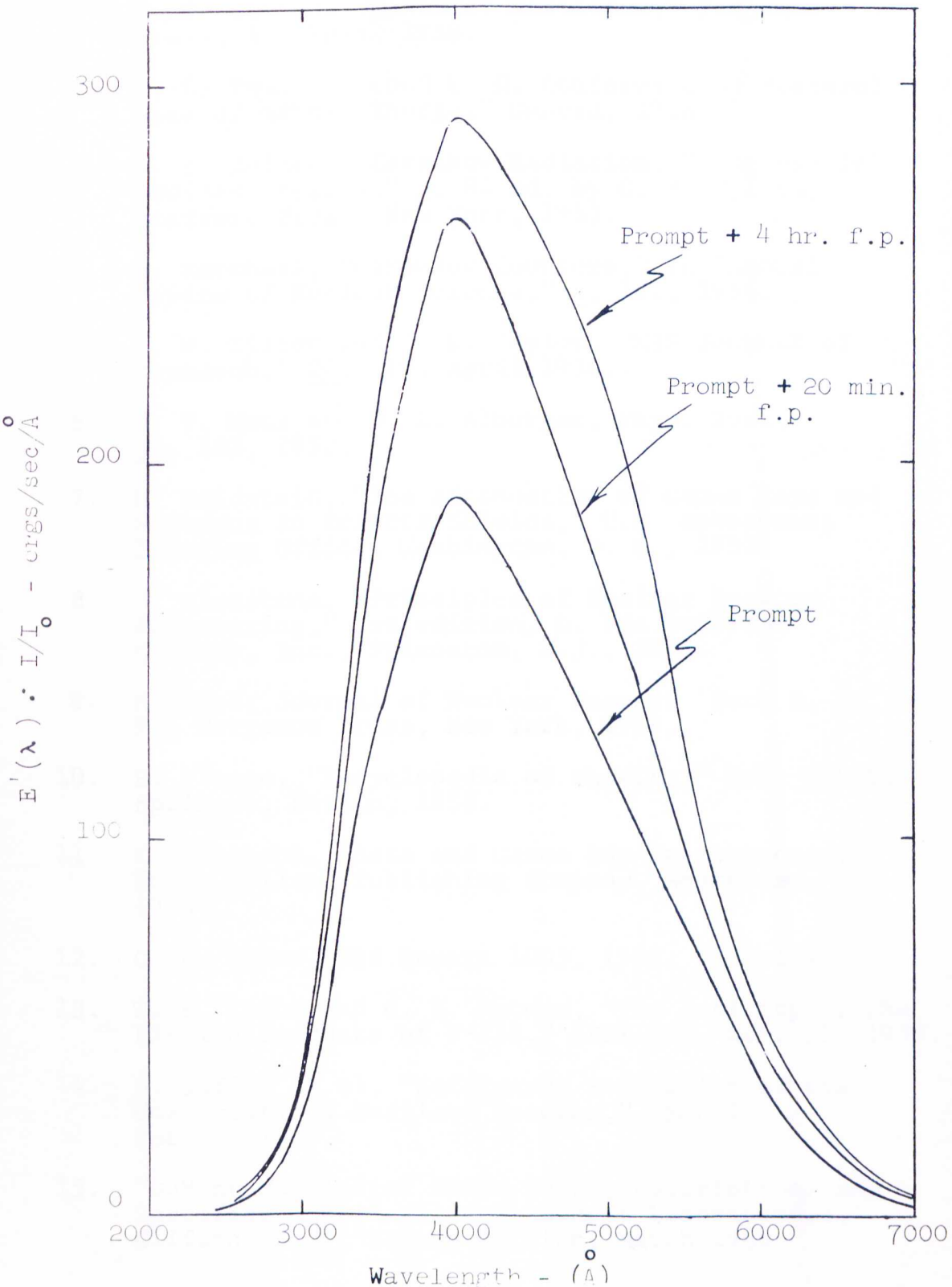

SELECTED BIBLIOGRAPHY

1. J. V. Jelley, "Cerenkov Radiation," Pergamon Press, New York, 1958.

2. I. E. Tamm, "Second U. N. Conference on Peaceful Uses of Atomic Energy," Geneva, 1958.

3. J. V. Jelley, "Cerenkov Radiation", "Progress in Nuclear Physics," 3, 84 ed. by O. R. Frisch, Academic Press, New York, 1953.

4. J. Marshall, "Cerenkov Counters," in "Annual Review of Nuclear Science," 4, 141, 1954.

5. L. W. Tilton and J. K. Taylor, "NBS Journal of Research," 20, 419, April 1938.

6. H. T. Motz and D. E. Alburger, Phys. Rev., 86, 165, 1952.

7. H. Goldstein, "The Attenuation of Gamma Rays and Neutrons in Reactor Shields," U.S. Government Printing Office, Washington, D. C., 1957.

8. S. Glasstone, "Principles of Nuclear Reactor Engineering," 1st edition, D. Van Nostrand Company, Inc., Princeton, N.J., 1955.

9. M. Ross, Journal of Nuclear Energy: Part B, 1, 98, Pergamon Press, New York, 1959.

10. S. Flugge, "Encyclopedia of Physics," Vol. XXXIV, Springer, Berlin, 1958.

11. K. Siegbahn, "Beta and Gamma Ray Spectroscopy," North Holland Publishing Company, Amsterdam, 1955.

12. G. R. White, NBS Report 1003, 1952, unpublished.

13. W. E. Knabe and G. E. Putnam, "The Activity of the Fission Products of U-235," APEX-448, Oct. 31, 1958.

14. D. Duffey et al, "Safeguards Evaluation of the University of Maryland Reactor," UMNE-1, Feb. 7, 1960.

15. "DuMont Multiplier Photo Tubes, Descriptions and Specifications," Allen B. DuMont Laboratories, Clifton, N.J., Second Edition, March 1960.

16. Private Communication.

17. G. R. Harrison, R. C. Lord, and J. R. Loffbourow, "Practical Spectroscopy," Prentice Hall, New Jersey, 1948.

18. "Kodak Plates and Films for Science and Industry," Eastman Kodak Company, 1962.

19. G. H. Eggers, and A. H. Kazi, "DOFL-TRIGA Acceptance Test Report," GA-2995, March 1962.

20. F. E. Obenshain and A. Foderaro, "Energy from Fission Product Decay," WAPD-P-652, May 1955.

21. C. F. Miller, "Gamma Decay of Fission Products from the Slow Neutron Fission of U-235," USNRDL-TR-187, July 11, 1957.

22. C. B. Magee, "U-235 Fission Product Activity and Energy as a Function of Decay Time for a Specific Irradiation Time and Thermal Flux," APEX-530, April 1959.

23. H. I. West, Jr., "The Beta Ray Spectra of the Fission Products of U-235 1 to 300 seconds After Fission," UCRL-L, 1960.

24. R. E. Carter, F. Reines, J. J. Wagner and M. E. Wyman, Phys, Rev. 113, 280, 1959.

25. J. F. Perkins and R. W. King, "Energy Release from the Decay of Fission Products," Nuc. Sci. and Eng. 3, 726, 1958.

26. F. C. Maienschein, "Fission Gamma-Ray Energy Release as a Function of Time after Fission," ORNL-3193, pp. 189-191, Sept. 1, 1961.

27. R. W. Peelle, W. Zobel and T. A. Love, "Measurement of the Spectrum of Short Lived Fission Product Decay Gamma Rays Emitted from a Rotating Fuel Belt," ORNL-2081, pp.91-94, Sept. 10, 1956.

28. W. Zobel and T. A. Love, "Time and Energy Spectra of Fission Product Gamma Rays Measured at Short Times After Uranium Sample Irradiation," ORNL-2081, 95, Sept. 10, 1956.

29. W. Zobel and R. W. Peelle, T. A. Love and G. M. Estabrook, "Analysis of Fission Product Gamma Ray Spectra Experiment," ORNL-2389, pp. 97-98, Sept. 1, 1957.

30. F. C. Maienschein, R. W. Peelle and T. A. Love "Energy Spectrum of Prompt Gamma Rays Accompanying the Fission of U-235," ORNL-2389, pp. 99-110, Sept. 1, 1957.

31. C. J. Borkowski and R. J. Kerr, Nucleonics 14, 105, June 1956.

32. M. H. Sweet, Electronics, pp. 105-109, Nov. 1946.

33. R. E. Bell and R. L. Graham, Rev. of Sci. Inst., 23, 301, June 1952.

34. P. Hariharan and M. S. Bhalla, Journal of Sci. Inst. 33, 69, Feb. 1956.

35. H. E. Johns, J. E. Till and D. V.Cormack, Nucleonics 12, 40, Oct. 1954.

36. H. E. Johns, D. V. Cormack, S. A. Denesuk and G. F. Whitmore, Can. J. Phys. 30, 556, 1954.

37. R. G. Wymer and R. E. Biggers, ORNL-3180, Sept. 19, 1961.

38. E. H. Belcher, Proc. Royal Soc. London, A-216, 90, 1953.

39. A. T. Nelms, NBS Circular 577, 1956.

40. W. R. Sawyer, Can. Biol. and Fisheries Contr. N. S., 7, 75, 1931.

41. B. P. Fabricand, "A Detailed Investigation of the Absorption by Water of Electromagnetic Radiation," Colum. Univ. Hudson Lab. T. R. 73, 1957.

42. H. R. James and E. A. Birge, Wisc. Acad. Sci. Arts and Ltrs., 31, 18, 1938.

43. L. H. Dawson and E. O. Hulburt, J.O.S.A., 24 175, 1934.

44. E. O. Hulburt, J.O.S.A., 17, 15, 1928.